# NEOGENE STRATIGRAPHIC RELATIONSHIPS WITHIN THE NAM CON SON BASIN, OFFSHORE VIETNAM RESULTING FROM TECTONICS, EUSTASY, AND SEDIMENT FLUX

A Dissertation

by

CHRISTINE M. WRIGHT

Submitted to the Office of Graduate Studies of
Texas A&M University
in partial fulfillment of the requirements for the degree of

DOCTOR OF PHILOSOPHY

December 2006

Major Subject: Geology

# NEOGENE STRATIGRAPHIC RELATIONSHIPS WITHIN THE NAM CON SON BASIN, OFFSHORE VIETNAM RESULTING FROM TECTONICS, EUSTASY, AND SEDIMENT FLUX

A Dissertation

by

CHRISTINE M. WRIGHT

Submitted to the Office of Graduate Studies of
Texas A&M University
in partial fulfillment of the requirements for the degree of

DOCTOR OF PHILOSOPHY

Approved by:

| | |
|---|---|
| Chair of Committee | Steven L. Dorobek |
| Committee Members, | William R. Bryant |
| | Philip D. Rabinowitz |
| | David Sparks |
| | Brian J. Willis |
| Head of Department | Richard Carlson |

December 2006

Major Subject: Geology

# ABSTRACT

Neogene Stratigraphic Relationships Within the Nam Con Son Basin, Offshore Vietnam Resulting From Tectonics, Eustasy, and Sediment Flux. (December 2006)

Christine M. Wright, B.S., Central Missouri State University;

M.S., Louisiana State University

Chair of Advisory Committee: Dr. Steve Dorobek

The South China Sea is a region of significant importance in terms of the records of SE Asian tectonics, including Tibetan Plateau uplift, and the onset and evolution of the East Asian monsoon. The Mekong River has been a dominant sediment source since at least late Miocene time and has headwaters on the eastern Tibetan Plateau. Understanding the Pliocene to Recent stratigraphy of the paleo-Mekong Delta and associated shelf-edge deposits aids in understanding changes in accommodation, sea level, and sediment supply. This record might then be useful in interpreting the long-term history of basin evolution in the Nam Con Son Basin.

Nine sequence boundaries and associated sequences are recognized along the late Miocene to latest Pleistocene shelf in the East Nam Con Son Basin. Age constraints were assigned to key stratigraphic horizons by correlating sequence boundaries with published sea level curves. Accommodation in the study area is controlled by shelf -edge compaction, rift-related thermal subsidence, non-rift-related anomalous subsidence, eustatic change, and shelf edge faulting.

Two primary sources supplied sediment to the southwestern South China Sea during Pliocene to Recent time and likely include the paleo-Mekong Delta and a fluvio-deltaic system originating from the Sunda Shelf, such as the Molengraaff River. Changes in thickness, area, and location of Pliocene to Recent shelf-edge delta deposits reflect changes in accommodation and sediment supply over time, as well as progradation of the shelf edge during Pliocene to Recent time and avulsion of the shelf edge delta.

Anomalous subsidence of LGM shelf edge deposits is estimated at approximately 40-50 m deeper than expected. The current depth of the LGM deltaic wedge may indicate renewed rapid tectonic subsidence during the last 18,000 yrs, possible compaction effects or a combination of these.

# DEDICATION

I would like to dedicate this dissertation to my mother, who always told me I could do anything; to my husband who supported me; and to my son, William, who I hope has as many adventures in college as I did.

## ACKNOWLEDGMENTS

I would like to thank my advisor, Steve Dorobek, for his insight during the last four years. I would also like to thank my committee members for agreeing to serve on my committee. Appreciation is expressed to ConocoPhilips for donating the data. Steve Tran was instrumental in loading the data and maintaining the hardware. Help from Gabriel Grimaldi and several Chevron geoscientists was vital in learning to use the software. Financial support for this research was provided by AAPG student grants-in-aid. Financial support for academics was provided by ConocoPhillips, ChevronTexaco, and scholarships through the Department of Geology and Geophysics.

# TABLE OF CONTENTS

Page

Page

## LIST OF FIGURES

Page

Page

Page

# CHAPTER I

# INTRODUCTION

Uplift of the Tibetan Plateau is believed to be the result of collision of India with Eurasia beginning in early Eocene time (~50 Ma) (e.g., Dewey et al., 1989; Harrison et al., 1992; Harrison et al., 1998; Clark and Royden, 2000; Sun and Liu, 2000, Tapponnier et al., 2001). The timing and nature of uplift are complicated and controversial. Even less understood are the possible responses of Earth's surface processes to uplift of the Tibetan Plateau. Uplift of the Plateau is thought to have affected the evolution of the East Asian Monsoon (Ruddiman and Kutzbach, 1991; Raymo and Ruddiman, 1992; Fillipelli, 1997; Prell and Kutzbach, 1992; Prell and Kutzbach, 1997; Wang et al., 2000; An et al., 2001; Clift and Gaedicke, 2002; Liu et al., 2003), continental drainage across SE Asia (Lacassin et al., 1998; Replumaz et al., 2001; Clark et al., 2004), oceanic upwelling in the Arabian Sea (Ruddiman et al., 1997), and sediment flux into adjacent ocean basins (Olson and Dorobek, 2000; Clift and Gaedicke, 2002; Wehausen et al., 2003; Murray and Dorobek, 2004). Nonetheless, the geomorphologic evolution of Tibetan uplift and the geodynamic and tectonic driving forces for the uplift are yet to be fully resolved.

The South China Sea (SCS) is an area of great importance with respect to the uplift history of the Tibetan Plateau because several prominent Asian rivers have

---

This dissertation follows the style of AAPG Bulletin.

headwaters in Tibet and ultimately discharge into the SCS. The modern Mekong River drainage is one of the major river systems that drains Tibet and deposits sediment in the SCS of offshore Vietnam. Thus, the Neogene stratigraphy of offshore Vietnam serves as a proxy record for uplift and erosion of the eastern Tibetan Plateau. Changes in sediment flux within the paleo-Mekong delta and shelf system are linked to changes in exhumation rates, which in turn likely reflect rates of plateau uplift. Dorobek and Olson (2001), Clift et al. (2004), and Murray and Dorobek (2004) utilized the sedimentary record of the SCS as a proxy for uplift history. This study investigates the Neogene stratigraphy within the Nam Con Son Basin and places depositional patterns into a sequence stratigraphic framework in order to evaluate the effects of tectonics, eustasy, and sediment flux.

The tectonic history of the Nam Con Son Basin (NCSB) has been investigated by a number of workers (e.g., Taylor and Hayes, 1983; Su et al., 1989; Matthews et al., 1997; and Olson, 2001). Matthews et al. (1997) and Lee et al. (2001) described the sedimentary record and generalized stratigraphy of the NCSB. Cretaceous-Paleogene extensional tectonics have been examined by Taylor and Hayes (1983), Tapponnier et al. (1982), Jolivet et al. (1989), Rangin et al. (1990), Huchon et al. (1994), Lee and Lawver (1994), Zhou (1994), Zhou et al. (1995), Hall (1996), and Huchon (1998), although the mechanism responsible for extension is still poorly understood. Inversion structures within the basin have been studied by Matthews and Todd (1993), Tija (1994), Tija and Liew (1996), Olson and Dorobek (2000), Olson (2001), and Hall and Morley (2004). Wheeler and White (2002) investigated post-rift subsidence history and report

anomalous subsidence in the NCSB during the last 10 Ma. Detailed study of the stratigraphic relationships within Neogene strata should provide additional insight into the post-rift subsidence history of the basin. The combined effects of tectonic subsidence, sediment flux and eustatic sea-level fluctuations must be investigated simultaneously in order to assess the record of Tibetan uplift and continental drainage evolution that must be present in these strata.

Offshore Vietnam also contains economically important petroleum resources. The region has been explored since the early 1960's (Olson, 2001). Most source rocks are confined to Paleogene lacustrine, fluvio-deltaic, marine, and carbonate deposits with reservoir rocks largely found in: 1) fractured/weathered granitic basement; and 2) Miocene sands and carbonate platform facies (Howes, 1997; Matthews et al., 1997; Lee et al., 2001). The study interval (Pliocene to Recent) is not typically associated with economically significant hydrocarbon accumulations, although analysis of the Pliocene to Recent stratigraphic succession should be useful for basin modeling studies and may provide insight into potential drilling hazards that overlie deeper petroleum reservoirs.

This study will attempt to link the Neogene stratigraphy of offshore Vietnam to changes in accommodation resulting from eustatic fluctuations, tectonic subsidence, and changes in sediment flux. Changes in sediment flux will be used as a potential proxy for uplift of the Tibetan Plateau and possibly the related evolution of the East Asian monsoon. To date, few stratigraphic studies of the Vietnamese continental margin have utilized such an extensive seismic data set to evaluate the stratigraphic record and its relation to the uplift of the Tibetan Plateau.

# CHAPTER II

# BACKGROUND GEOLOGIC HISTORY

## UPLIFT OF THE TIBETAN PLATEAU

The Tibetan Plateau formed as a result of continent-continent collision between India and Asia, which began about 50 Ma (e.g., Dewey et al., 1989; Harrison et al., 1992; Fielding, 1996; Royden et al., 1997; Clark and Royden, 2000; Sun and Liu, 2000; Tapponnier et al., 2001) (Figure 2.1). Multiple hypotheses have been proposed for the origin of the Tibetan Plateau, including: underthrusting of India (Powell and Conaghan, 1973; Wang et al., 1982), delayed continental underplating (Powell, 1986), continental injection (Zhao and Morgan, 1985; 1987), distributed shortening (Houseman et al., 1981; Chang et al., 1986; Molnar et al., 1987; Willett and Beaumont, 1994; Fielding, 1996), and flow within a low-viscosity midcrustal channel (Beaumont et al., 2004; Jamieson et al., 2004). Some authors also argue for inherited elevation during Early Cretaceous time prior to initial hard collision (Yin et al., 1994; Murphy et al., 1997).

The timing of Tibetan uplift remains controversial. Sun and Liu (2000) argue for an episode of uplift as young as Middle Pleistocene (~1.1 and 0.9 Ma) to account for a part of present elevation. Other authors have argued for uplift over the last 5 Myr (Powell, 1986) or a major uplift event at 10 Ma (Zhao and Morgan, 1985). Fielding (1996) suggests that the Tibetan Plateau attained its current elevation before ~8 Ma, based on volcanism in northern Tibet and extension in southern Tibet. Chung et al. (2005) propose that uplift occurred during two main stages in Eocene and late Oligocene

time and that uplift was diachronous, with uplift propagating from south to north. Molnar et al. (1993) suggest there were two phases of uplift, with an initial phase of

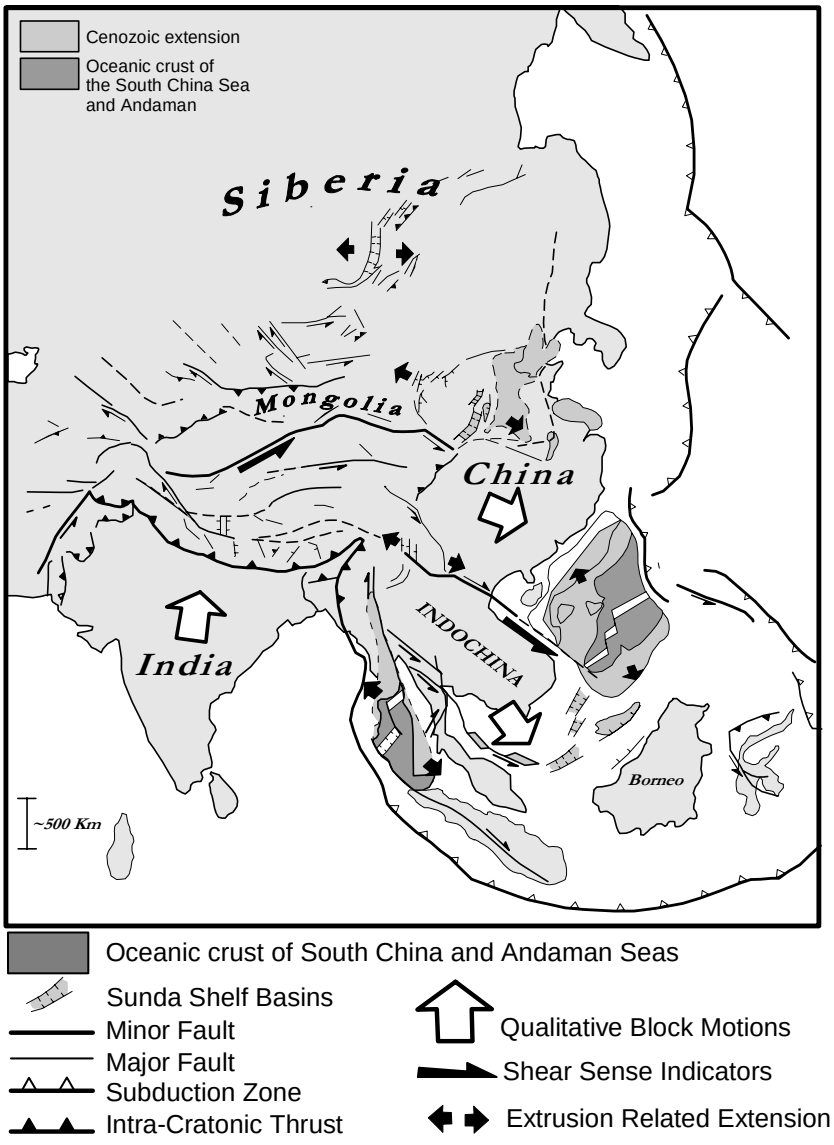


**Figure 2.1:** Cenozoic tectonic elements across southeast Asia related to oceanic subduction in western Pacific, indentation of India, and extrusion of the Indochina and South China blocks. After Tapponnier et al. (1982).

uplift at about 50 Ma and a second at around 6-9 Ma. Yin et al. (1994) and Murphy et al. (1997) propose that the Tibetan Plateau had already attained significant elevation (as much as 3-4 km) prior to hard collision between India and Eurasia. Many authors now suggest that the onset of east-west extension in the southern Plateau reflects attainment of some critical maximum elevation, which triggered orogenic collapse (e.g., Molnar et al., 1993; Fielding, 1996; Harrison et al., 1998; Garzione et al., 2003).

Uplift of the Tibetan Plateau probably had significant impacts on global ocean chemistry (i.e., major flux of siliciclastic sediment and dissolved load to the world's oceans) and climate (i.e., onset of global cooling and evolution of the East Asian monsoon). Thus, understanding the timing of uplift events is crucial for establishing a link between Plateau uplift, sediment flux to the SCS, and evolution of the East Asian monsoon. This study, in effect, will attempt an inverse approach, where changes in sediment supply to the NCSB will be used as an indicator of progressive uplift in the Tibetan Plateau.

## EXTENSIONAL HISTORY OF THE SOUTH CHINA SEA

The proto-southeast Asian margin was an Andean-type convergent margin during mid-Jurassic to mid-Cretaceous time (Taylor and Hayes, 1983). Extension of continental crust in the SCS region began during Late Cretaceous-Early Paleocene time (Holloway, 1982; Taylor and Hayes, 1983; Zhou et al., 1995; Schluter et al., 1996). Seafloor spreading began in the north South China margin during late Oligocene time (~32 Ma) along a WSW-ENE to NE-SW axis (Hamilton, 1979; Taylor and Hayes, 1983; Briais et

al., 1993, Zhou, 1994). Spreading in the Northwestern Sub-basin ended at ~30 Ma, but continued in a nearly north-south direction farther east with ridge segments arranged in a right-stepping, en echelon pattern (Briais et al., 1993). Briais et al. (1993) report a shift from ENE-WSW ridge segments to more E-W oriented ridge segments at about 30-26 Ma. The ridge jumped south at ~26-24 Ma with a corresponding change in ridge-axis orientation (Briais et al., 1993). A second ridge jump occurred at ~20.5 Ma and was coeval with maximum lateral propagation of the spreading system (Briais et al., 1993). At this time the direction of spreading shifted from NW-SE to N-S (at ~19 Ma) and back to NW-SE (at ~17.8 Ma) (Briais et al., 1993). Seafloor spreading propagated into the Southwestern Sub-basin of the SCS, with the southwestern propagating tip of the youngest ridge system attaining its nearest position to the NCSB by middle Miocene time (~15.5 Ma) (Briais et al., 1993) (Figure 2.2).

The mechanisms controlling seafloor spreading in the SCS are not well understood. Some authors attribute seafloor spreading to large-scale extrusion of continental blocks during the Indo-Eurasian collision (Tapponnier et al., 1982; Briais et al., 1993; Huchon et al., 1994; LeLoup et al., 2001). Zhou et al (1995) propose three phases of extension and spreading, each with a separate primary driving factor: 1) Late Cretaceous-Early Eocene extension was controlled by trench rollback of the West Pacific subduction zone and extension across the SCS upper plate; 2) influence of the initial and subsequent “hard” collision of the Indian Plate with Eurasia, which controlled extension and spreading during mid- Eocene to mid-Miocene time; and 3) during mid-Miocene through Quaternary time the primary factors influencing the tectonics of the

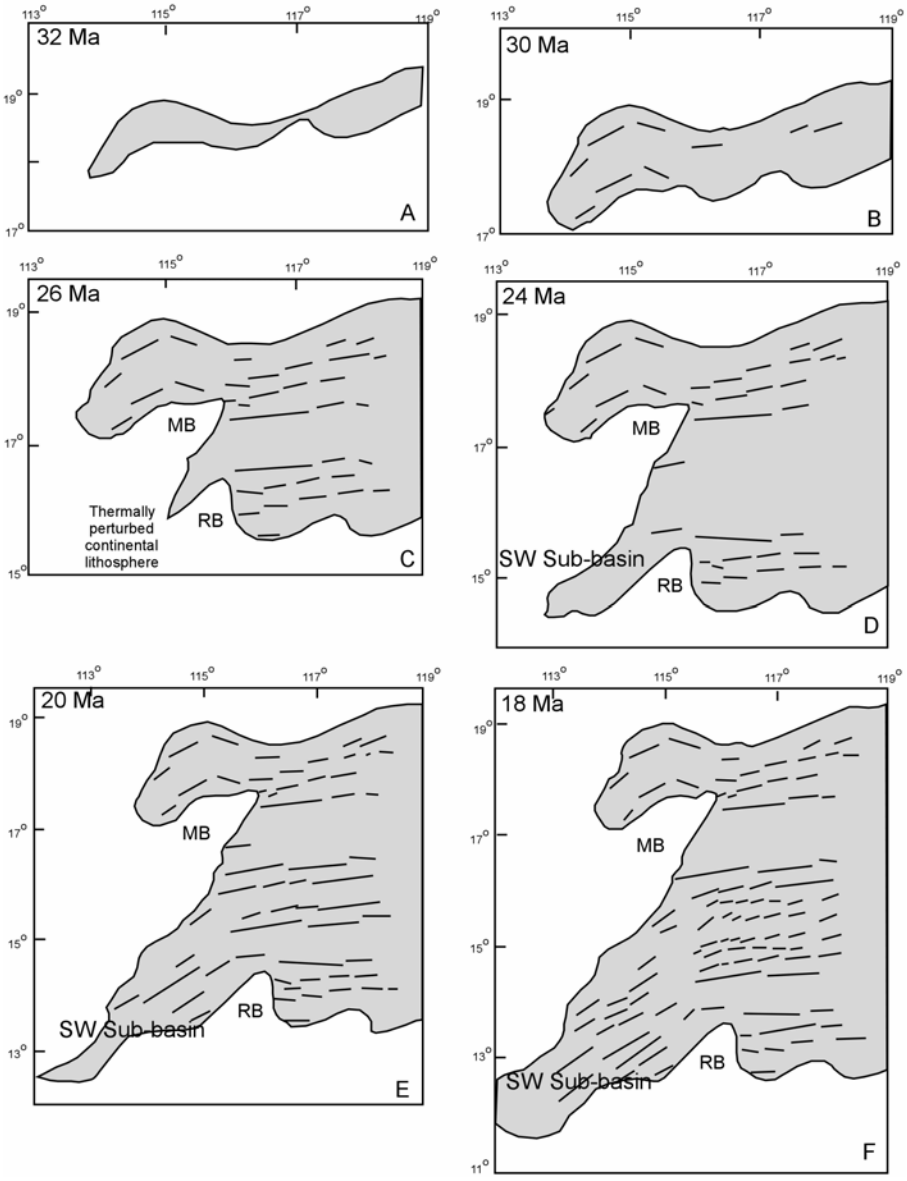


**Figure 2.2:** Seafloor spreading history in the SCS. Gray shows the area of oceanic crust. Solid black dashes show trend of magnetic lineations. *Early to Middle Miocene time (Figures 2.2d and 2.2e):* propagation of spreading axis into the southwestern sub-basin. *Middle Miocene time (Figure 2.2f):* ridge tip had propagated to its most southwestern location with respect to the NCSB (After Briais et al., 1993).

SCS include northward subduction of the Indian Ocean-Australian plate and the northward shift of the Philippine Block. Extension in the SCS was minimal during mid-Miocene to Quaternary time.

## NEOGENE BASIN INVERSION

Many basins across the southern SCS underwent a period of tectonic inversion during Miocene and later time (Matthews and Todd, 1993; Ginger et al., 1994; Tija, 1994; Tija and Liew, 1996; Madon, 1997; Matthews et al., 1997; Olson and Dorobek, 2000; Olson, 2001; Hall and Morley, 2004). The West Natuna Basin, Malay Basin, Western Nam Con Son Basin (WNCSB), and Eastern Nam Con Son Basin (ENCSB) (Figure 2.3) experienced variable compressional stress orientations and magnitudes, resulting in a variety of inversion features (Olson, 2001).

Inversion began in the West Natuna Basin and WNCSB during late Oligocene to early Miocene time. Inversion was more pronounced in the West Natuna Basin (Olson, 2001). Inversion continued in the West Natuna Basin and WNCSB during middle Miocene time and expanded to the Malay Basin and ENCSB (Olson, 2001). Inversion shifted northward in the Malay basin during late Miocene time, while minor inversion continued in the West Natuna Basin (Olson, 2001).

Only mild inversion structures related to reactivated Paleogene extensional faults are observed in the ENCSB (Matthews and Todd, 1993; Matthews et al., 1997). While inversion across the Sunda Shelf generally migrated from east to west-northwest,

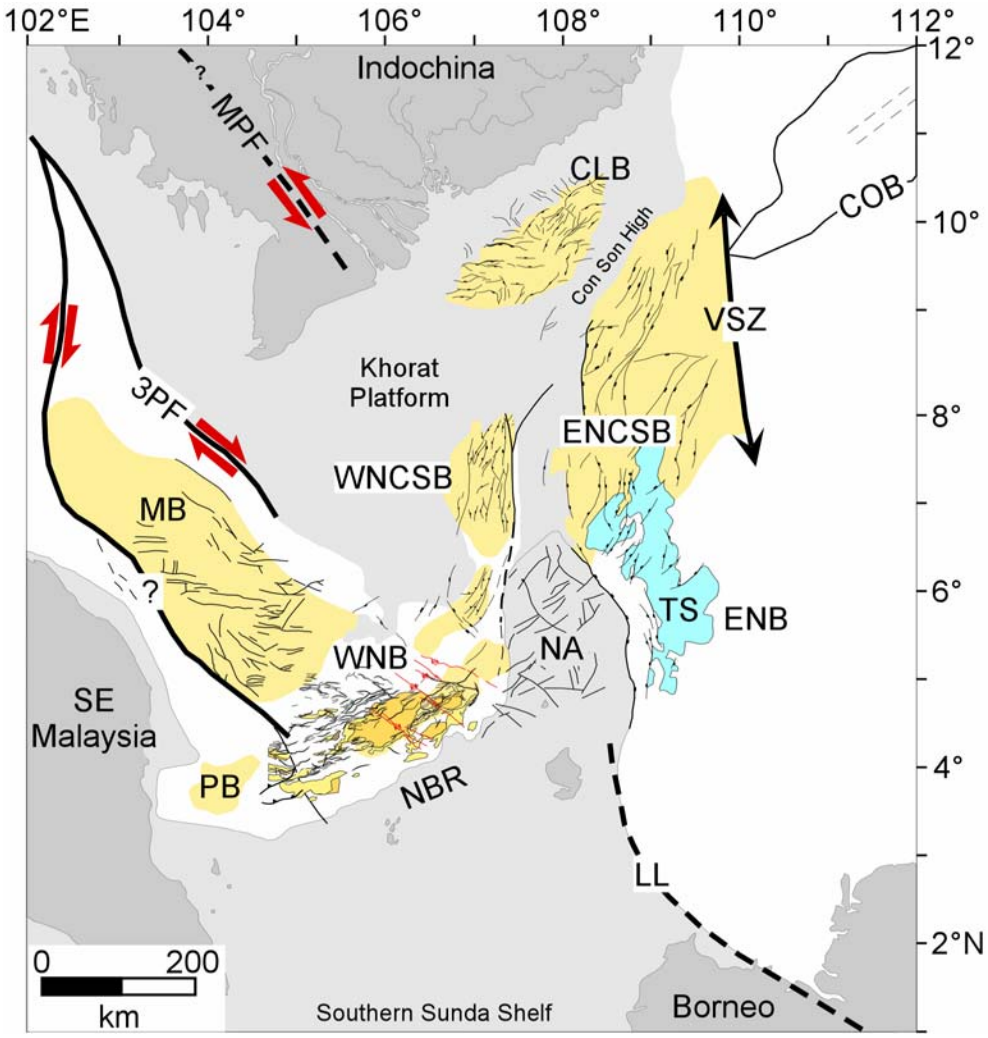


**Figure 2.3:** Regional map of SE Asia including basin locations and important regional highs. Regional strike-slip faults are shown in bold black lines. Faults are dashed where inferred. Major Tertiary depocenters are shown in yellow. Light blue highlights the Terumbu Shelf, which is a region of extensive carbonate sedimentation characterized by isolated carbonate platforms and pinnacle reefs. VSZ, Vietnam Shear Zone; ENCSB, East Nam Con Son Basin; WNCSB, West Nam Con Son Basin; CLB, Cuu Long Basin; NA, Natuna Arch; ENB, East Natuna Basin; WNB, West Natuna Basin; LL, Lupar Line; PB, Penyu Basin; MB, Malay Basin; MPF, Mae Ping Fault; 3PF, Three Pagodas Fault; COB, Continental-Oceanic Boundary. From Olson (2001).

inversion in the ENCSB behaved independently due to tectonic isolation resulting from the Vietnam Shear Zone and the Natuna Arch (Olson, 2001).

## STRATIGRAPHY

The deposits in the SCS are generally separated into syn-rift and post-rift strata (Lee et al., 2001). Tectonostratigraphic and lithostratigraphic information from Matthews et al. (1997) can be seen in Figure 2.4. As this study will focus on post-rift strata, syn-rift strata will not be discussed here.

Post-rift strata in the NCSB are composed of both carbonate and siliciclastic units. Carbonate deposition began in early Miocene time and continued through late Miocene time (Matthews et al., 1997). Matthews et al. (1997) separated the stratigraphy of the NCSB into ten units of Tertiary age (designated T10 to T100) and one Quaternary age unit (labeled Q10). Sequence T80 of Matthews et al. (1997) was deposited during early late Miocene time. Carbonate strata in the lower part of T80 primarily consist of isolated platform facies that were deposited on fault-bounded preexisting topographic highs (Matthews et al., 1997). A sea-level lowstand during T80 temporarily disrupted carbonate growth, which was reestablished as isolated buildups and pinnacle reefs (Matthews et al., 1997). Carbonate deposition was confined to the west NCSB during late Miocene time (Matthews et al., 1997).

Silicilastic deposition records a transition along the shelf in the western part of the study area from more terrestrial environments to marine environments (Matthews et

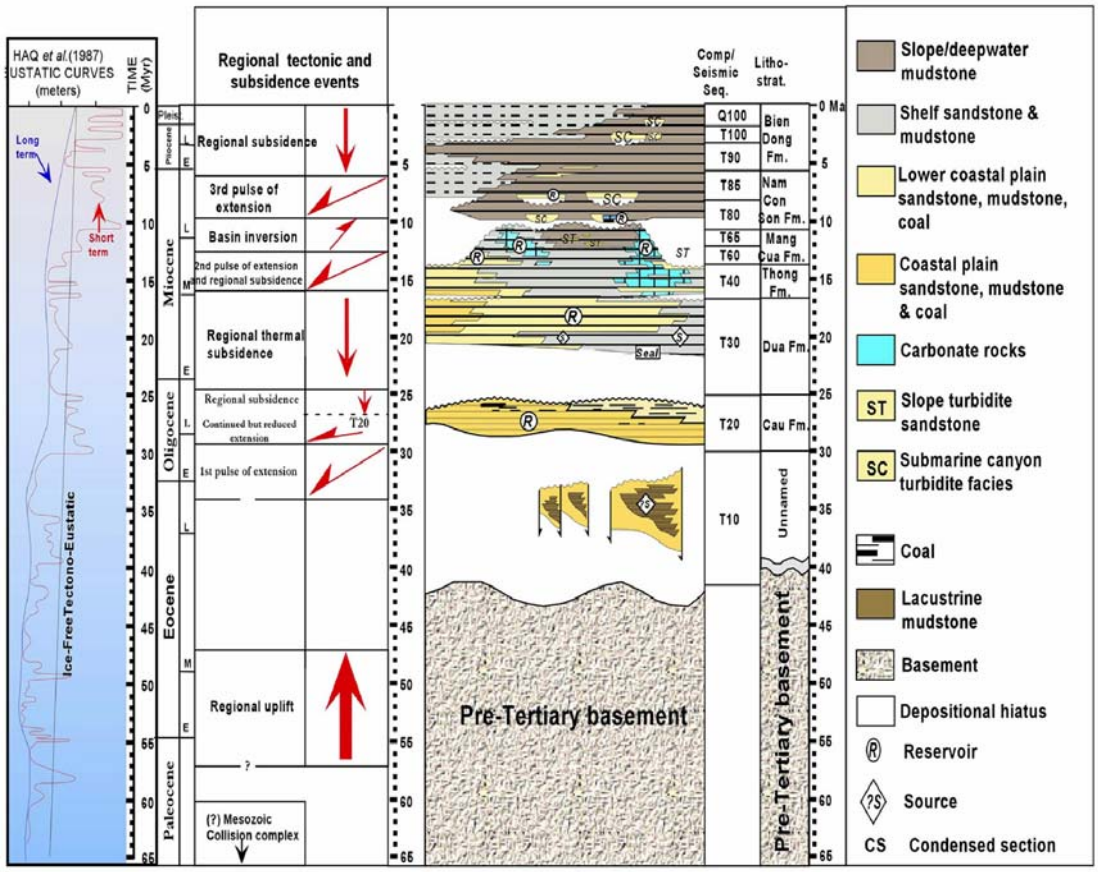


**Figure 2.4:** Nam Con Son Basin tectonostratigraphic summary (from Olson, 2001). Tectonstratigraphic and lithostratigraphic information from Matthews *et al.*(1997). Eusatic sea-level curves from Haq *et al.*(1987).

al., 1997; Lee et al., 2001). The oldest post-rift reflectors in the western NCSB are believed to represent marginal marine to shelf facies (Lee et al., 2001). Seafloor topography, created during renewed late Early to mid-Miocene rifting, controlled depositional environments. During late Early to mid-Miocene time, shelf siliciclastic deposition dominated in the east while carbonate deposition occurred in the west (Matthews et al., 1997). Sediment supply rates were outpaced by subsidence as evidenced by backstepping shelf edges during late Early to mid-Miocene (T40 through T60 interval of Matthews et al., 1997). Middle Miocene facies consist of shelf siliciclastic and carbonate facies with deeper water siliciclastics near the top of the section (T60 horizon of Matthews et al., 1997). During late Miocene time, clastic shelf deposition was confined to the southwest and deeper water mudstone and pelagic facies are found between carbonate buildups (Matthews et al., 1997). In the eastern and southern NCSB, late Miocene strata record the late phase of a second rifting episode, and are characterized by channels and channel-like features that form valley systems extending eastward into deeper water settings (Lee et al., 2001). Shelf siliciclastics prograded and supplied sediment to deep water environments via a system of canyons (Matthews et al., 1997). In the east, Upper Miocene deep water mudstone and local sandy turbidite facies surround carbonate buildups (Matthews et al., 1997). Shelf and slope siliciclastics with some carbonate facies characterize western deposits during late Miocene time (Matthews et al., 1997). Shelf siliciclastics and deepwater mudstone facies in the east characterize a basinward facies shift during early to late Pliocene time (Matthews et al., 1997). During late Pliocene time, western shelf siliciclastics prograded

eastward and transition to slope deposits in the east (Matthews et al., 1997). Pleistocene deposits in the west consist of eastward prograding shelf facies with intermittent subaeial exposure and flooding, while in the east, submarine fans record periods of erosion and bypass in the west (Matthews et al., 1997).

# CHAPTER III

# OBJECTIVES

This project focuses on developing a more detailed understanding of the stratigraphic relationships within the Pliocene to Recent succession in the Nam Con Son Basin, offshore Vietnam. The objectives of this project include:

1) Characterization of modern seafloor channel morphology and distribution on the shelf, slope and basin floor in areas dominated by clastic deposition in an effort to distinguish between fluvial channels, incised valley, slope channels, gullies, submarine canyons, turbidite channels, and basin floor channel-levee deposits, and to evaluate sediment dispersal pathways related to eustatic changes since the Last Glacial Maximum (LGM);
2) Description of the vertical and horizontal variations in seismic facies on the shelf, slope and basin floor in clastic dominated areas within the Pliocene to Recent strata (upper 2 seconds (TWT) of data) in an effort to interpret depositional facies (i.e., delta, shelf, slope fan, basin floor fan) and place these environments in a sequence stratigraphic framework;
3) Analysis of modern seafloor features (shelf edge and deltaic wedge) to determine the amount of subsidence since the Last Glacial Maximum (LGM);
4) Interpretation of changing sediment flux, tectonic regimes, and third-order eustatic fluctuations as recorded in the Pliocene-Recent interval in an effort to construct a detailed history of post-rift basin evolution, sediment flux

from the paleo-Mekong drainage, and influence of the East Asian monsoon on sedimentation.

Specific questions and hypotheses that this study can address include:

- How do the stratigraphic stacking patterns within the paleo-Mekong delta and shelf system vary temporally and spatially since Early Pliocene time?
- How do modern seafloor features relate to sea-level change since the LGM?
- How do changes in the stratigraphic stacking patterns record changes in accommodation space due to tectonics, third-order eustatic changes, climatic changes, and changing sediment flux into the NCSB during Pliocene to Recent time?
- Can changes in sediment flux from SE Asia be ascertained with this data set and can this record be used as a proxy for evaluating uplift of the eastern Tibetan Plateau and evolution of the East Asian monsoon since Early Pliocene time?

# CHAPTER IV

# DATA, METHODS AND DATA QUALITY

## DATA

The data consist of approximately 9,320 line kilometers of 2D, post-stack, depth-migrated seismic data, donated by ConocoPhillips, that cover an area of ~37,000 $km^2$ located southeast of the modern Mekong Delta (Figure 4.1). Nine well logs with limited biostratigraphic and chronostratigraphic picks are also available within the dataset. Twelve wells have been time-depth converted and there is one well in the south with well log data. Additional lithologic and facies information are available in scientific literature on the NCSB.

## METHODS

Detailed mapping of the modern seafloor was completed using SeisWorks$_{TM}$, seismic interpretation software from Landmark Graphics Corporation. Channels were identified based on characteristics outlined by Murray and Dorobek (2004). Depositional facies maps were constructed using depositional features recognizable in the seismic data along with locations of fluvial channels, incised valleys, canyons and turbidite channels in order to evaluate sediment dispersal since the Last Glacial Maximum (LGM). These data were used to investigate the areal extent and distribution of LGM shelf, slope and basin floor channels, which aid in understanding: 1) the regional distribution and nature of sediment dispersal systems and 2) the ultimate sites of

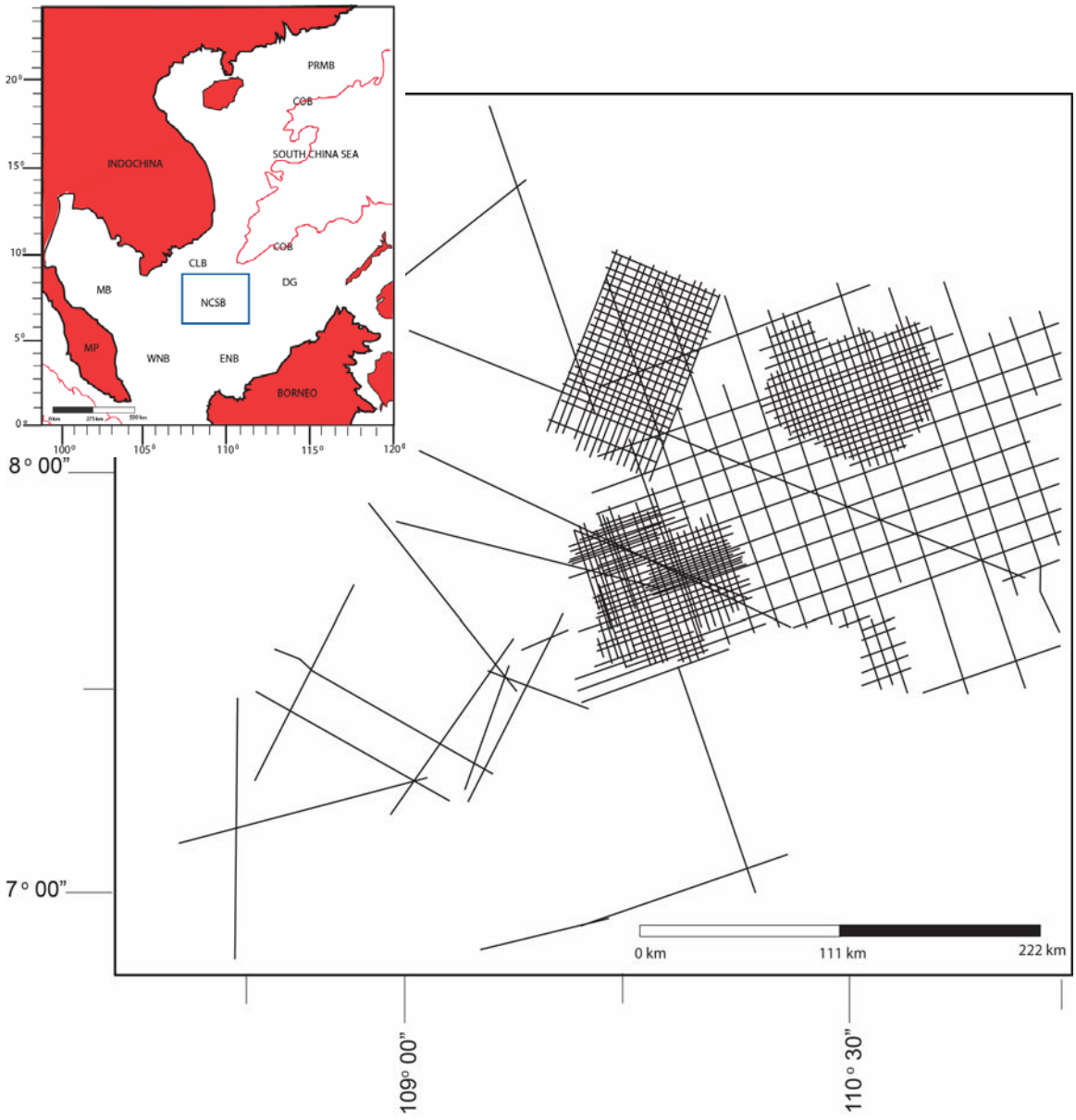


**Figure 4.1:** Map of available seismic profiles in the data set. Small inset map in upper left corner shows the study area (outlined in blue). NCSB, Nam Con Son Basin; CLB, Cuu Long Basin; MB, Malay Basin; WNB, West Natuna Basin; ENB, East Natuna Basin; MP Malay Peninsula; DG, Dangerous Grounds; COB, Continent-Ocean Boundary. The location of the basemap has been shifted 10 km in an unspecified direction in order to protect proprietary interests. Modified from Huchon et al. (1998).

sediment accumulation. Sediment accumulation can be determined by identifying features such as deltas, slope fans and basin floor fans. Delta, shelf edge, slope fan, and basin floor fan deposits can be distinguished by geometry and internal seismic facies. Incisions were identified based on morphology, size and geographic distribution following the definitions of Normark et al. (2003) and characteristics outlined by Murray and Dorobek (2004). Width was measured from levee crest to levee crest and depth from levee crest to the maximum depth to channel base for each basin floor incision. Channel measurement data can be found in Appendix A. Reflector geometry, seismic facies, and depositional facies were interpreted based on descriptions of Mitchum et al. (1977).

The southwestern LGM shelf margin of the SCS within the NCSB was investigated in terms of thickness and present-day water depth (Figure 4.2). Water depth was measured by estimating the depth in milliseconds of the seafloor reflector. A seismic wave velocity of 1500 m/sec was used to determine water depth in meters. Thickness was measured for both the LGM shelf edge and shelf-edge delta by estimating depth values in milliseconds. Velocities used for stratal thickness measurements were obtained from the closest well with available data. The velocity data and calculations are included in Appendix A.

A series of asymmetrical ridges were observed at the seafloor in the southern part of the southwestern SCS shelf margin (Figure 4.3). Width and depth measurements were taken for approximately thirty ridges over a random ~5 km distance to obtain representative depth and width values. Width was measured in meters from crest to crest

between adjacent ridges. Ridge height was measured in milliseconds from the top of the crest to the base of the adjacent trough. This measurement was then converted to meters using a seismic wave velocity of 1500 m/sec.

The dataset includes dip-trending and oblique-to-shelf-trending seismic profiles of the Pliocene-Recent stratigraphic succession of offshore Vietnam, which allow for analysis of regional stratigraphic relationships. Wells in the study area penetrate the

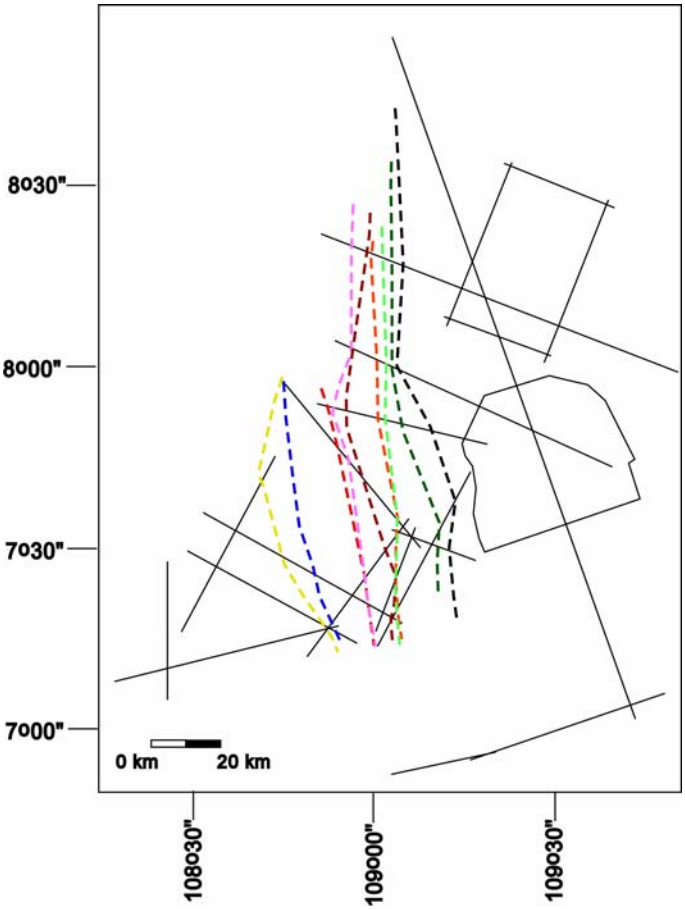


**Figure 4.2:** Thickness and present-day water depth of shelf margin deposits were measured near the LGM shelf edge (approximate location marked with black dashed line). This illustration also depicts the progradation of the shelf edge during Pliocene to Recent time.

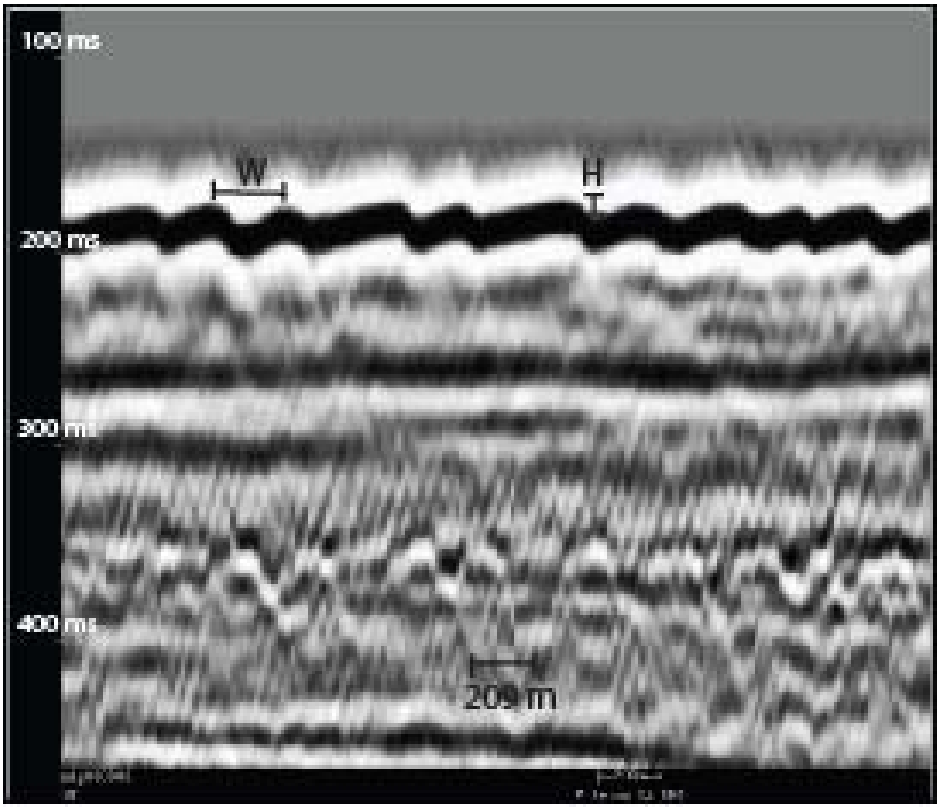


**Figure 4.3:** Asymmetrical seafloor ridges. W: Width measurements were taken between successive ridge crests. H: Depth/height measurements were taken from the top of the ridge crest to the base of the adjacent trough. The left side of the image is toward the west.

upper 2.5 seconds (TWT) of seismic data and well data include “picks” of key stratigraphic horizons within the study area. The youngest stratigraphic pick is early Pliocene in age and is found at roughly 2.5 seconds, above the Mid-Miocene Unconformity, which is a regionally recognizable unconformity across the study area (Matthews et al., 1997). The upper 2.0 seconds, which includes the entire Pliocene to Recent interval, has only limited age control from wells and previous studies.

Key stratigraphic boundaries were identified based on seismic facies and patterns of reflector terminations (onlap, downlap, and erosional truncation). Several regional chronostratigraphic markers are observable within the NCSB and were mapped across the study area. These picks were compared to previous studies which identified similar stratigraphic units (Matthews et al., 1997; Lee et al., 2001; Murray, 2003).The mid-Miocene unconformity (MMU) is a regional unconformity formed during a time of tectonic inversion and sea-level fall. The MMU is recognized across many parts of the SCS, except in deep-water settings or areas that underwent insignificant inversion (Murray, 2003). The MMU was recognizable as an angular unconformity located at ~2000 to 3000 ms and was mapped across the study area. Reflectors identified as “top Pliocene” and “top late Pleistocene” by Murray (2003) based on well reports were identified and mapped across the study area. These two horizons were used to constrain age assignments when correlating sequence boundaries with published sea-level curves.

Sequence boundaries were identified based on fluvial incision on the shelf, incision at the shelf edge, overall internal reflector geometry, and the nature of slope and

basin floor seismic facies. These sequence boundaries were then correlated across the study area to establish possible relationships between observed stratigraphic patterns and eustatic sea-level fluctuations. Stratal stacking patterns were used to investigate: 1) the patterns and importance of thickness variations across the shelf and shelf edge; 2) whether the shelf edge/paleo-Mekong delta vary in location, geometry and internal seismic facies, both temporally and spatially, since early Pliocene time, and 3) whether these variations record changes in tectonic subsidence and eustatic change. Lowstand Systems Tract and Highstand Systems Tract strata were identified based on reflector terminations and comparison with published stratigraphic models of Van Wagoner (1990) in an effort to evaluate the changing response of sediment deposition over Pliocene to Recent time.

Sequence boundaries and related sequences were described in detail and compared with sea-level curves of Worndardt et al. (2001) and Haq et al. (1987). The number of sequence boundaries and magnitude of sea-level fall was more closely correlatable with the curves of Worndardt et al. (2001), thus, the Wornardt curve was used to assign ages to the interpreted sequence boundaries in this study. The “top Pliocene” and “top lower Pleistocene” horizons identified by Murray (2003) were used to help constrain ages.

Isopach maps were constructed along the shelf and shelf edge for each sequence using MapIt!, a mapping application within SeisWorks$_{TM,}$ by computing gridded contours. Maps were constructed within a work session in depth utilizing the velocity model within the project to determine thickness in meters. A mapping file was first

constructed based on a mapped horizon. The gridding option builds a matrix of nodes and searches the mapping file for shot line points and control points that fall within a specified radius of each node. The program then computes an averaged z value for the node and weighs the z values of map points according to proximity to the node. The grid interval (distance between nodes) used was 6000 m in both the x and y direction, which is approximately one half the average distance between seismic line locations. The search radius around nodes was 50000 m, which is slightly larger than the maximum distance between seismic lines. The location of the terminal shelf edge and shelf-edge thickness were recorded for each sequence in the thickest part of the shelf edge on each line. The location of the terminal shelf edge for each sequence was identified by the point of maximum change in clinoform angle and was overlain on the isopach maps to evaluate shelf edge thickness accumulations. These isopach maps and thickness measurements were used to evaluate changes in sediment thickness and shifts in sediment accumulation on the shelf and at the shelf edge over time. Limited data and wide line spacing make features outside the limits of the data speculative in that they may not represent true geologic structures or depositional features. Thickness variations within the data limits are useful, however, for examining thickness trends along the shelf and shelf edge.

## DATA QUALITY

Data quality issues posed significant challenges in addressing the objectives. While two more tightly spaced seismic grids record basin floor deposition, the shelf area

is only imaged by a limited number of seismic lines that are very widely spaced. This made correlation of sequence boundaries along the shelf difficult because of inadequate cross-lines to check ties. The northern part of the shelf is thickened compared to the southern shelf so that the character of stratigraphic patterns varies making verification using cross-ties important. Additionally, data were lacking in several key areas where additional data would have strengthened identification of sequence boundaries. In several key locations, shelf lines ended just updip of the shelf edge making it more difficult to assign particular horizons as sequence boundaries.

In addition, three different migration schemes were used throughout the data set, making it difficult to correlate between lines that were migrated differently. Data quality was also poor in many parts of the study area. Throughout the data set, seismic quality decreased drastically with depth and seismic character became extremely noisy and "washed out". Multiples overprinted the data in many areas, cutting through key intervals in terms of sequence boundary identification. Syn-depositional slope failure and slumping is common at the shelf edge and in basinal areas over mid- to late-Miocene highs, which further complicates stratigraphic correlations. Gas charged sediments are common in the study area and are observed on seismic profiles within the data set. Much of the basin floor data is washed out and cut by multiples, making meaningful detailed seismic facies analysis impossible.

# CHAPTER V

# STRATIGRAPHY

## INTRODUCTION

The SCS is a region of significant importance in terms of the records of SE Asian tectonics, including Tibetan Plateau uplift, and the onset and evolution of the East Asian monsoon. The Mekong River has headwaters on the eastern Tibetan Plateau and has been a significant source of sediment to the southwestern SCS since at least late Miocene time (Murray and Dorobek, 2004). Increased understanding of the Pliocene to Recent stratigraphy of the Mekong point source and associated shelf-edge deposits will be useful in understanding changes in accommodation, sea level, and sediment supply. These changes might then be used to interpret the long-term history of basin evolution in the NCSB.

Seismic facies and reflector geometry were characterized across the Pliocene to Recent shelf edge in order to evaluate depositional environments and to identify sequence boundaries (Figure 5.1). Deposition during Pliocene to Recent time was dominated by sediment input from two fluvio-deltaic systems; one depositing along the Pliocene to Recent shelf edge in the northern part of the study area and a second in the south. Nine third-order sequence boundaries were identified on the basis of updip fluvial incision and the geometry of underlying and overlying reflectors. Third-order sequence boundaries and the associated sequences are labeled with Arabic numbers (i.e. 1, 2, 3). Pliocene sequence boundaries are designated with “P” and Pleistocene sequence

boundaries with “PL” immediately before Arabic numerals (i.e. P1, P2, PL 1, PL2). Results from this study are useful in evaluating the history of sea-level change, sediment fill patterns and subsidence in the NCSB during Pliocene to Recent time.

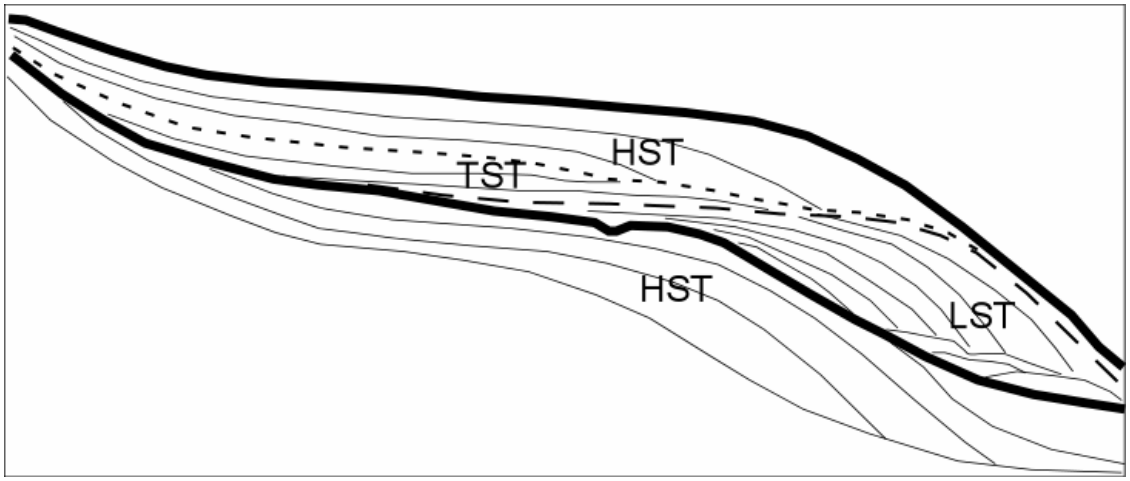


**Figure 5.1:** Idealized conceptual model of systems tracts and sequence boundaries. Bold solid line represents a sequence boundary; Small dash indicates a maximum flooding surface; Large dash indicates a tansgressive surface. LST-Lowstand Systems Tract; TST-Transgressive Systems Tract; HST-Highstand Systems Tract. (After Van Wagoner, 1990).

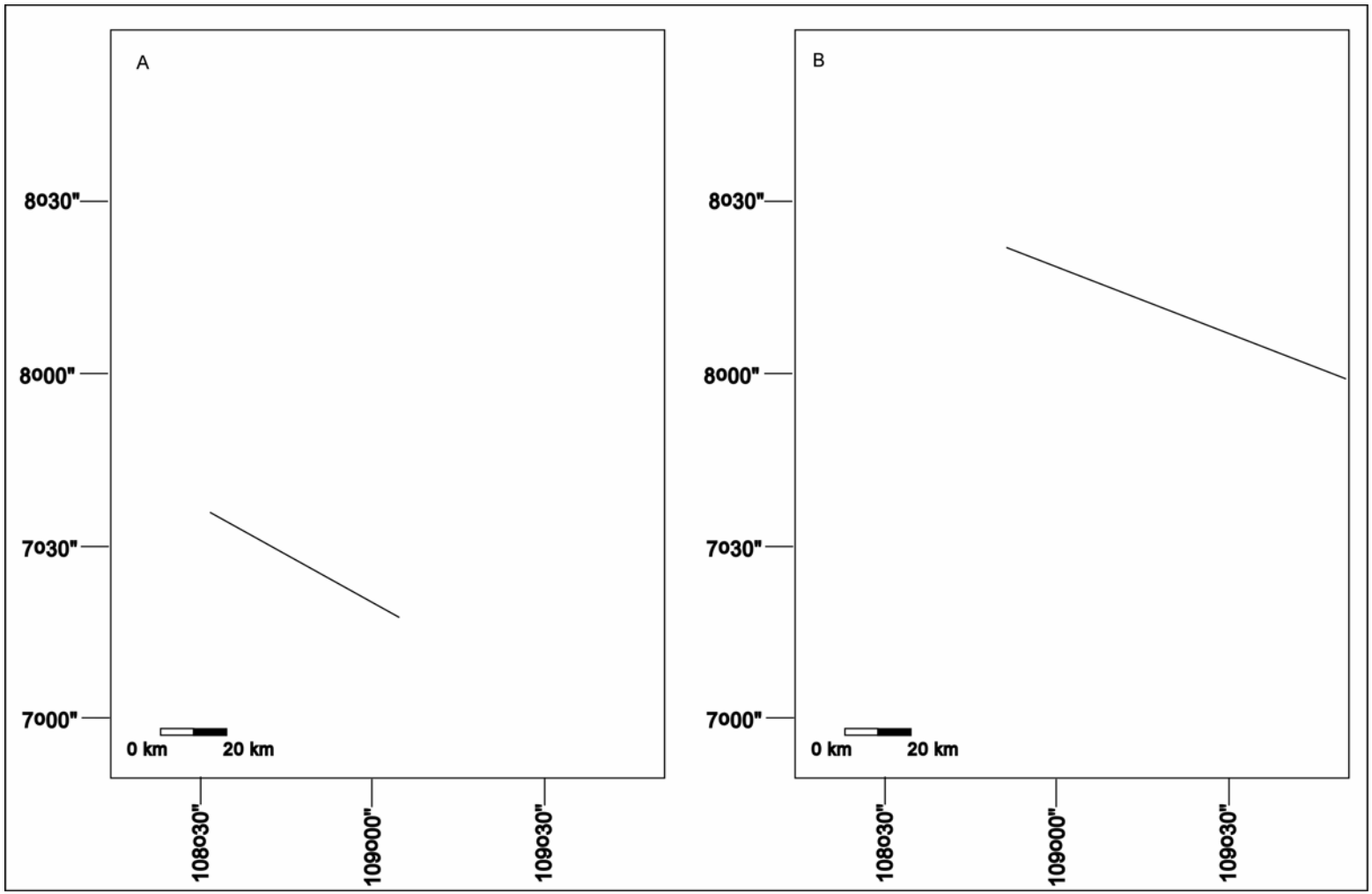


**Figure 5.2**: Base map showing locations of seismic profiles in Figures 5.3, 5.4, 5.5, and 5.6 A) Basemap for figures 5.3 and 5.4 from the southern part of the study area. B) Basemap for figures 5.5 and 5.6 from the north.

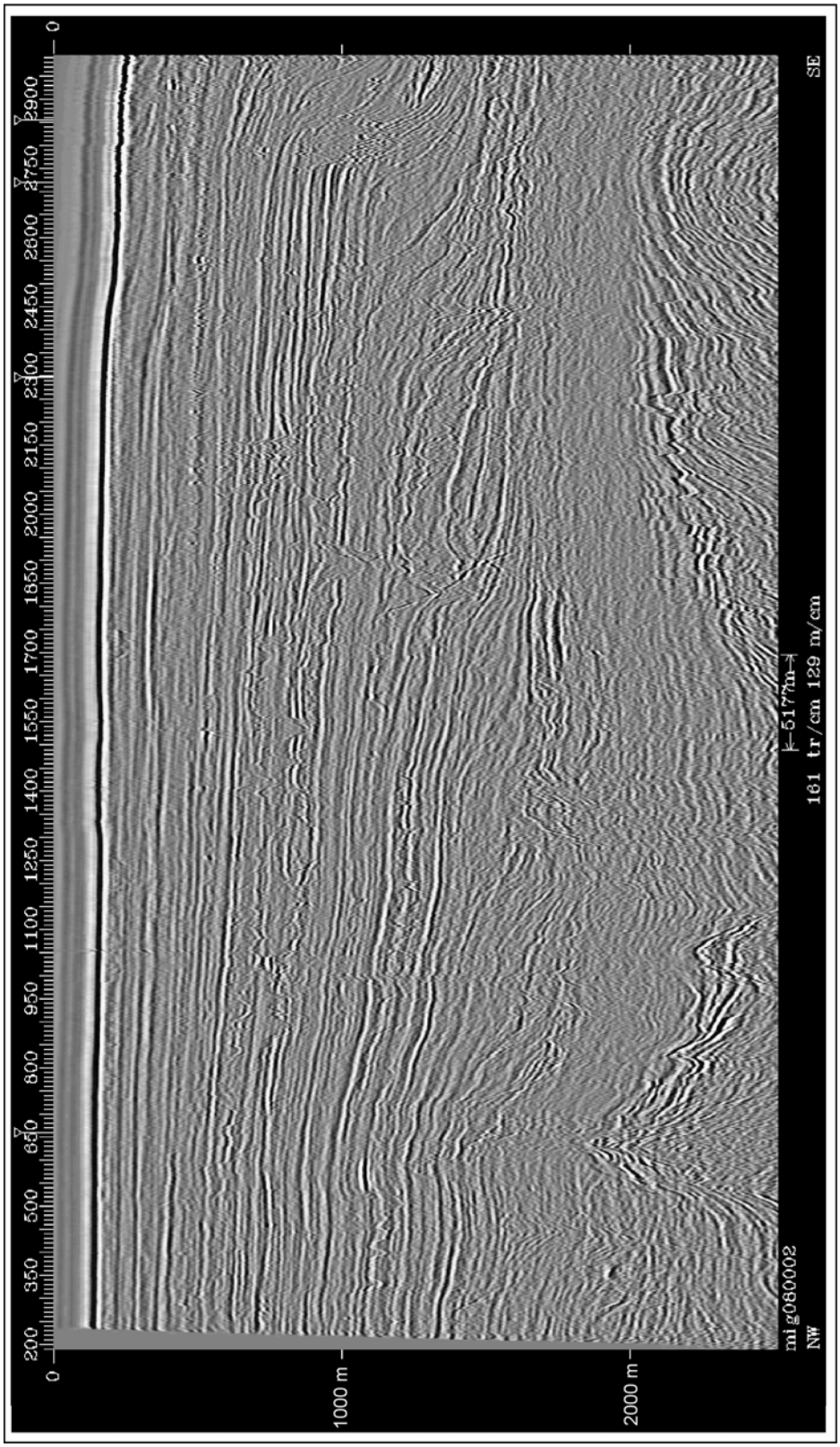


**Figure 5.3**: Uniterpreted seismic profile from the southern part of the study area.

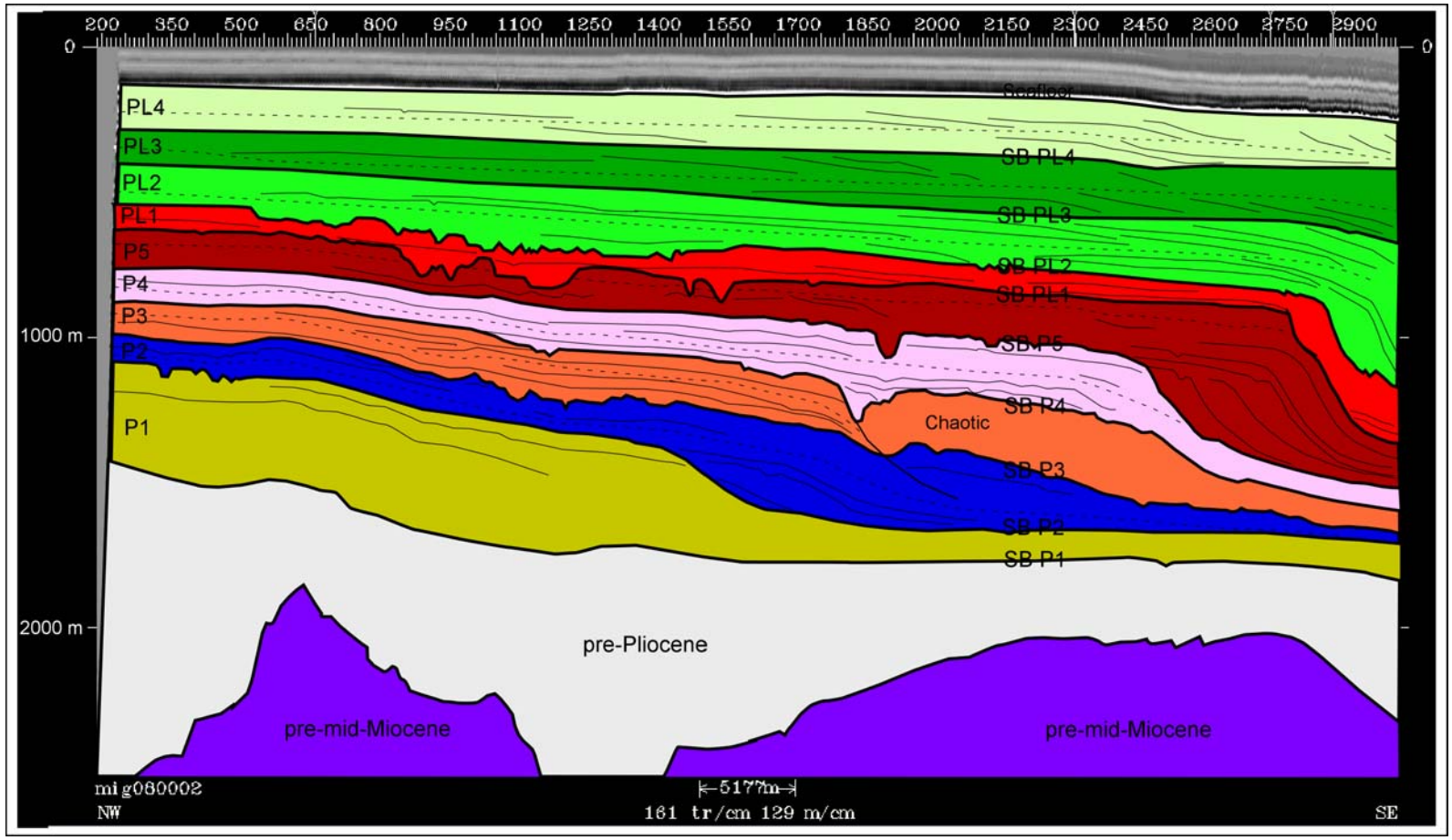


**Figure 5.4**: Line drawing based on the previous seismic profile. The nine sequence boundaries and associated sequences are shown. Thick black lines denote sequence boundaries. Dashed black lines denote the observed boundary between the LST and HST deposits. Thin solid black lines show the internal geometry of some reflectors

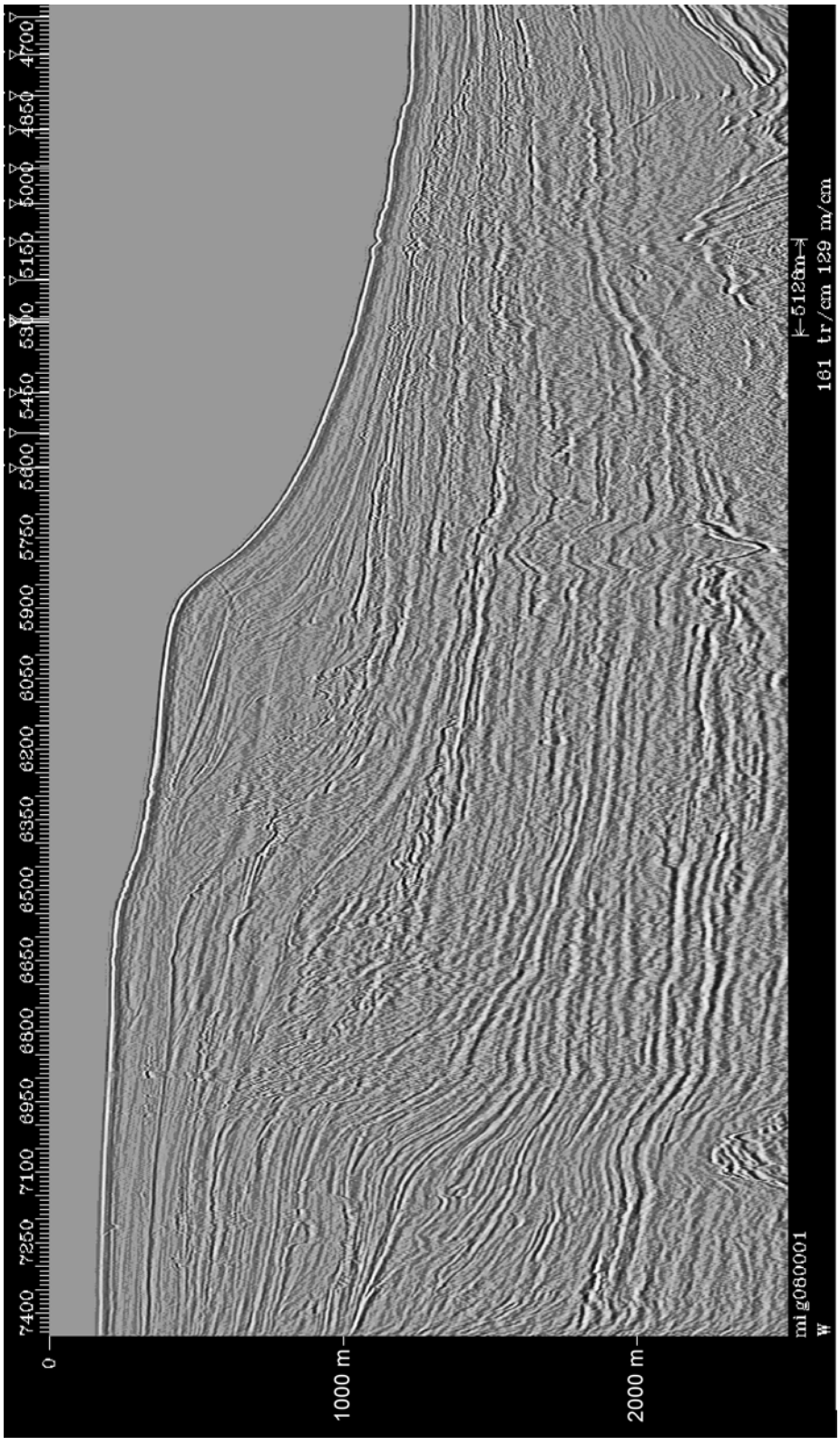


**Figure 5.5**: Uniterpreted seismic profile from the northern part of the study area.

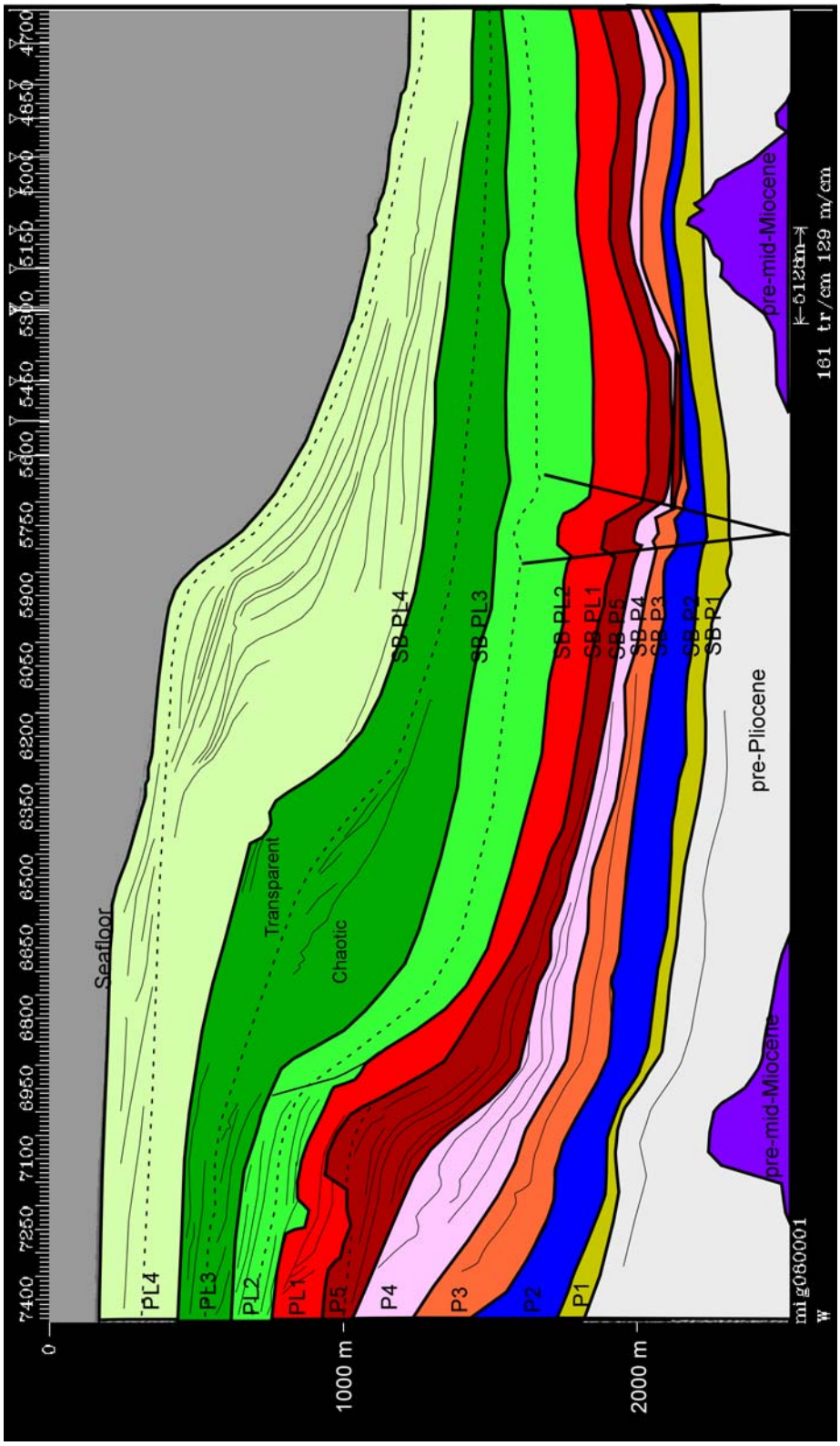


**Figure 5.6**: Line drawing based on the northern seismic profile shown in previous figure. The nine sequence boundaries and associated sequences are shown. Thick black lines denote sequence boundaries. Dashed black lines denote the observed boundary between the LST and HST deposits. Thin solid black lines show the internal geometry of some reflectors

# OBSERVATIONS

Nine sequence boundaries are recognized in the NCSB within Pliocene to Recent strata and divide the stratigraphy into nine third-order depositional sequences (Figures 5.2 through 5.6). The character of shelf-edge deposits within sequences P1, P2, P3, and P4 is best observed in the central and southern parts of the study area because the shelf edge is not observed within these sequences in the north. It is assumed that the shelf edge is located outside the limits of available data and Sequences P1 through P4 are represented by deep-water deposits in the north. Sequences thin updip and downdip of the shelf edge, which is recognized by an abrupt increase in reflector dip angle to > $1^{o}$. Two main thickness accumulations, one in the central to northern part of the study area and one in the south, are recognized along the Pliocene to Recent shelf edge based on isopach maps generated for each sequence using MapIt!$_{TM}$, a gridding and contouring application within SeisWorks$_{TM}$.

## Seismic Facies

Six seismic facies are observed within the Pliocene to Recent strata in the western part of the study area: 1) channelized facies, 2) prograding clinoform wedge facies, 3) shingled clinoform facies, 4) parallel to sub-parallel facies, 5) transparent facies, and 6) chaotic facies (Figures 5.7 and 5.8). Gas washout and multiples obscure the seismic facies in some parts of the study area so facies must be studied with care.

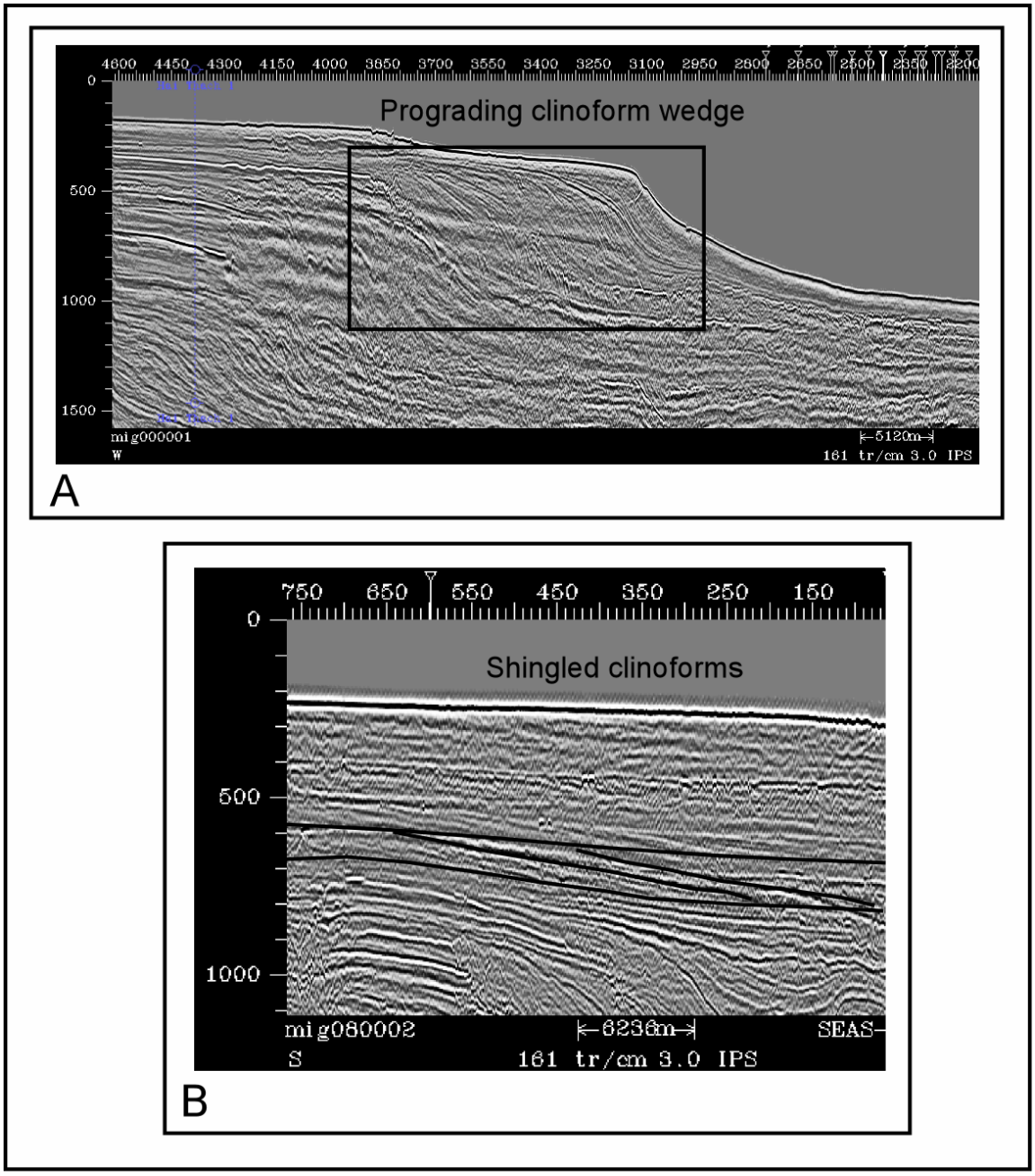


**Figure 5.7:** Characteristic prograding clinoform and shingled clinoform seismic facies observed within the study area. A) Prograding clinoform wedge facies is characterized by steep clinoforms and is generally found near the shelf edge. Black box outlines typical reflector pattern. B) Shingled clinoform facies is observable in the central part of this dip-trending seismic profile. Nearly horizontal, solid black lines mark the boundary of the facies example. Dipping solid black lines show the dip of internal reflectors.

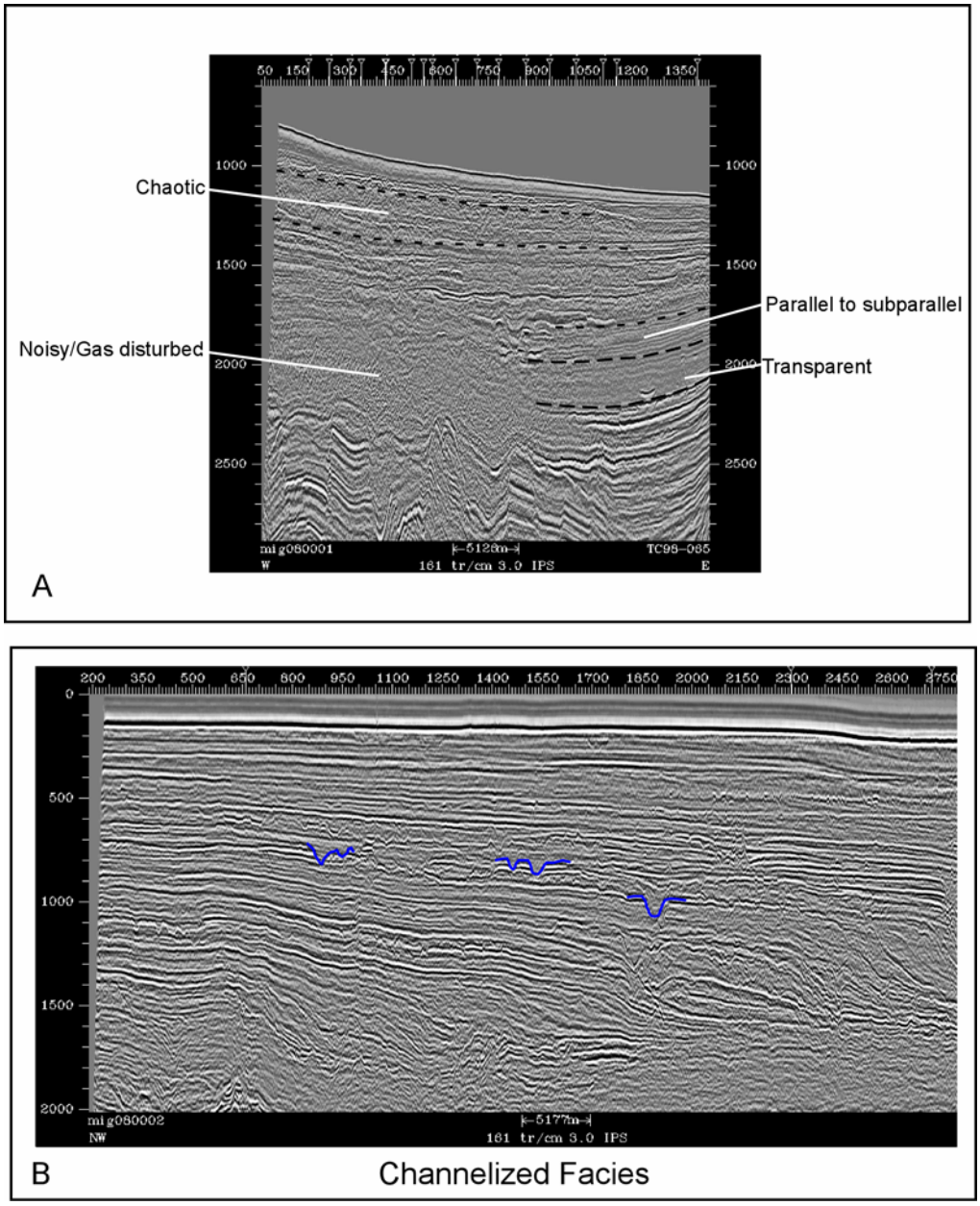


**Figure 5.8:** Characteristic seismic facies observed within the study area. A) Seismic profile located downdip of the shelf edge shows characteristic examples of chaotic, parallel to sub-parallel, and transparent seismic facies. Dash lines mark the boundaries of each facies. An example of noisy or gas disturbed reflectors is also shown. B) Typical example of channelized seismic facies. Several channels have been outlined in blue.

*Channelized Facies*

Channelized facies within Pliocene to Recent strata are typically found along sequence boundaries (SB) and indicate areas that have been incised. Individual incisions observed in this data set range in size from ~90 m to ~3 km wide and <10 m to ~200 m deep. Morphology of channels varies and includes v-shaped, u-shaped, flat-bottomed, and irregular. Channel types include fluvial channels, shelf margin incised valleys and canyons, slope channels and basin floor channels. Criteria for recognition of channels within Neogene strata of the southwestern SCS were outlined by Murray and Dorobek (2004). The channelized facies is recognized on seismic profiles by at least one of the following: observation of individual channels; incision into underlying generally continuous reflectors; abrupt changes in reflector amplitude; and chaotic channel fill.

*Prograding Clinoform Wedge Facies*

The prograding clinoform wedge facies is characterized by large-scale (> 200 ms) clinoforms. The general character of seismic reflector amplitude ranges from low to high, reflector continuity is generally moderate to high. This facies is interpreted to represent deposition near the shelf edge. This facies is often cut by shelf-edge faults, or overprinted by multiples and gas washout.

*Shingled Clinoform Facies*

The shingled clinoform facies is composed of shingled clinoforms less than about 100 ms thick. Reflectors within this facies downlap onto the upper bounding surface of

underlying layers. Reflectors are often erosionally truncated at the top of the interval. Seismic amplitude varies from low to high and reflector continuity is generally moderate to high. This facies represents deposition in shallow marine and shelf delta settings.

*Parallel to Sub-parallel Facies*

This seismic facies is typified by laterally continuous, sub-horizontal to gently seaward-dipping reflectors. This facies is observed within the study area both updip and down dip of the shelf edge. In updip reaches this seismic facies is characterized by moderate to high amplitude, very continuous reflectors interpreted to record deposition in inner-shelf environments. This facies is also observed in deep-water environments in the eastern part of the study area. Here reflector continuity is high and seismic amplitude varies from low to high.

*Transparent Facies*

Extremely low seismic amplitude characterizes the transparent facies. Reflector continuity is ranges from moderate to high, but is often indistinguishable due to low seismic amplitude. Transparent facies are primarily observed in basin floor settings, but are also recognized within the shelf edge wedge.

*Chaotic Facies*

Reflector amplitude in the chaotic facies is generally moderate to high, whereas reflector continuity is extremely low. Chaotic facies are generally recognized on the basin floor, at the toe-of-slope, and as channel fill deposits.

**Sequences**

*Sequence P1- early Pliocene*

Sequence P1 is latest Miocene to earliest Pliocene in age. The basal sequence boundary is ill defined due to poor data quality and limited data coverage. Updip regions of Sequence P1 are characterized by channelized and parallel/sub-parallel facies. Prograding clinoform wedge facies characterize the strata downdip and record shelf edge deposition. Seismic character of the prograding clinoform wedge facies within Sequence 1 is typically noisy. Thickness of this sequence varies from ~ 300 m to ~ 530 m at the thickest part of the prograding clinoform wedge facies and the direction of progradation is toward the southeast/east and north. Maximum thickness of prograding clinoform wedge facies is focused in the southwestern part of the study area immediately updip of the shelf edge (Figure 5.9). In more basinal areas, Sequence P1 is characterized by parallel/subparallel seismic facies that thin basinward to less than 100 ms (~ 130 m). LST and HST strata cannot be distinguished due to poor data quality.

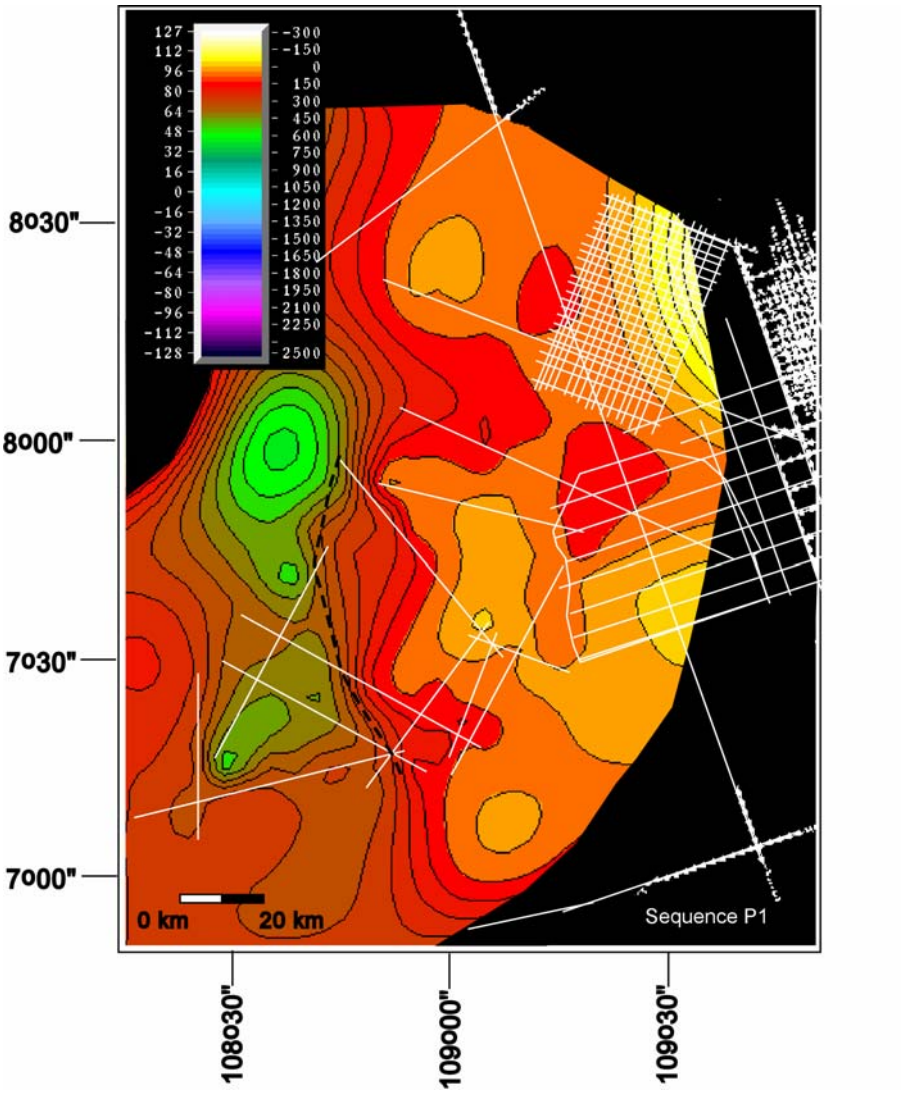


**Figure 5.9:** Isopach map of Sequence P1. Note the thickened shelf edge accumulation immediately updip of the shelf edge located in the southwestern portion of the study area. Scale bar is in meters. Contour interval is 50 m. The terminal shelf edge for Sequence P1 is identified by the black dashed line.

*Sequence P2-late Pliocene*

Sequence P2 is bounded at the base by Sequence Boundary (SB) P2. SB P2 is recognized by up-dip fluvial incision, shelf edge incision and overlying reflectors that onlap up-dip. SB P2 incised into underlying Sequence P1 near the shelf edge in the central part of the study area. This incision is u-shaped ~700 m wide and ~110 m deep, and is interpreted to be a shelf edge canyon or incised valley. The LST and HST are observed as relatively thin system tracts within this sequence. Both the LST and HST are characterized by parallel/sub-parallel seismic facies with gently seaward dipping reflectors. Channelized facies also comprise the HST. Truncation of the LST reflectors by the overlying HST marks the boundary between the two and represents the TST. Most of the HST has been removed from the shelf and shelf edge by subsequent incision and reworking. Slope deposits are characterized by chaotic facies or faulted and deformed parallel facies. Thick accumulations of prograding clinoform wedge facies are located in the central and southern regions of the study area (Figure 5.10). Down dip of the shelf edge, basin floor deposits are composed of parallel/sub-parallel and chaotic to transparent seismic facies.

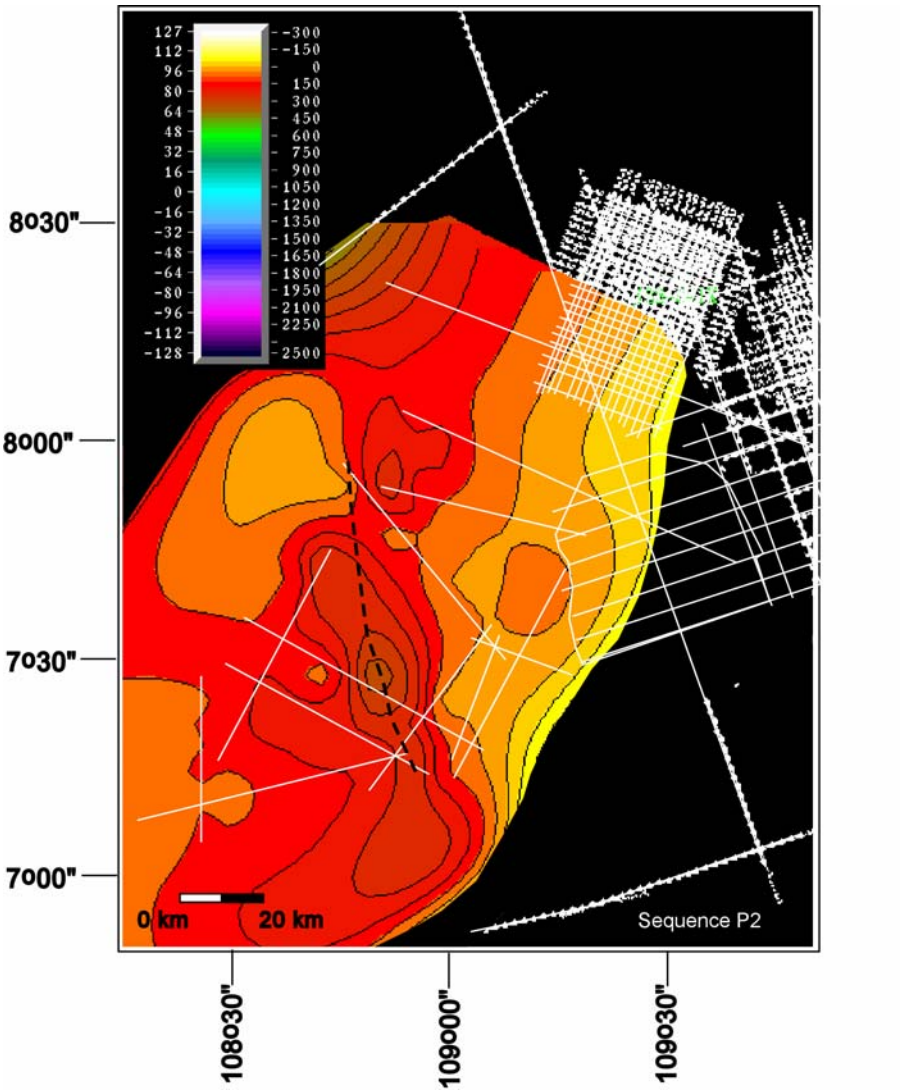


**Figure 5.10:** Isopach map of Sequence P2. Note the thickened shelf edge accumulations located in the central and southern portion of the study area at or immediately downdip of the terminal shelf edge. Scale bar is in meters. Contour interval is 50 m The location of the terminal shelf edge is identified by the black dashed line.

*Sequence P3-late Pliocene*

SB P3 is the basal bounding surface for Sequence P3. SB P3 truncates the underlying HST of Sequence P2 and is recognized by up-dip fluvial incision and overlying reflectors that onlap up-dip. Updip deposits are characterized by parallel/sub-parallel seismic facies. Prograding clinoform wedge (PCW) seismic facies is observed downdip. The sequence averages ~ 300 m thick within the PCW facies (Figure 5.7).

LST deposits are recognized as a parallel/sub-parallel seismic facies interval that onlaps the SB updip. Downdip the LST is observed as shingled clinoform seismic facies that downlap onto SB P3. The HST is observed as parallel/sub-parallel seismic facies that truncate reflectors of the underlying LST and is incised by the subsequent SB. In the south, the shelf edge is faulted and the shelf edge deposits within the LST and HST is characteristically deformed internally indicating shelf edge failure. The isopach map produced for this sequence shows a thickness accumulation in the central part of the study area immediately updip from the terminal shelf edge (Figure 5.11).

*Sequence P4-late Pliocene*

Sequence P4 is bounded by SB P4 at the base and SB P5 at the top of the sequence. SB P4 is recognized by up-dip fluvial incision, erosional truncation of underlying reflectors, and overlying reflectors that onlap SB P4 in updip parts of the study area. Both LST and HST are recognized in this sequence. The LST is characterized by shingled clinoform seismic facies with reflectors that downlap onto SB

P4 and are truncated by the overlying HST. The HST is typified by parallel-subparallel facies and reflectors that gently dip seaward.

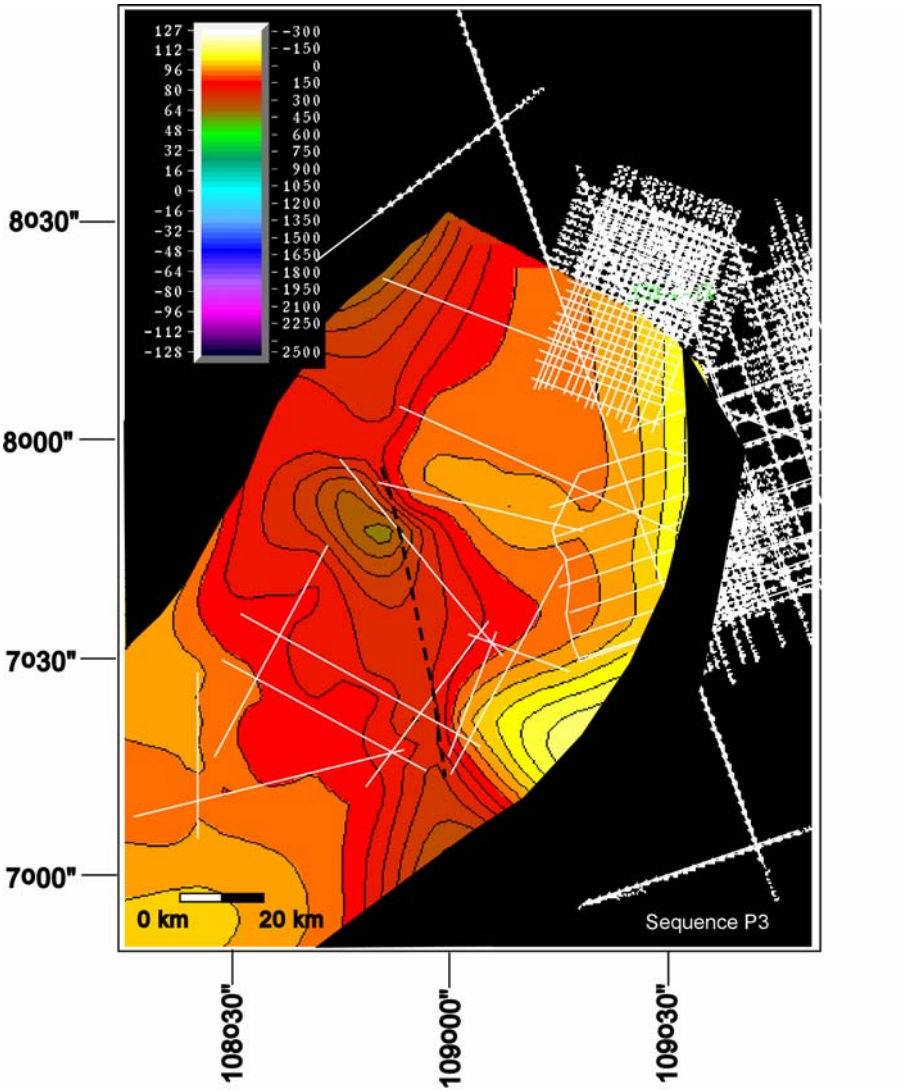


**Figure 5.11:** Isopach map of Sequence P3. Note the thickness accumulation immediately updip from the terminal shelf edge near the central portion of the study area. Scale bar is in meters. Contour interval is 50 m. The terminal shelf edge is identified by the black dashed line.

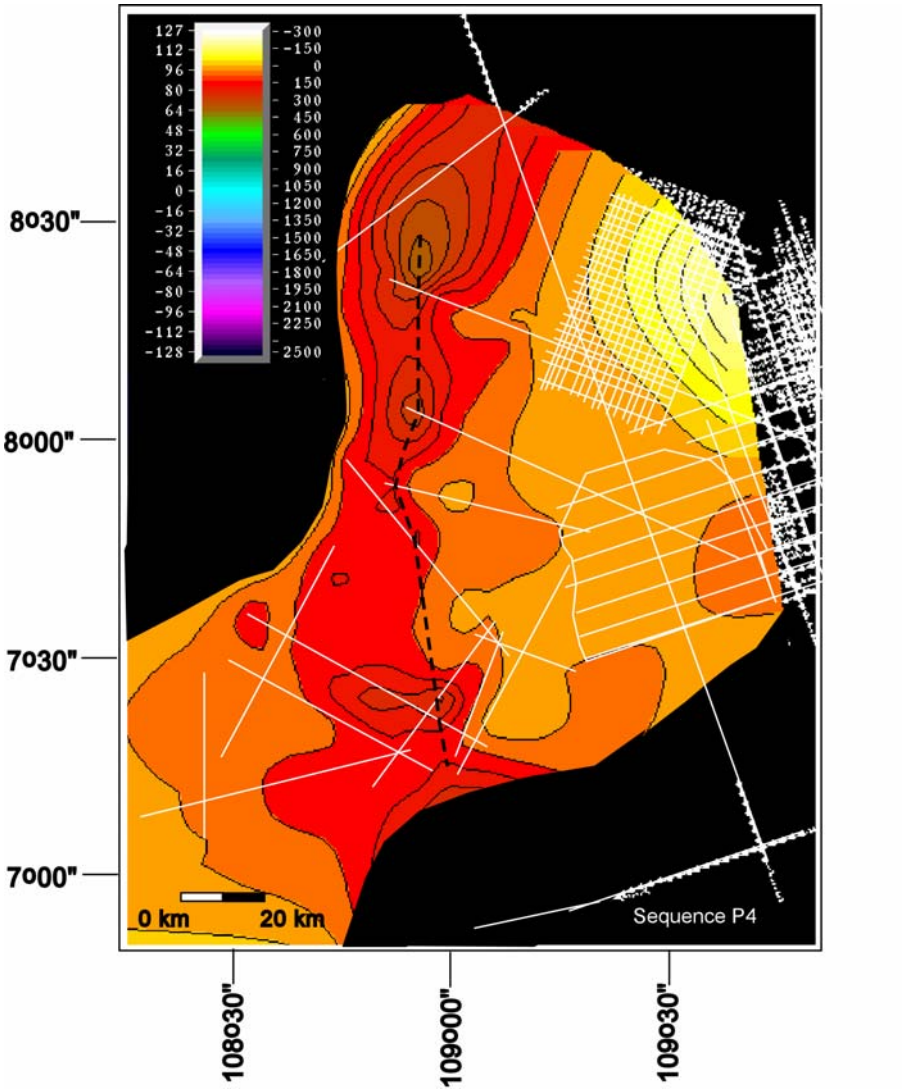


**Figure 5.12:** Isopach map of Sequence P4. Thickness accumulations are recognized in northern and southern parts of the study area. The location of the northern accumulation is coincident with the terminal shelf edge, while the southern accumulation is located immediately updip from the shelf edge. Scale bar is in meters. Contour interval is 50 m. The terminal shelf edge is identified by the black dashed line.

The HST is erosionally truncated and incised by SB P5. Downdip the sequence is characterized by PCW facies, which interpreted as the shelf edge. Thickness averages ~300 m in the PCW facies across the southern and central regions of the study area. Two thickness accumulations are observed along trend with the shelf edge (Figure 5.12). Basin floor strata range from chaotic to transparent in seismic facies character.

*Sequence P5-late Pliocene*

Sequence P5 is characterized by prograding clinoform wedge facies at the shelf edge. The basal sequence boundary for the interval is SB P5, which is recognized by downstepping and onlapping reflectors at the shelf edge within the overlying strata. SB P5 is deeply incised near the shelf edge and farther updip on the shelf. Major incisions near the shelf edge have a maximum incised depth equal to the depth of onlapping reflectors at the shelf edge (Figure 5.13). Updip regions of this sequence are composed of parallel/sub-parallel and channelized facies. The LST is recognized by downstepping reflectors within the PCW facies that onlap SB P5 indicating sea-level fall below the previous shelf edge. Shelf margin reflectors are progradational and become aggradational up-section. Downdip from the shelf edge, seismic facies within Sequence P5 is chaotic, parallel/sub-parallel or transparent. This sequence is commonly gas disturbed within basin floor deposits. The HST of Sequence P5 is characterized by parallel/sub-parallel and channelized facies, which are generally thin and erosionally truncated.

Maximum thickness for Sequence P5 is coincident with the shelf margin. The northern and southern depocenters described previously are observed during this interval (Figure 5.14). Thicker regions of PCW facies are observed at the shelf edge in both the northern and southern parts of the study area. Shelf edge failure is observed in the south.

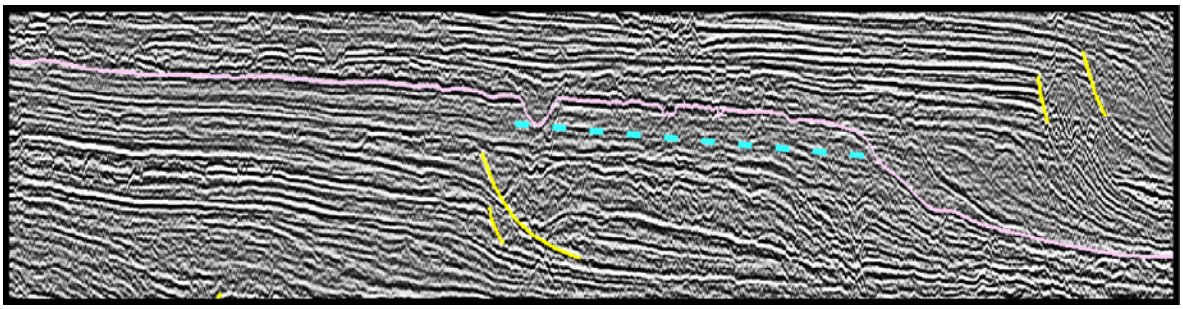

**Figure 5.13:** Seismic profile displays that incision depth on SB P5 correlates closely with the level of onlap in the first downstepping shelf edge reflectors. Yellow: faults; pink: SB P5; blue dash: line projecting the depth of surface incision to the depth of onlapping reflectors.

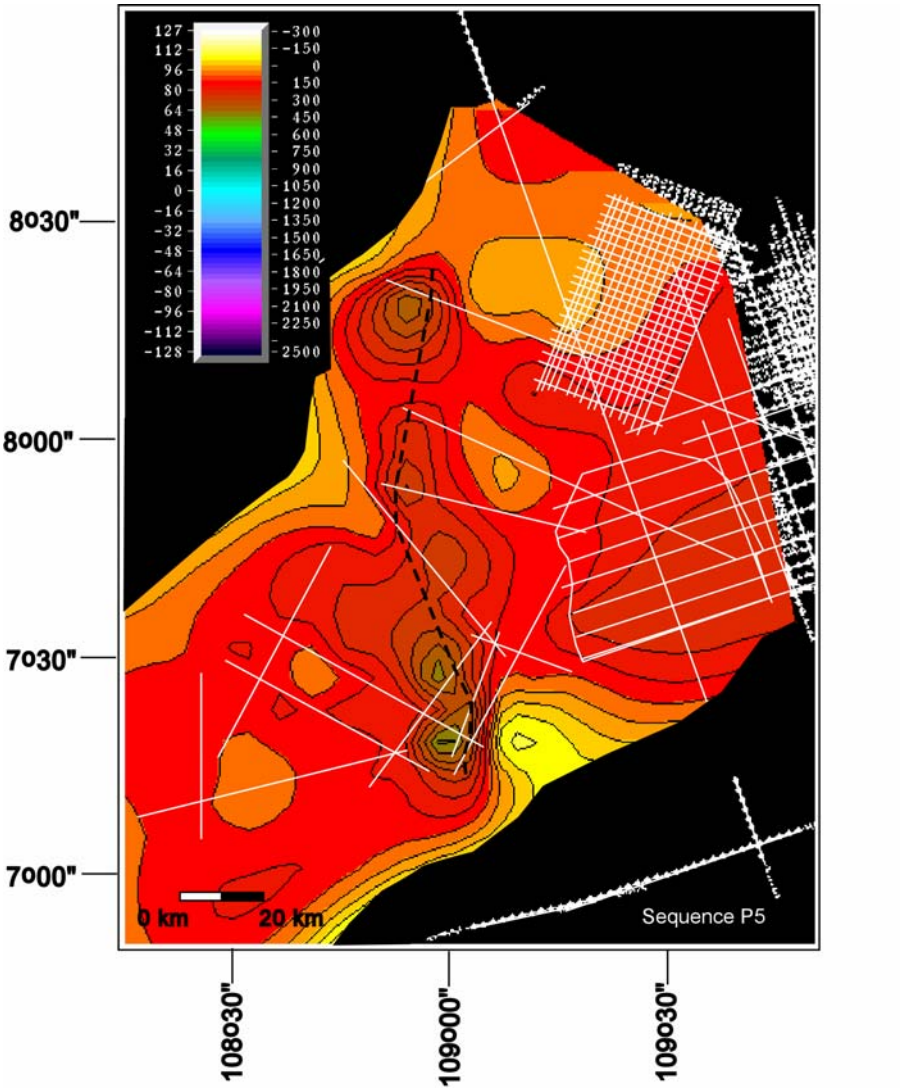


**Figure 5.14:** Isopach map of Sequence P5. Thickness accumulations are observed in the northern and southern parts of the study area located immediately updip from the terminal shelf edge. Scale bar is in meters. Contour interval is 50 m. The terminal shelf edge is identified by the black dashed line.

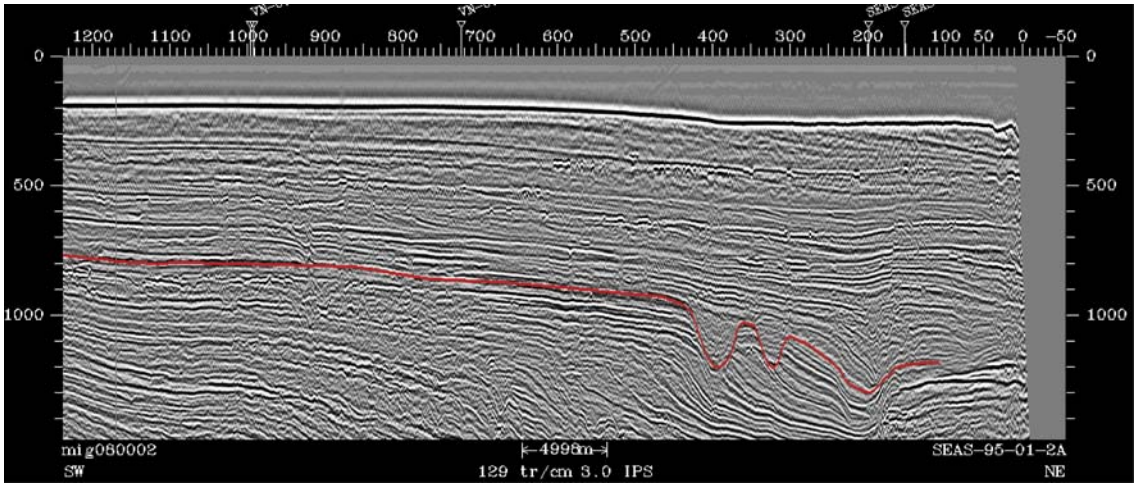


**Figure 5.15:** Shelf edge incisions associated with sequence boundary PL1.

*Sequence PL1-early Pleistocene*

Sequence PL1 shelf-edge deposits range from ~250 m to nearly 700 m thick. Shelf and shelf-edge deposits are thinner within Sequence PL1 compared to both older and younger sequences. The base of Sequence PL1 is bounded by SB PL1, which is recognized by significant shelf edge and updip shelf incision (Figure 5.15). Major incisions, ~1100 to ~1800 m wide and ~130 to ~200 m deep with chaotic fill, are observed near the shelf margin in the south. Updip the LST is composed of predominantly channelized and parallel/sub-parallel seismic facies. The LST near the shelf edge is characterized by PCW facies and overlying reflectors that onlap the sequence boundary at the base of slope and in up-dip, shelf areas. Possible slope fan deposits are recognized in the south as part of the LST (Figure 5.16) Shelf margin failure is observed in the southern part of the study area. Basinward of the shelf edge basin floor strata are typified by transparent and parallel/sub-parallel seismic facies that are generally noisy or gas disturbed. Normal faults are observed within this sequence located over relict mid-Miocene inversion highs. The HST is not observed within this sequence. Shelf edge thickness accumulations are observed in the central and southern regions of the study area (Figure 5.17).

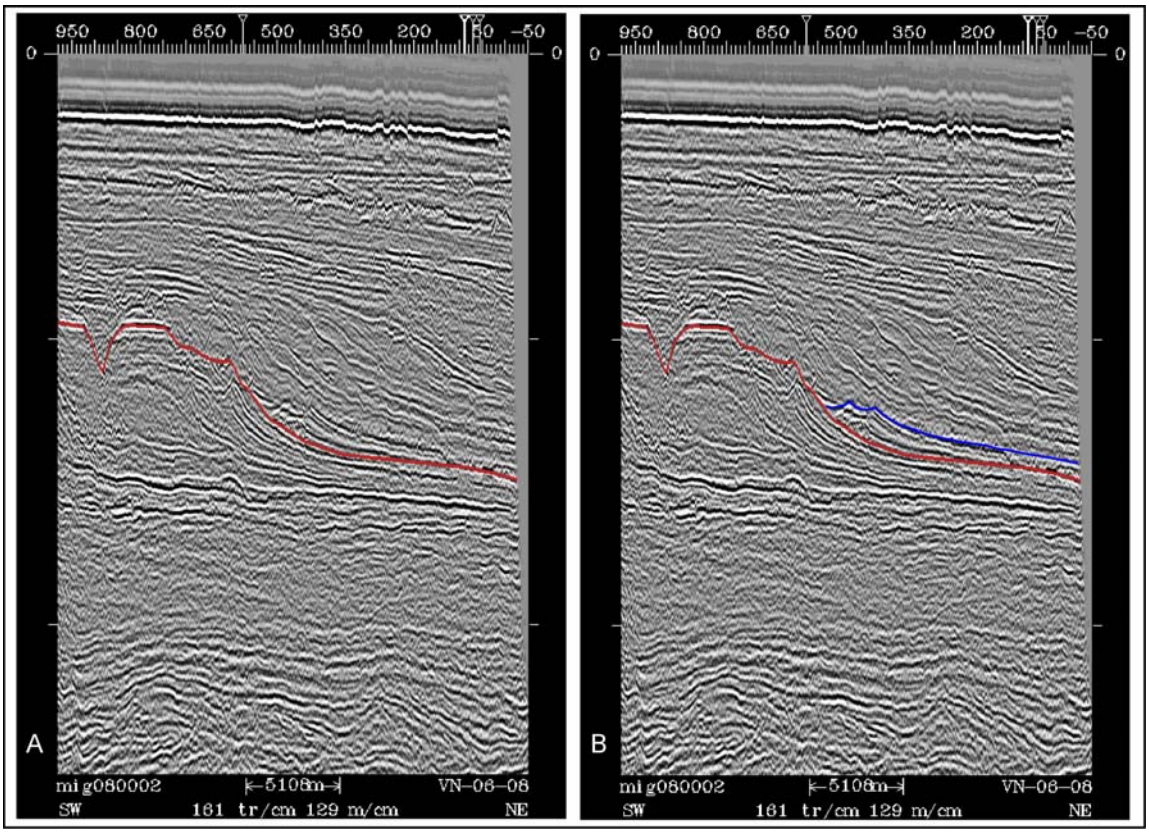


**Figure 5.16:** Slope fan deposits within the LST of Sequence P5. A) Uninterpreted seismic profile showing SB PL1 (red). B) Interpreted seismic profile showing SB PL1 (red) and slope fan deposits (blue).

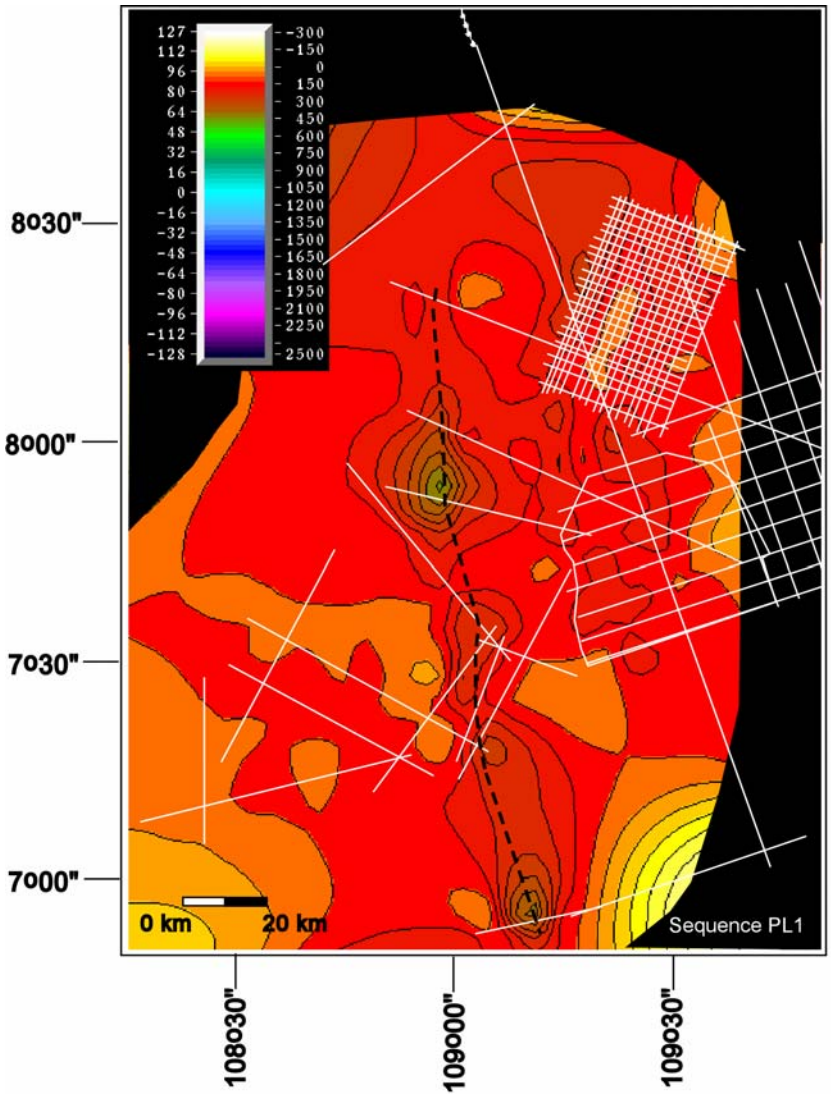


**Figure 5.17:** Isopach map of Sequence PL1. Thickness accumulations are recognized in the central and southern parts of the study area coincident with the terminal shelf edge. Scale bar is in meters. Contour interval is 50 m. The terminal shelf edge is identified by the black dashed line.

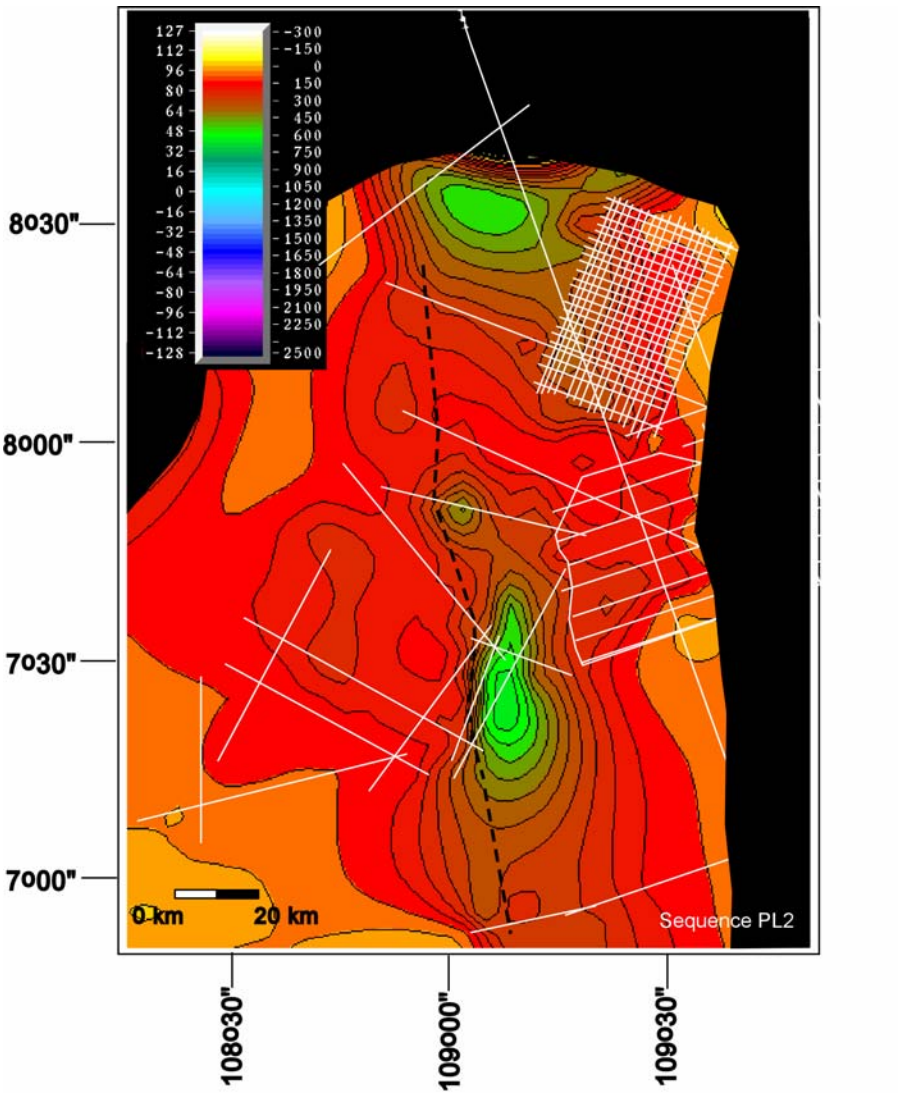


**Figure 5.18:** Isopach map of Sequence PL2. Thickness accumulations are observed in the central and southern parts of the study area immediately down dip from the terminal shelf edge. Scale bar is in meters. Contour interval is 50 m. The terminal shelf edge is identified by the black dashed line.

*Sequence PL2-early Pliocene*

Sequence PL2 is bounded below by SB PL2, which is identified by up-dip shelf incision and shelf margin incision. Reflectors downlap onto the sequence boundary downdip and onlap the sequence boundary up-dip within the overlying strata. The LST of Sequence PL2 is characterized updip by channelized facies and parallel/sub-parallel facies with gently seaward dipping reflectors. At the shelf edge the LST is comprised of downstepping PCW seismic facies. Thickness at the shelf edge varies from ~300 m to ~600 m where not faulted. Downdip from the shelf edge basin floor deposits display chaotic, transparent or parallel/sub-parallel seismic facies. The TST is recognized as a transgressive surface of erosion that truncates the underlying reflectors of the LST overlain by backstepping reflectors that onlap the sequence boundary progressively farther updip. Strata within the TST are characterized by seaward dipping reflectors displaying parallel/sub-parallel seismic facies. Strata overlying the TST are typified by shingled clinoform seismic facies that reflects deposition during the HST. Failure is common at the shelf edge. Shelf edge thickness accumulations are observed in the central and southern parts of the study area (Figure 5.18).

*Sequence PL3-middle Pleistocene*

The base of Sequence PL3 is bounded by SB PL4 and is identified by localized updip incision on the shelf, overlying reflectors that onlap updip and downlap downdip. Both the LST and HST are recognized within this interval. Updip the LST is defined by seaward dipping reflectors that are characterized by the parallel/sub-parallel seismic

facies and shingled clinoform facies. At the shelf edge PCW, chaotic, and transparent seismic facies distinguish shelf edge deposits. Shelf edge strata are commonly disturbed by faulting and failure as evidence by chaotic zones and disrupted reflectors. Downdip from the shelf edge, strata at the toe of slope onlap the sequence boundary. Seismic character in basinal settings is defined by parallel/sub-parallel, chaotic and transparent seismic facies. The top of the LST is identified by truncation of underlying reflectors and overlying reflectors that downlap onto the system tract boundary.

HST strata are recognized as parallel/sub-parallel and shingled clinoform seismic facies. Reflectors within the overlying strata downlap onto the LST and are truncated by SB PL4 at the top. Near the shelf edge HST strata display a more transparent seismic facies. HST strata thin updip and downdip of the shelf edge. The HST is characterized by thin parallel/sub-parallel to transparent seismic facies in basinal areas.

Shelf edge thickness varies from ~150 m to ~640 m across the study area with maximum thickness occurring near the shelf edge concentrated in shelf edge thickness accumulations from the north to the south (Figure 5.19).

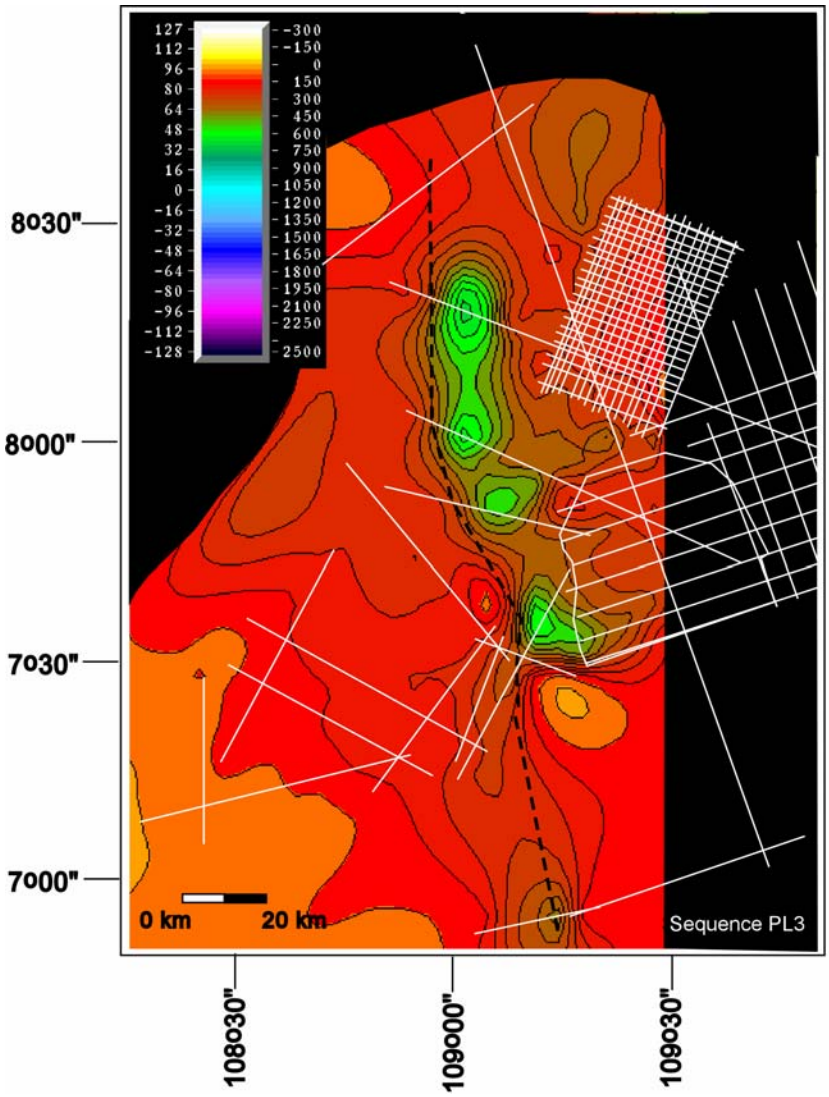


**Figure 5.19:** Isopach map of Sequence PL3. Thickness accumulations are concentrated immediately downdip from the shelf edge in the northern, central and southern parts of the study area. Scale bar is in meters. Contour interval is 50 m. The terminal shelf edge is identified by the black dashed line.

*Sequence PL4-late Pleistocene*

Sequence PL4 is bounded by SB PL4 at the base and the seafloor at the top. SB PL4 is recognized by incision near the shelf edge, shelf incision up-dip, and onlapping reflectors at the base of slope within overlying strata. Updip the LST is expressed as shingled clinoform facies and parallel/sub-parallel facies with gently seaward dipping reflectors that onlap the sequence boundary. The LST is characterized by PCW facies at the shelf edge. Topset reflectors within the PCW facies dip seaward in the northern and central parts of the study area. Shelf-edge failure is observed in the central part of the study area. Shelf edge reflectors in the southern region of the study area are interrupted by cross-cutting multiples and gas washout. Downdip from the shelf edge, the nature of seismic facies is characterized by chaotic facies near the base of slope in units that onlap the basal sequence boundary both updip and downdip. Further basinward, seismic facies is generally parallel/sub-parallel to transparent.

The upper part of the LST is characterized by more aggradational reflector pattern. The top of the LST is recognized on the shelf and at the shelf edge by truncation of LST reflectors at the upper boundary and shingled clinoform facies at the seafloor located updip from the shelf edge, which record transgression. Along the shelf edge and updip shelf regions in the south, low angle, shingled clinoforms of the TST are truncated at the seafloor. Asymmetric ridges and a deltaic wedge are observed on the seafloor, which will be discussed in detail in Chapter VI. The HST is not observed within this sequence.

Thickness of Sequence PL4 varies across the study area from ~300 m to ~800 m at the shelf edge (Figure 5.20). Two thickness accumulations are observed, one in the north and a second in the south. Both thickness accumulations are located immediately downdip of the terminal shelf edge.

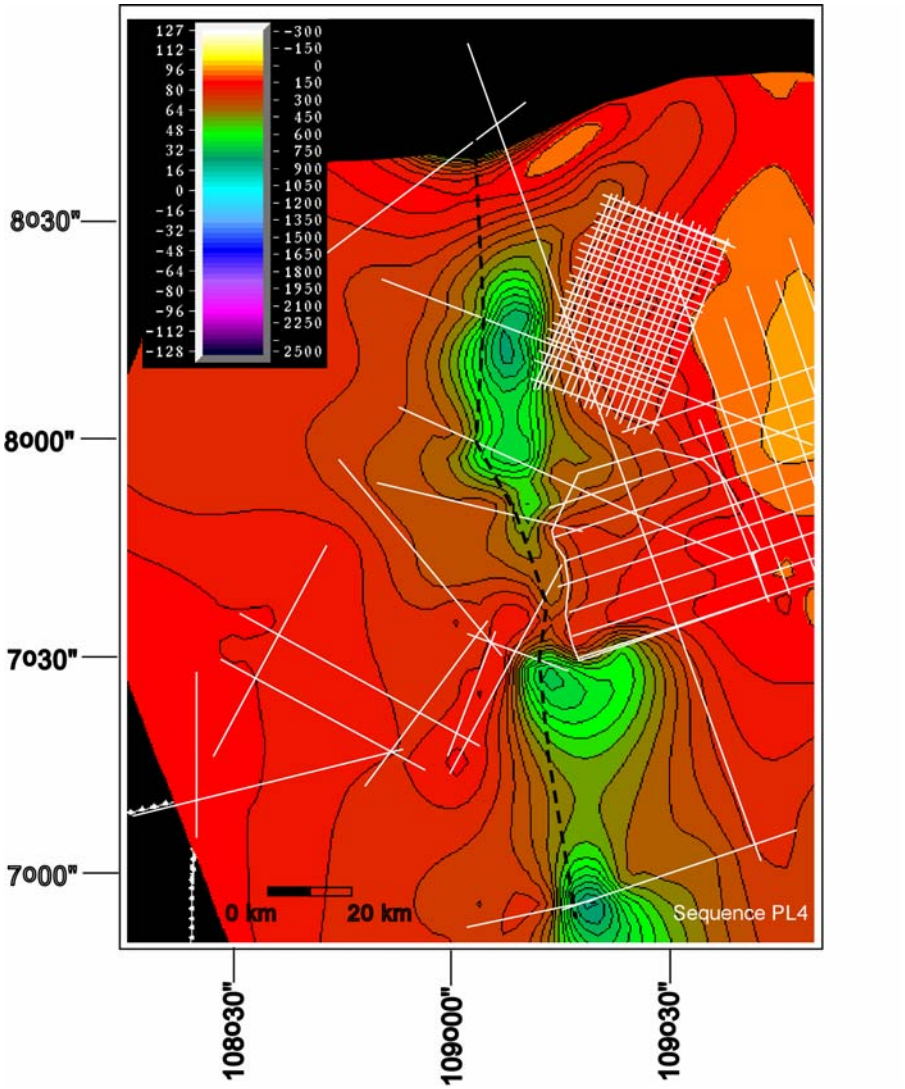


**Figure 5.20:** Isopach map of Sequence PL4. Shelf edge thickness accumulations are recognized in the northern and southern parts of the study area immediately downdip from the shelf edge in the north and coincident with the shelf edge in the south. Scale bar is in meters. Contour interval is 50 m. The terminal shelf edge is identified by the black dashed line.

# DISCUSSION

## Sequence Stratigraphy and Sea-level History

Comparison of duration and magnitude of sequences and sequence boundaries of Wornardt et al. (2001) and limited biostratigraphic constraints allow estimated age constraints to be assigned to the stratigraphic section (Figure 5.21). Pliocene sequence boundaries P1, P2, P3, and P4 may correlate with lowstand events at ~3.95 Ma, ~3.21 Ma, ~2.76 Ma, and 2.55, respectively. SB P5 may correlate with the ~2.00 Ma sea-level lowstand of Wornardt et al. (2001). SB PL1 and SB PL2 can be correlated with the ~1.56 Ma and ~1.40 Ma sea-level lowstands (Wornardt et al., 2001). SB PL3 may record the ~0.8 Ma lowstand event reported by Wornardt et al. (2001). SB PL4 likely correlates to the ~0.2 lowstand.

Minor sea-level fall is recognized during early Pliocene to earliest late Pliocene time (~3.95-3.21 Ma) according to the sea-level curve of Wornardt et al. (2001). A significant sea-level fall observed at ~3.21 Ma, followed by a long-term sea-level rise from ~3.21 to ~0.8 Ma (Wornardt et al. 2001). Long-term sea-level rise continues until ~0.8 Ma, when fourth- and fifth-order sea-level fluctuations dominate eustatic patterns. Long-term sea-level fall is observed within fourth-order sea-level changes during middle Pleistocene time (~0.8 to ~0.2 Ma).

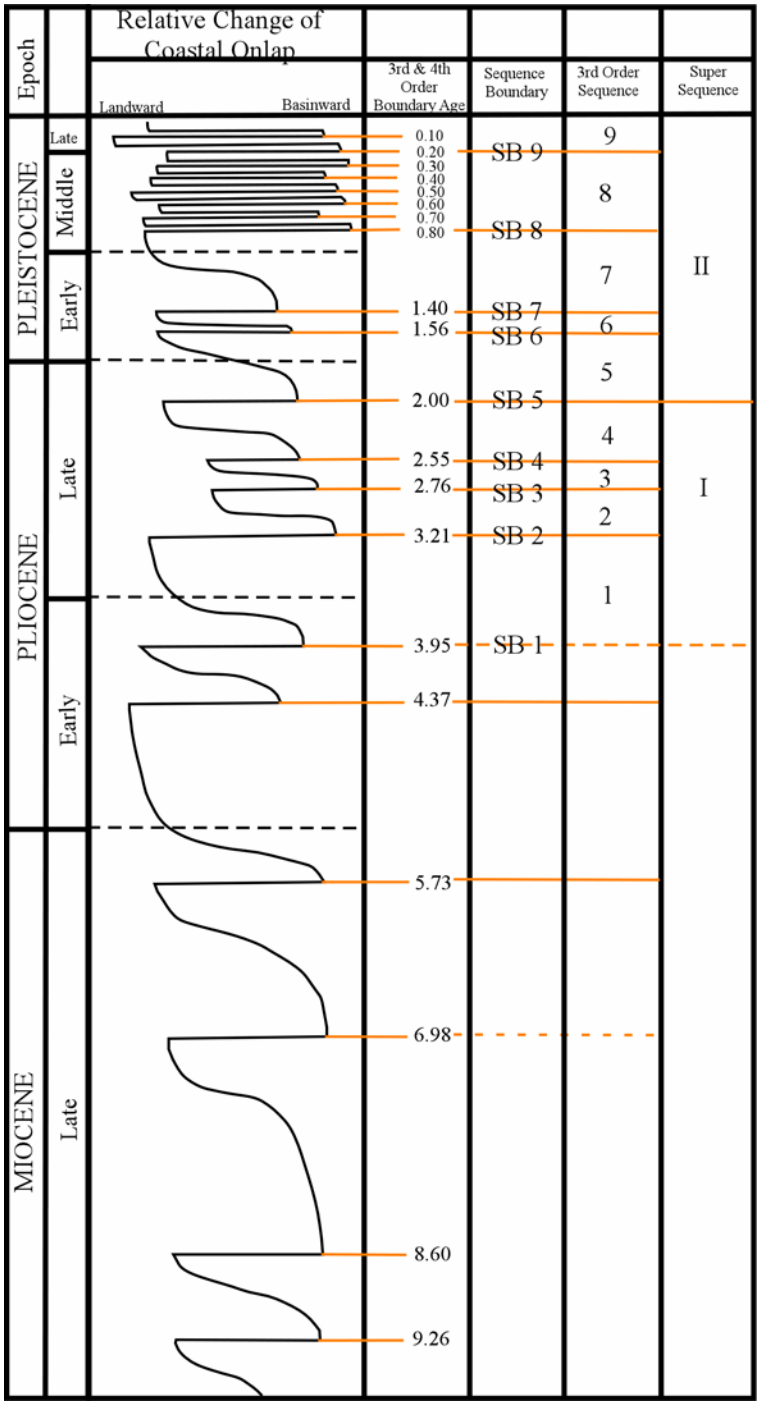


**Figure 5.21:** Sequence boundaries and sequences from this study correlated to the Wornardt et al. (2001) sea-level curve. Sequence boundaries are labeled SB 1 through SB 8. Third-order sequences are labeled A through I. Second-order sequences are labeled I and II. Modified from Yarbrough, 2005).

Sequences P2 through P3 display progradational character despite deposition during long-term sea-level rise. The prograding nature of sequences P2 through P3, which is a contradictory reflector pattern during sea-level rise, indicates significant sediment flux to the ENCSB during late Pliocene time. Alternatively, this may indicate that the sea-level curve of Wornardt et al. (2001) does not adequately reflect changing accommodation within the ENCSB during this interval. Third-order sea-level fall within late Pliocene through latest Pliocene strata produced decreased accommodation and resulted in incision of the shelf during third-order lowstands.

A more aggradational character is observed in Sequence P4 indicating that accommodation change nearly equaled the rate of sediment supply. This may indicate decreased sediment supply compared with deposition during Sequences P2 and P3 or may reflect increased accommodation resulting from sea-level rise between ~2.55 and ~2.00 Ma as reported by Wornardt et al. (2001).

Sequence boundary P5 marks a change in depositional style within LST deposits. Lowstand strata within Sequences P5 through PL4 are characterized by well-developed LST that fall below the position of the former shelf edge (Figures 5.22 and 5.23).

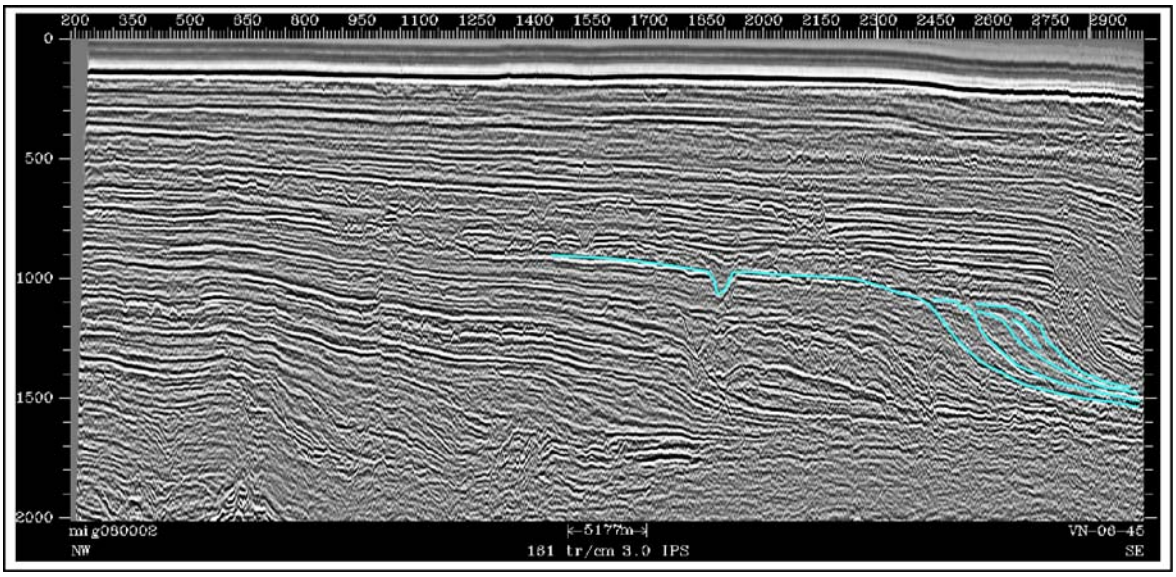


**Figure 5.22:** Sequence boundary P5 and downstepping shelf-edge clinoforms are marked with blue.

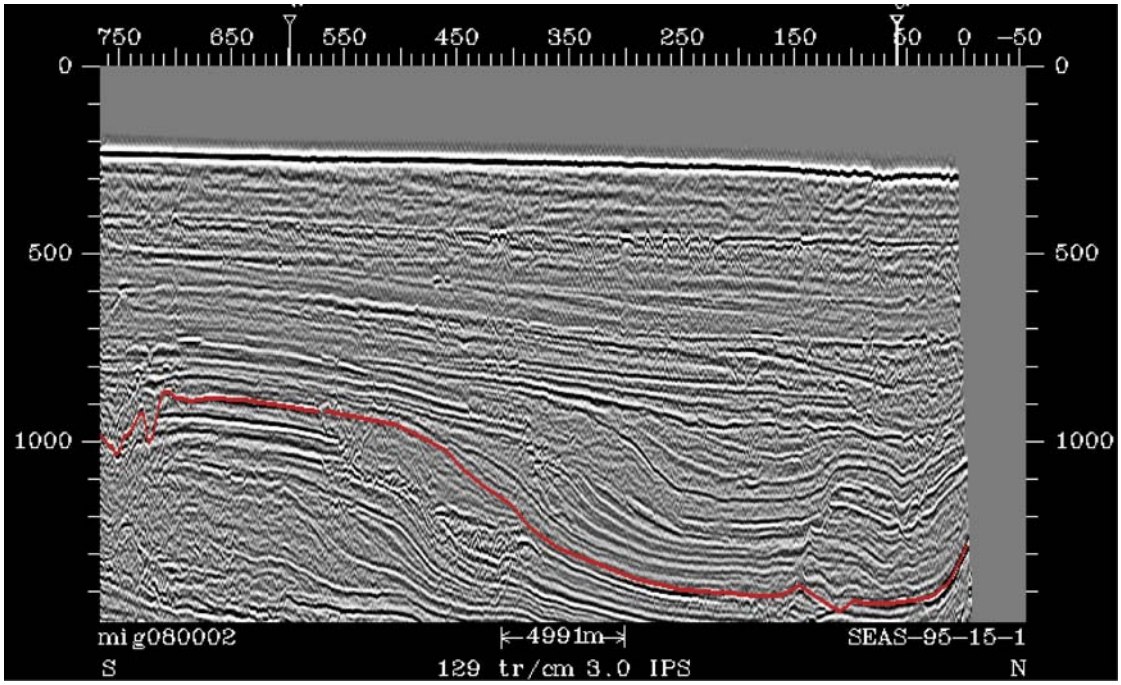


**Figure 5.23:** Sequence boundary P6 is marked in red. Note the downstepping prograding wedge clinoform facies downdip from the previous terminal shelf edge.

SB 5 divides the Pliocene to Recent strata into two second-order trends in accommodation: Supersequence I, which is comprised of Sequences P1, P2, P3, and P4; and Supersequence II, which consists of Sequences P5 through PL4.

Sequences 1 through 4 likely record highstand progradation during Supersequence I. Long-term, relatively high accommodation favored progradation during this interval. Third-order sea-level falls resulted in episodic updip incision and the formation of third-order sequence boundaries. No evidence of shelf edge incision is observed in the southernmost part of the study area indicating that sea-level did not fall significantly below the previous shelf edge. Relative sea-level started to fall during the second-order accommodation decrease observed in Super sequence II, beginning at ~3.21 Ma. The impact of this long term decrease in accommodation produced a more dramatic response to third-order sea-level falls. Significant fluvial incision of shelf settings and slope to basin floor deposition are observed in Sequences 5 and 6 as a result.

Sequences 7 through 9 represent third-order sea-level cycles and likely formed during the rising limb of the second-order accommodation trend within Supersequence II. The sea-level of Wornardt et al. (2001) suggests accommodation increased slightly during latest Pliocene to early Pleistocene time. Sequences 7, 8, and 9 formed as a result of third-order sea-level cycles within this period. The long-term increasing accommodation trend produced a less dramatic response to third-order sea-level falls as compared to Sequences 5 and 6. Chaotic units on the slope and basin floor observed in Sequences 7, 8, and 9 indicate that mass transport processes were active in the ENCSB during latest Pliocene to late Pleistocene time. Large incisions, such as those observed

along the shelf edge in Sequences 5 and 6, are not observed in Sequences 7, 8, and 9. This may be a reflection of a less dramatic response to sea-level fall within the climbing limb of Supersequence II. It may also result from limited data coverage in that large incisions may have formed on the latest Pliocene to late Pleistocene shelf edge, but are not captured due to the wide spacing between seismic lines.

**Accommodation Change**

Accommodation in the ENCSB was controlled by global, regional and local factors, which are influenced by eustasy, tectonics and sediment flux. Post-rift thermal subsidence related to Oligocene rifting in the SCS influenced subsidence in the basin during Pliocene to Recent time. Anomalous and poorly understood basin subsidence, added to the thermal subsidence rates inherited from earlier rifting events, has been reported for the ENCSB by Wheeler and White (2002). The effects of this anomalous subsidence decrease drastically to the west so the WNCSB and the Mekong Basin do not display similar anomalous subsidence. The combined effects of rift-related thermal subsidence and younger anomalous subsidence act to increase accommodation in the ENCSB.

Accommodation in the ENCSB was also influenced by eustatic changes. In addition to the third-order sea-level cycles interpreted from stratal patterns in the ENCSB during Pliocene to Recent time, two long-term trends in accommodation are recognized. During Super-Sequence I (late Pliocene time), long-term sea-level rise indicates that accommodation increase should have been recorded. However, late

Pliocene deposits record progradation, suggesting that sediment supply outpaced accommodation change during this interval.

Sequences P5, PL1 and PL2 were deposited during long-term sea-level rise between ~3.21 to ~0.8 Ma, which should have resulted in increased accommodation producing aggradational or backstepping stratigraphic patterns. LST strata within Sequences P5, PL1 and PL2 are characterized by lowstand prograding wedge deposits that downstep and onlap the basal sequence boundary suggesting significant accommodation decrease. This is contrary to the reported sea-level trend during this interval. The sea-level curve of Wornardt et al. (2001) was constructed based on strata in the Gulf of Mexico. This may reflect an exaggerated response to sea-level rise in the Gulf of Mexico due to sediment loading from point sources along the northern margin of the Gulf of Mexico.

Sequence PL3 was deposited during sea-level fall between ~0.8 to ~0.2 Ma. The progradational character of Sequence PL3 suggests that sediment supply kept pace or may have outpaced accommodation decrease due to sea-level fall. Sequence boundary PL4 records sea-level lowstand at ~0.2 Ma followed by short-term sea-level rise and fourth-order sea-level fall at ~0.1 Ma. The progradational nature of Sequence PL4, particularly in the north, suggests that sediment supply outpaced accommodation due to sea-level rise between ~0.2 to ~0.1 Ma.

Shelf-edge faulting and slumping also played a role in affecting local accommodation. Shelf-edge faulting seems to be related to the progradation of highstand

deposits past most antecedent LST shelf edges. Steep antecedent topography also seems to have favored shelf-edge failure.

Compaction near the shelf edge probably significantly influenced accommodation increase at least over the last 18 to 20 kyrs. Approximately 40-50 meters of subsidence has occurred since the LGM and is recognized in the ENCSB during this study and on the Sunda Shelf by Wong et al. (2003). Subsidence rates of ~ 2.5 m/kyr are estimated by this study and by Wong et al. (2003). This rate is similar to compaction rates reported for the Mississippi Delta (Wong et al., 2003). This will be discussed in additional detail in following chapters.

Normal faulting in the Pliocene to Recent section is observed over deep mid-Miocene inversion highs in present-day deep-water settings. Occasionally, faults within late Miocene to Recent strata link with basement-involved faults which controlled inversion during mid-Miocene time. This suggests possible reactivation of rift or inversion related faults during Pliocene to Recent time. This may reflect renewed rifting in the SCS or continued deformation through at least latest Pleistocene time.

**Sediment Supply**

Thickness variations across the study area were investigated for Pliocene sequences P1 through P5 and Pleistocene sequences PL1 through PL4 using gridded time-thickness maps created using MapIt!$_{TM}$, a mapping program in SeisWorks$_{TM}$. The gridding option within MapIt!$_{TM}$ was used to compute contours. Within MapIt!, averaged *z* values are computed by the program for each node in a matrix

built by the software. Contours are then created and smoothed by means of the algorithms in the software. Care must be taken when interpreting gridded isopach maps because *z* values are extrapolated between known points and contours are smoothed. Features lying outside the data area may not reflect true geologic structures or stratigraphic features. However, these isopach maps are useful for examining regional trends in thickness during early Pliocene to Recent time.

Two main areas of thickened shelf-edge accumulations and adjacent slope-to-basin floor deposits are recognized throughout late Pliocene to Recent time, one in the central/north and one in the south. These shelf-edge "thicks" likely reflect deposition near a point source. Two main point sources supplied sediment to the NCSB during Pliocene to Recent time: the paleo-Mekong River in the north and the paleo-Molengraff River in the south (Murray and Dorobek, 2004). The northern depositional "thicks" likely record deposition from the paleo-Mekong River, which has been a significant sediment source to the southwestern SCS since at least Miocene time according to Murray and Dorobek (2004). Recognition of east/southeast prograding shelf edge deposits during Sequence P1 (early Pliocene) suggests that the Cuu Long and WNCS Basins had filled by at least early Pliocene time and became sites of sediment bypass allowing rapid seaward migration of fluvio-deltaic systems into the eastern NCSB during third-order highstand condition. The Mekong River continued to be a dominant sediment source throughout Pliocene to Recent time in the NCSB.

The southern shelf depositional "thicks" most likely reflect deposition from fluvio-deltaic systems that originated from the Sunda Shelf, such as the Molengraaff

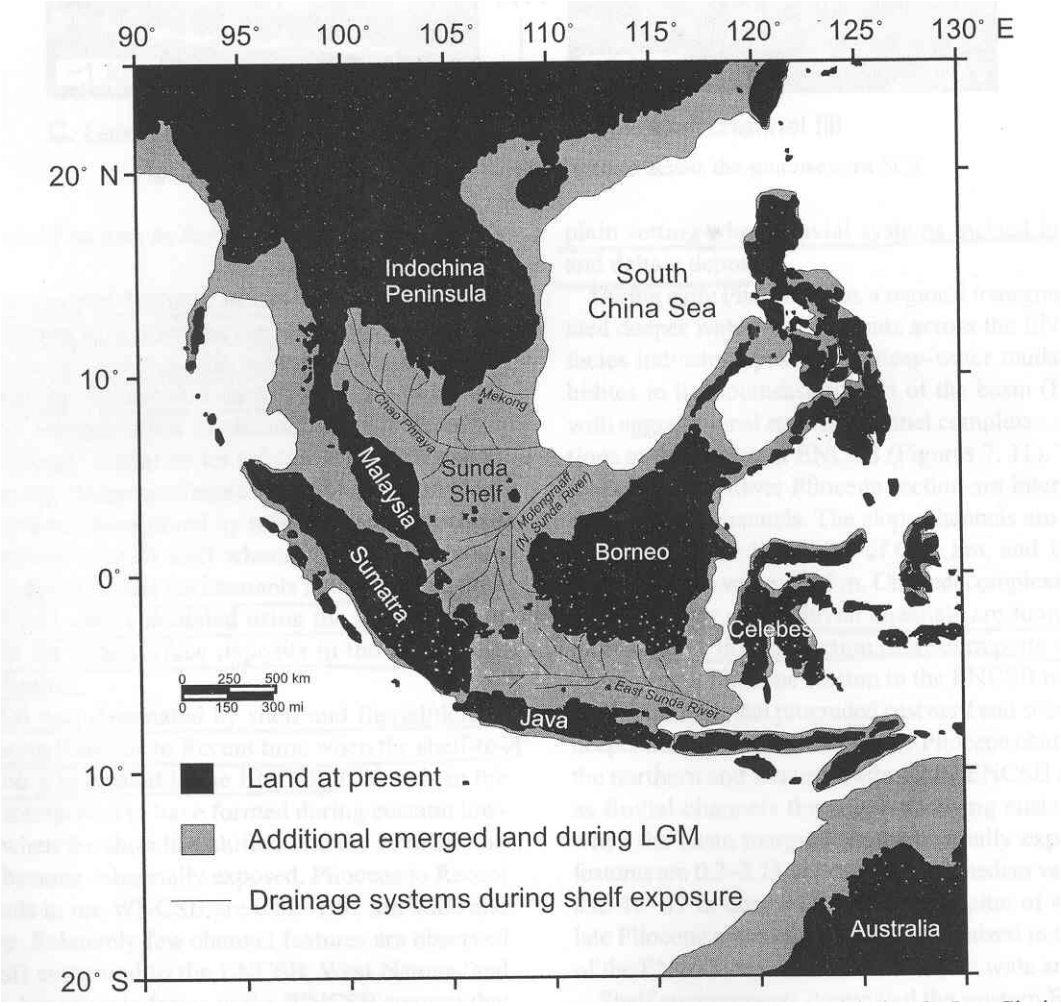


**Figure 5.24:** Shelf-edge depositional thicks were likely sourced from the paleo-Mekong River in the north and southern rivers originating from the Sunda Shelf, such as the Molengraaff River.

River (North Sunda River) or possibly the Chao Phraya River (Figure 5.20). North to northeast progradation observed within Sequence P1 suggests that basins on the Sunda Shelf, such as the Malay and West Natuna Basins, had filled and were areas of sediment bypass by at least latest Miocene-early Pliocene time (Murray and Dorobek, 2004). Evidence of significant Pliocene to Recent shelf edge deposits in the south suggests that these Sunda Shelf river systems remained an important sediment source at least through the LGM.

The location of the shelf-edge "thick" with respect to the terminal shelf edge has implications for slope and basin floor deposition. Shelf-edge "thicks" located updip from the terminal shelf margin indicate periods when slope and basin floor deposition would likely have been minimized. Shelf-edge "thicks" located downdip from the terminal shelf edge or coincident with it would have more likely resulted in deposition on the slope and basin floor.

*Paleo-Mekong and paleo-Molengraaff Shelf Edge Systems*

There is an overall shift in sediment thickness to the east as the shelf edge prograded eastward during Pliocene to Recent time (Figure 5.25). Within the paleo-Mekong point source, lateral shifts in sediment accumulation are also observed. These are likely due to minor shifts in the location of the delta due to avulsion during times of decreased accommodation resulting from sediment infill. The presence of shelf edge thicks in Sequences P1 through P4 suggest that the Mekong River supplied sediment in

the ENCSB by at least Sequence P1, or early Pliocene time, and remained an influence through the end of Sequence P4

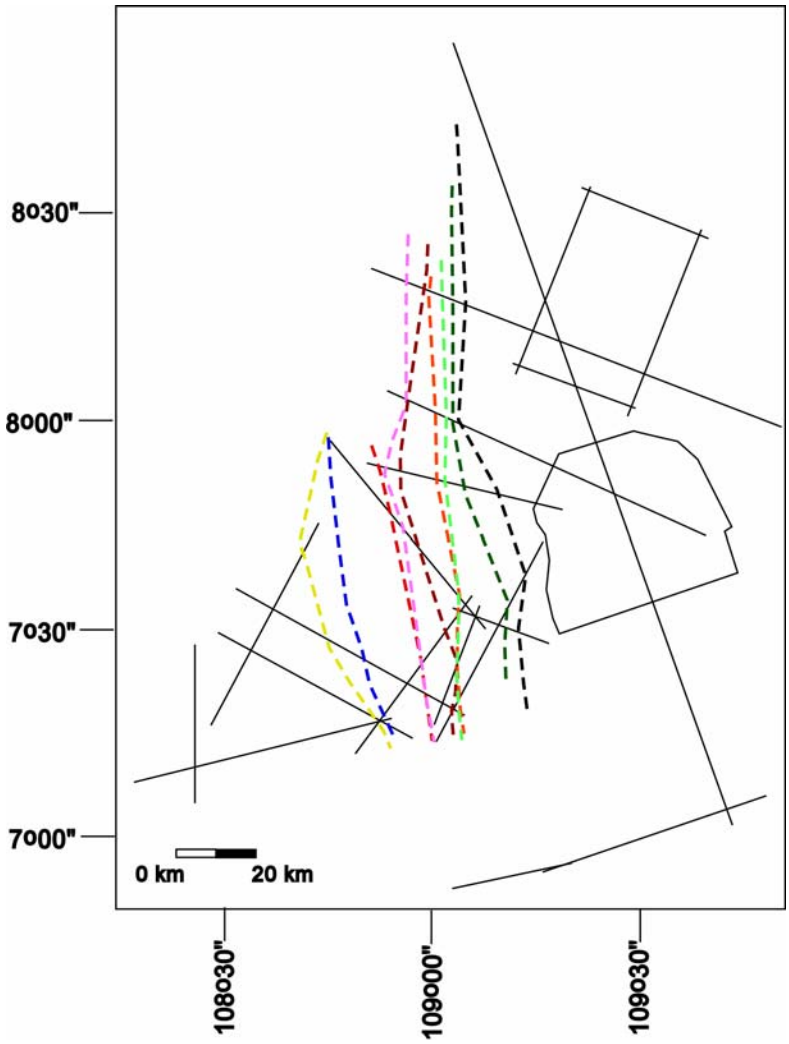


**Figure 5.25:** Progradation of the shelf edge across the ENCSB from Early Pliocene through Recent time (Sequences P1 through PL4). Yellow: Sequence P1 shelf edge; Blue: Sequence P2 shelf edge; Ruby Red: Sequence P3 shelf edge; Pink; Sequence P4 shelf edge; Brick Red: Sequence P5 shelf edge; Orange: Sequence P6 shelf edge; Light Green: Sequence P7 shelf edge; Dark Green: Sequence P8 shelf edge; Black: Sequence P9 shelf edge.

(~2.00 Ma). The progradational nature of Sequences P1, P2, and P3 suggests steady sediment supply that slightly outpaced long-term slow accommodation increase. The similar shelf edge location and aggradational nature of sequences P3 and P4 (late Pliocene) suggests that sediment supply kept pace with changes in available accommodation space.

Sequence P2 shelf-edge thick, located in the central part of the study area, is thinner than that observed in Sequence P1, which may suggest decreased sediment supply from the paleo-Mekong point source at this time. The shelf-edge “thick” observed in the central part of the study area increased in thickness during Sequence P3 and decreased thickness during Sequence P4. This may reflect increased sediment supply from during Sequence P3 and decreased supply during Sequence P4. The Sequence P4 isopach map also indicates that two separate “thicks” formed during this interval. This may reflect increasing influence of the paleo-Molengraff point source during this time.

Shelf-edge “thicks” observed during Sequences P1 and P3 are situated updip from the terminal shelf edge indicating that slope and basin floor deposition would more likely have been limited. Slope and basin floor deposits are not observed as well-developed stratigraphic units within Seqences P1 and P3. During Sequences P2 and P4, shelf-edge “thicks” are coincident with the terminal shelf margin. However, significant slope and basin floor deposits are not recognized within the data set during Sequences P2 and P4. This may be due to limited data such that slope and basin floor deposits were more significantly formed, but they are not observed within this data set.

Two separate shelf-edge “thicks” are observed and likely reflect influence of the paleo-Mekong River in the north and the paleo-Molengraaff River in the south. The northern “thick” changed little in thickness compared to Sequence P4 and was situated immediately updip from the terminal shelf edge. The southern “thick” increased in thickness and areal extent suggesting increased sediment supply from the paleo-Molengraaff River.

During Sequence PL1 (early Pleistocene) the northern “thick” migrated into the central part of the study area and increased in thickness, suggesting avulsion of the paleo-Mekong River system and possibly increased sediment supply. The southern “thick” decreased in thickness and areal extent, which may reflect decreased sediment supply from the paleo-Molengraaff River during early Pleistocene time. Both shelf-edge “thicks” were located coincident with the terminal shelf edge.

The northern shelf edge “thick” decreased in areal extent and thickness during Sequence PL2 (early Pleistocene), whereas the southern shelf-edge “thick” increased significantly. This may reflect increased sediment supply from the paleo-Molengraaff River during this sequence. Both shelf-edge “thicks” were located downdip from the terminal shelf edge.

Both the northern and southern “thicks” were located immediately downdip from the terminal shelf edge during Sequence PL3. The northern “thick” increased in thickness and areal extent suggesting increased sediment supply from the paleo-Mekong River during middle Pleistocene time (~0.8 Ma). Thickness of the southern “thick”

remained unchanged since Sequence PL2 (early Pliocene), suggesting continued sediment supply from the paleo-Molengraaff River.

During Sequence PL4 (late Pleistocene) the northern “thick” increased in areal extent, while the southern “thick” maintained thickness during this time. This may reflect continued or slightly increased sediment supply from the paleo-Mekong and paleo-Molengraff Rivers during late Pleistocene time. Both shelf-edge “thicks” were situated immediately downdip from the terminal shelf edge.

The locations of “thicks” during Sequences PL2, Pl3, and Pl4 (early to late Pleistocene) were immediately downdip from the terminal shelf edge suggesting that slope and basin floor deposition would have been well-developed. Slope and toe-of-slope deposits are recognized during early to late Pleistocene age strata within the data set and were likely linked with these updip shelf-edge accumulations.

**Trends Within Third-order Sequences**

Sequence boundary P5 divides the stratigraphy into two intervals based on trends in the strata below that differ from trends observed within the strata above. In general, strata below sequence boundary P5 (Super-seqeunce I) display less well developed LST deposits, are less deeply incised, and have less dramatic variations in thickness between the shelf and shelf edge deposits compared with strata above sequence boundary P5.

Sediment supply likely outpaced long-term sea-level rise during Sequences P1 through P4 (early to late Pliocene). The long-term progradational character of these sequences may have minimized effects of third order eustatic changes resulting in less

deeply incised shelf areas and less developed LST. Deeper incision and better developed LST are observed within the strata above sequence boundary P5 (late Pliocene) and comprise Super-sequence II. These changes may reflect more balance between sediment supply and third-order eustatic changes such that each third-order lowstand is more dramatic. This would likely have produced deeper incision on the shelf and LST deposition below the previous shelf edge, which may have resulted in more dramatic thickness variations between shelf and shelf edge strata.

## CONCLUSIONS

- Nine sequence boundaries and associated sequences are recognized along the late Miocene to latest Pleistocene shelf in the ENCSB.
- Loosely defined age constraints can be assigned by comparing the stratigraphic analysis with published sea level curves of Wornardt et al. (2001) and correlating sequence boundaries.
- Regional accommodation is controlled by a combination of compaction, rift-related and non-rift-related anomalous subsidence, and eustatic change.
- More localized accommodation on the shelf is influence by avulsion of shelf margin systems and shelf edge faulting.
- Two point sources, likely the paleo-Mekong and paleo-Molengraaff Rivers, deposited sediment in the NCSB and influenced stratigraphic patterns as well as location of shelf-edge thickness accumulations during Pliocene to Recent time.

- Shifts in the location of shelf-edge thicks likely records avulsion of the point source systems and changes in thickness may record evolving sediment supply.
- Sediment supply during early to late Pliocene time overwhelmed deposition on the shelf and shelf edge such that the effects of third-order lowstands were limited.
- Sediment supply during late Pliocene to late Pleistocene time was not sufficient to overprint third-order lowstands.

# CHAPTER VI

# MODERN SEAFLOOR FEATURES

## INTRODUCTION

It is generally accepted that sea-level fall during the Last Glacial Maximum (LGM) was ~ 120 m below present day sea level (e.g., Fairbanks, 1989; Roberts et al., 2004). The LGM lowstand exposed significant portions of the present-day shelf regions around the SCS, including most of the Sunda Shelf (Wang et al., 1999; Hanebuth et al., 2003; Schimanski and Statteger, 2005). During the LGM, two major rivers incised on the emergent shelf and deposited sediment near the shelf break (Wang et el., 1999). Incised valleys and deltaic deposits associated with the LGM paleo-Mekong River have been observed on the Vietnam Shelf (Schimanski and Statteger, 2005). Extensive up-dip incision and shelf margin deposition has been reported for the Molengraaff River on the Sunda Shelf (Hanebuth et al. 2000; Thi et al., 2001; Wong et al., 2003). This study uses extensive 2D seismic data from the ENCSB to provide a detailed history of latest Pleistocene to Recent seafloor features related to shelf margin deposition and to evaluate sediment dispersal pathways across the southwestern margin of the SCS during the LGM.

# OBSERVATIONS

## Shelf Margin System

Two prominent depositional features are found in the western part of the study area: 1) a large-scale progradational package ranging from ~300 ms to ~800 ms (TWT) (~300-700 m calculated from nearest well velocity data; see Appendix A Table 2 for calculations), which is overlain by 2) a smaller scale (~90-160 ms, ~100-150 m; Appendix A Table 3) prograding unit interpreted to be an associated outer shelf to shelf-edge delta. The shelf break is observed at present-day water depths of ~310 m. The deltaic offlap break, however, is found at ~160 m present day water depth, and becomes shallower toward the south. Additional seafloor features include asymmetric ridges on the shelf to the south. Distance between ridge crests ranges from ~100-270 m (Appendix A Table 4). Ridge height ranges from ~3-8 m. The steep face is in on the basinward side of the ridge.

The study area can be segregated into three regions based on the distribution of dip-trending seismic profiles along the shelf margin: 1) a northern area dominated by progradational shelf edge system clinoforms with horizontal to sub-horizontal topset reflectors; 2) a central area dominated by progradational shelf edge clinoforms with seaward dipping reflectors; and 3) a southern are dominated by prograding shelf edge clinoforms and erosional truncation of shelf reflectors.

Late Pleistocene (Sequence PL4 described in Chapter V) shelf-edge deposits in the northern part of the study area are characterized by prograding clinoforms that are approximately 700 m thick. A deltaic wedge formed during late lowstand to early

transgression is observed at the seafloor. Asymmetric seafloor ridges observed in the south are at ~ 140 m present day water depth, approximately 3-8 m high, and ~100 m to ~240 m wide.

The deltaic offlap break in the north is located at ~170 m present-day water depth. The deltaic unit is composed of low angle, shingled clinoforms ~130 m thick, which are subtly truncated at the present day shelf seafloor. In the central part of the study area, the deltaic offlap break is located at ~160 m and internal deltaic character is typically low angle, shingled clinoforms approximately 145 m thick. Clinoforms are erosionally truncated along the modern shelf surface. In the south, the deltaic wedge is recognizable as a thin unit of shingled, erosionally truncated clinoforms. The offlap break is not recognized in the south, due to extensive removal of seafloor deposits.

**Seafloor Channels and Sediment Dispersal Pathways**

The modern shelf edge trends roughly N-S across the study area. A single, flat-bottomed, v-shaped channel approximately 16 m deep and 290 m wide was observed incised within the delta top clinoforms at the seafloor in the northwestern part of the study area (Figure 6.1). South of ~ $8^{o}00$” N longitude, no channels were observed across the shelf at the seafloor, but seafloor reflectors in the south are erosionally truncated. With the exception of localized channels and canyons along on the shelf edge, channels were not recognized across the modern shelf in the southern part of the study area.

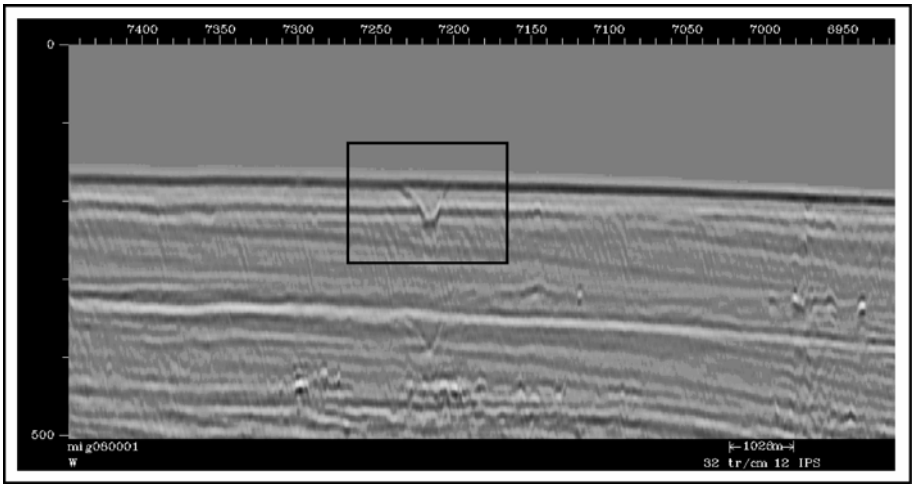


**Figure 6.1:** V-shaped channel observed on the shelf in the northern part of the study area.

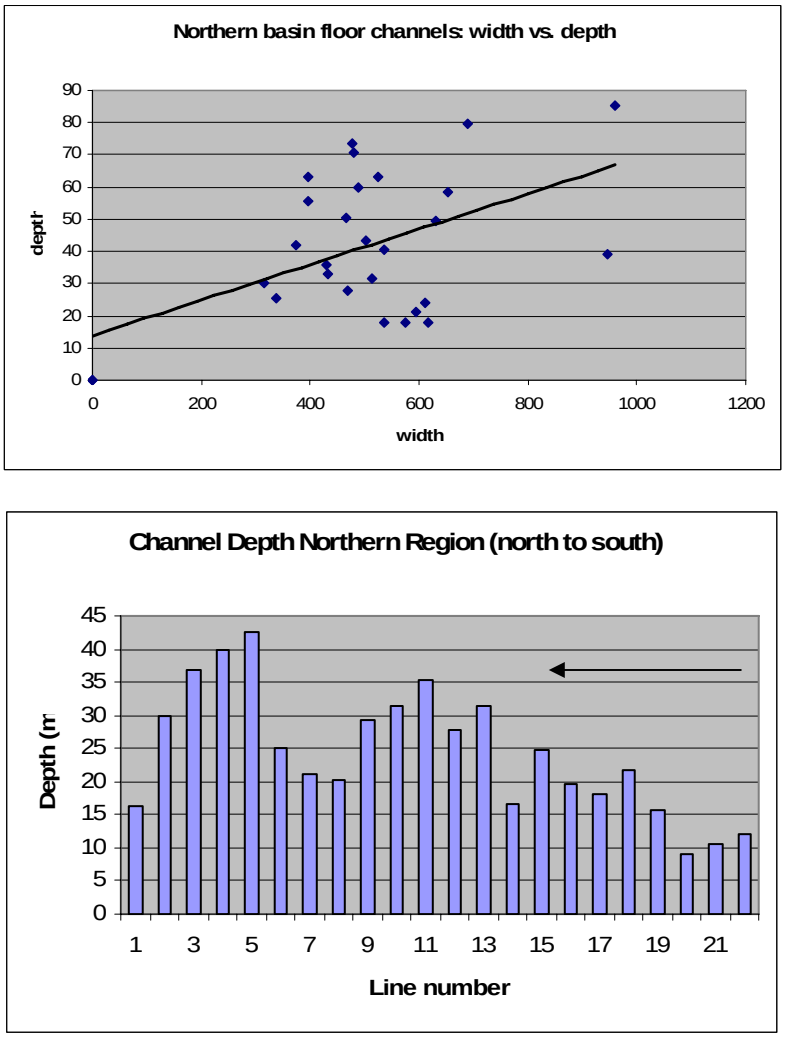


**Figure 6.2:** Top: Basin floor channel depth vs. width in the northern part of the study area taken on southwest-northeast seismic lines from the north to the south. Depth is on the y-axis in meters. Width is on the x-axis in meters.Bottom: Basin floor channel depth in the northern part of the study area taken on southwest-northeast seismic lines from the north to the south. There is an overall decrease in depth values toward the south. Arrow indicates direction of flow from the shelf edge into the basin (southwest to northeast). Depth is on the y-axis in meters. Line number denotes the location of the seismic line with 1 being towards the northeast and 22 being towards the southwest.

Basin floor channels are observed in both northern and southern parts of the study area. In the northern part, channels range from ~5 m to ~ 40 m deep and ~300 m to ~1 km wide (measured from the levee crest to the deepest part of the channel). Channel width (measured levee crest to levee crest) varies little (Figure 6.2). Channel depth displays a general trend of increasing depth toward the north (away from the shelf edge) with a sudden decrease in channel depth at the northern boundary of the study area (Figure 6.2). Channels on the basin floor are leveed closer to the shelf edge and levees decrease in width and height downdip from the shelf edge (Figure 6.3). The gradient of the basin floor in the northern part of the study area from the shelf edge to the north and east has a gradient of about 7 m/km.

In the southern part of the study area, basin-floor channels range from ~3 to ~70 m deep. Channel width varies from ~300 to ~1000 m. Incision is significant within strata deposited over topographic highs formed by carbonate buildups, with channels being more frequent, wider and deeper than the basin floor. Channels display a stong relationship of increasing width with increasing depth (Figure 6.4). Width and depth decrease away form the shelf edge. Channels on the basin floor likely correlate with updip canyons and slope channels observed in the south and southwest.

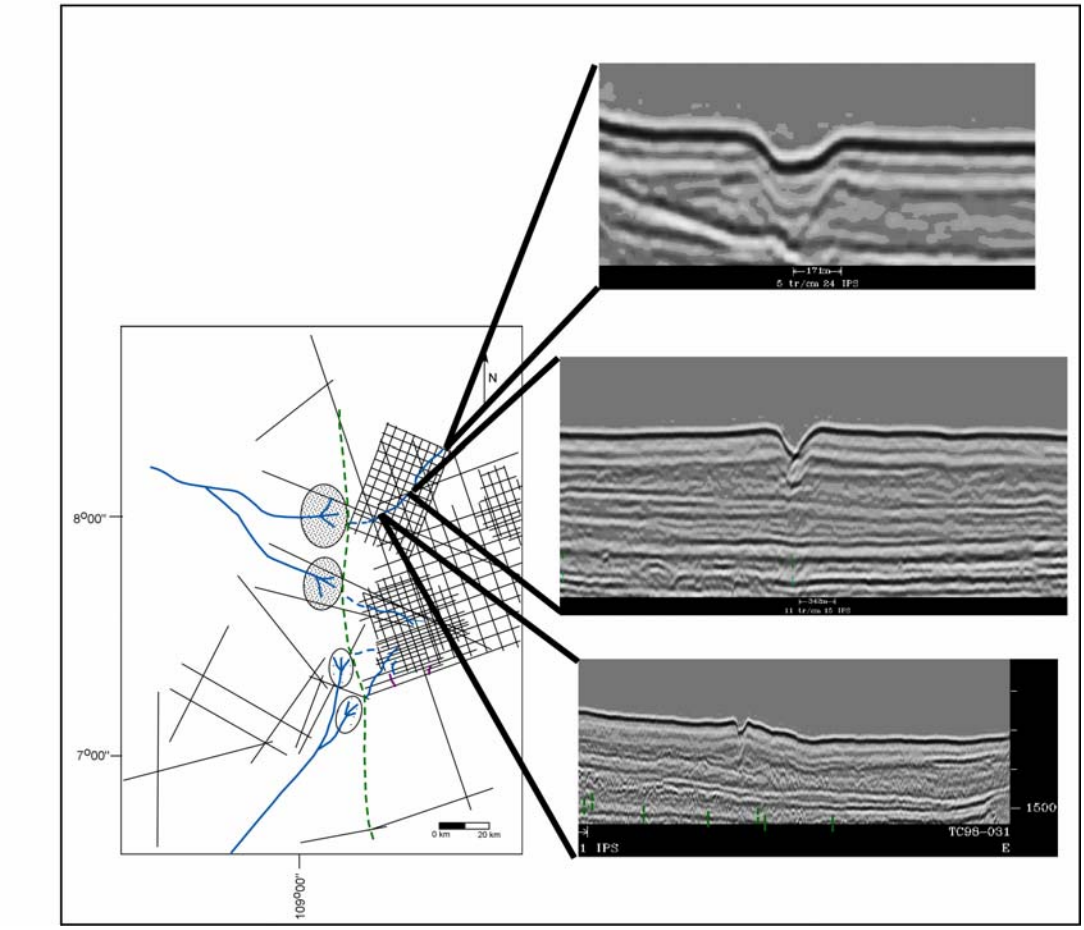


**Figure 6.3:** Levees associated with basin floor channels in the northern part of the study area decrease in width and height away from the shelf edge

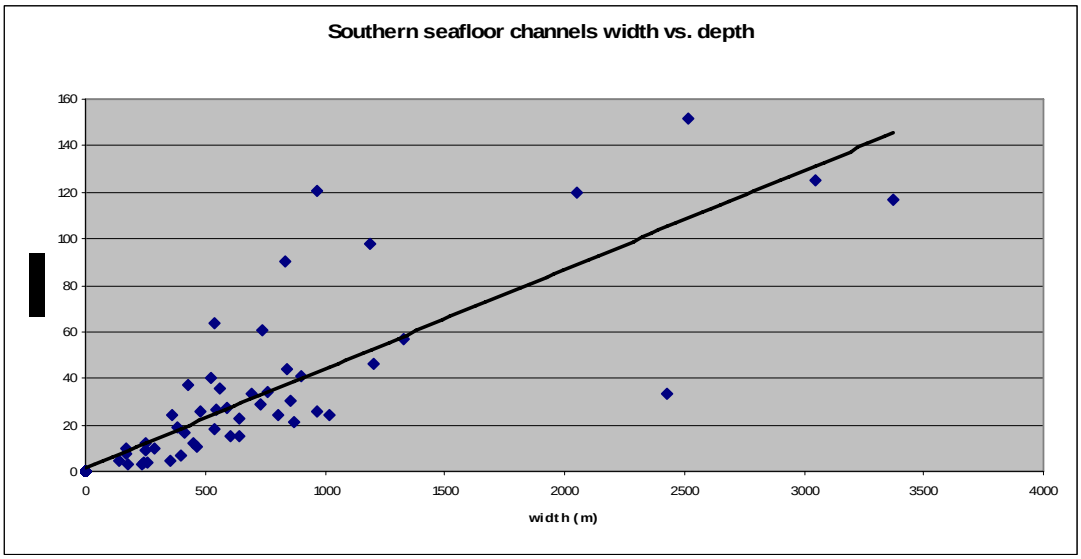


**Figure 6.4:** Depth of present-day basin floor chanels in the south increases linearly with width. Depth is on the y-axis in meters. Width is on the x-axis in meters.

# DISCUSSION

## Shelf Margin System

Sea level fall during the LGM has been reported to have been ~120 m below present sea level (e.g. Fairbanks, 1989; Roberts et al., 2004). Therefore the position of the modern offlap break of latest Pleistocene deltaic clinoforms records where sea level intersected the Vietnamese Shelf during the LGM (Wong, 2003; Roberts et al., 2004). The delta observed on the seafloor within the study area is interpreted to be related to paleo-Mekong Delta lowstand deposition during the LGM. The latest Pleistocene offlap break of paleo-Mekong Delta clinoforms is located at ~160 to ~170 m current water depth and yields an estimated sea-level fall that is ~40-50 m greater than the accepted ~120 m below present day sea level. The additional ~40-50 m water depth must be accounted for in some way.

Wong et al. (2003) studied Quaternary (570 kybp to Recent) sedimentation in the Molengraff paleo-delta in the Zengmu Basin, located on the Sunda Shelf in the southwestern SCS. These authors estimated ~50 m of subsidence over the last 20 kyrs with an average subsidence rate of 2.5 m/kyrs, which very closely matches the magnitude and rates of subsidence estimated in this study. Wong et al. (2003) attribute this ~50 m of subsidence to the combined effects of compaction and shelf edge normal faults. Wong et al. (2003) point to compaction rates of the modern Mississippi Delta ranging from 30-60 cm/100 yrs, which is comparable to the rates observed in the Zengmu Basin. Normal faults at the shelf edge observed in air gun and PARASOUND profiles in the Zengmu Basin indicate an important tectonic component also affects

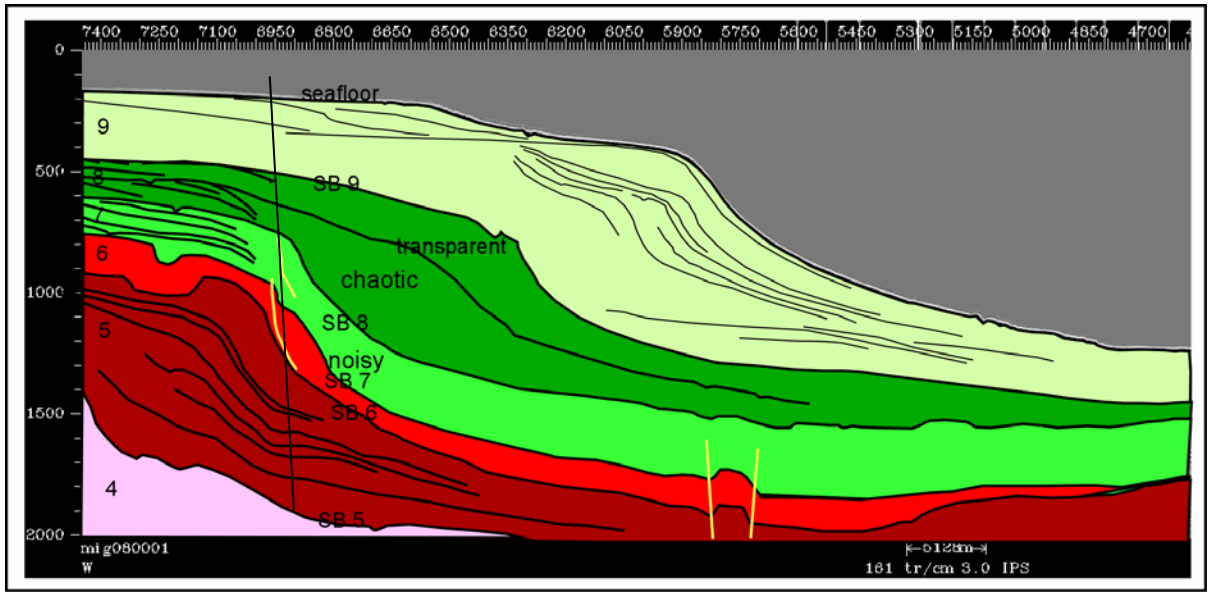


**Figure 6.5:** Seaward dipping seismic reflectors observed within middle Pleistocene strata immediately overlie a steep antecedent shelf edge, which forms a compaction hinge. Vertical black line shows the location of the antecedent shelf edge.

subsidence rates (Wong et al., 2003). Backstripping methods used by Wong et al. (2003) estimate latest Pliestocene to LGM tectonic subsidence rates on the order of 27 cm/kyrs. Wong et al. (2003) indicate that the magnitude and rates of subsidence in the Zengmu Basin is only applicable to the shelf edge and does not reflect earlier reports of tectonic stability on the Sunda Shelf.

Seaward dipping seismic reflectors are observed within older strata immediately overlying a steep antecedent shelf edge (Sequence PL3, middle Pleistocene) in the ENCSB (Figure 6.5). This relationship suggests that the location of the antecedent shelf edge in Sequence PL2 formed a compaction hinge, which resulted in rotation of strata downdip of the hinge line. A similar relationship was observed by Wong et al. (2003) within late Pleistocene age strata along areas of the Sunda Shelf to the south of the present study area. Seaward dipping reflectors are observed within late Pleistocene strata in the central part of the study area (Figure 6.6), indicating that similar compaction effects influence present-day water depth of LGM shelf edge deposits in the ENCSB.

At least part of the additional 40-50 m of water may be attributed to a pulse of rapid tectonic subsidence since the LGM. Wheeler and White (2002) report anomalous tectonic subsidence in the central and eastern Nam Con Son Basin. Wheeler and White (2002) conclude that this subsidence must have occurred in the last ten million years and calculate rates between 8 to 98 meters per million years with an average rate of 49 meters per million years. This rate is not sufficient alone to account for the ~40-50 m anomalous water depth and is significantly less than the 27 cm/kyrs reported by Wong et al. (2003). Forty to fifty meters of subsidence over the last 18,000 years suggests

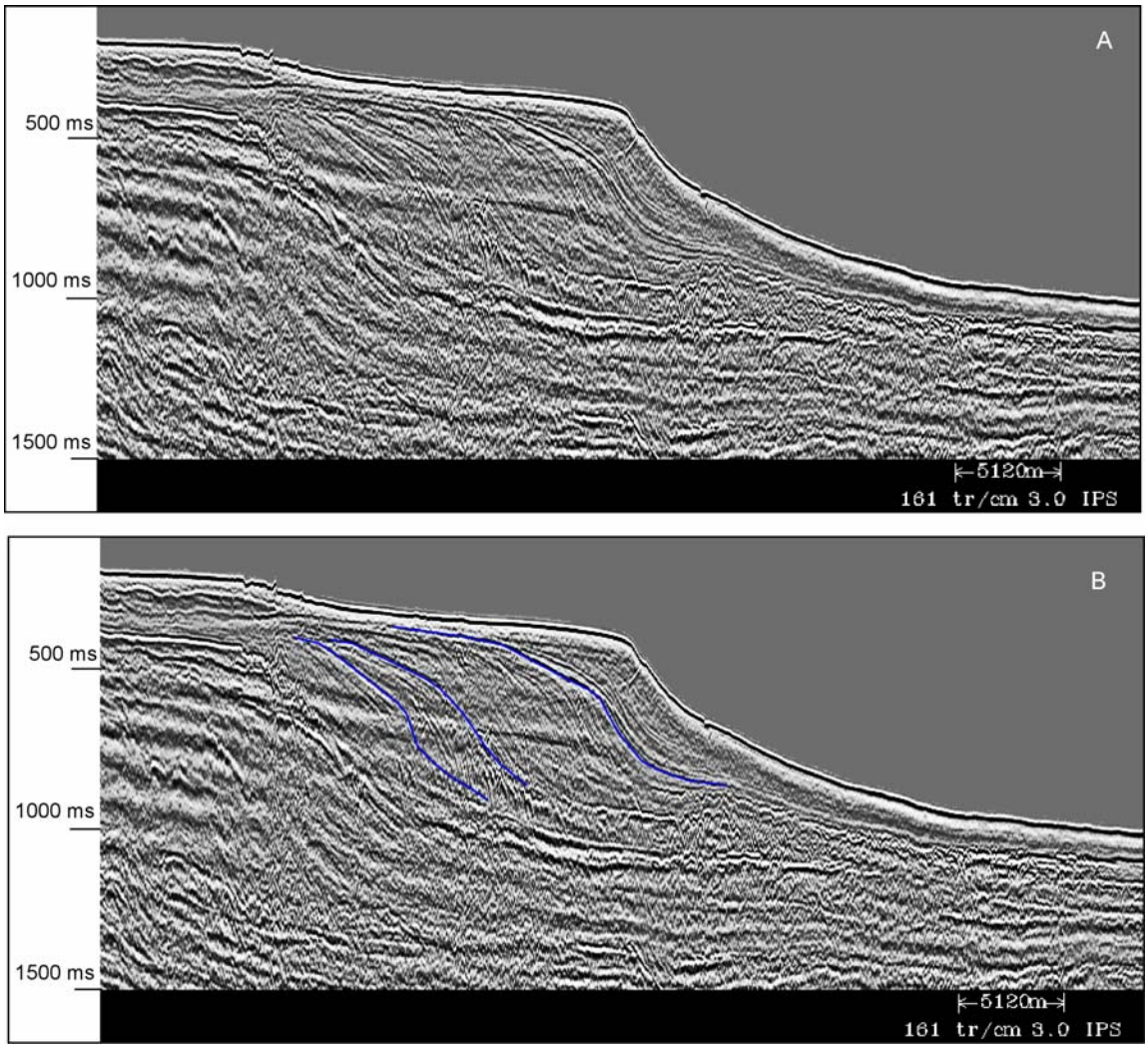


**Figure 6.6:** Seaward dipping reflectors observed within late Pleistocene strata in the central part of the study area. A) Uninterpreted seismic profile. B) Several seaward dipping reflectors have been traced in blue.

subsidence rates on the order of ~2.2 m/1000 years to ~2.7 m/ 1000 years, which correlates well with the subsidence rates determined by Wong et al. (2003). This far exceeds the calculated subsidence rates reported by Wheeler and White (2002). Thus, the current depth of the LGM deltaic wedge might reflect renewed tectonic activity in the NCSB.

The delta observed at the seafloor near the shelf margin likely records late lowstand deposition during the LGM. Hanebuth et al. (2000) and Basset et al. (2005) report rapid flooding of the Sunda Shelf after the LGM lowstand and suggest that a large meltwater pulse from the Antarctic ice sheet may have contributed to rapid post-LGM sea-level rise across the Sunda Shelf by as much as ~15 m. This meltwater pulse plus anomalous subsidence would have increased the preservation potential of the late lowstand LGM to transgressive deposits.

The southern regions of the study area are truncated by transgressive reworking over a large portion of the study area. Progradation and aggradation of the shelf edge suggest that a second sediment source, such as the Molengraaff River, was likely active on the Sunda Shelf and depositing sediment near the shelf edge during the LGM lowstand. Asymmetric ridges seen in this part of the basin are similar in character to ridges described by other authors. Wong et al. (2003) reported asymmetric erosional sand ridges on the Sunda Shelf up-dip from erosionally truncated delta wedges in a region just to the south of the present study area and interpreted these ridges as aggradational transgressive deposits. The asymmetric ridges observed in the present study are similar in shape and height and are found in similar present-day water depth as

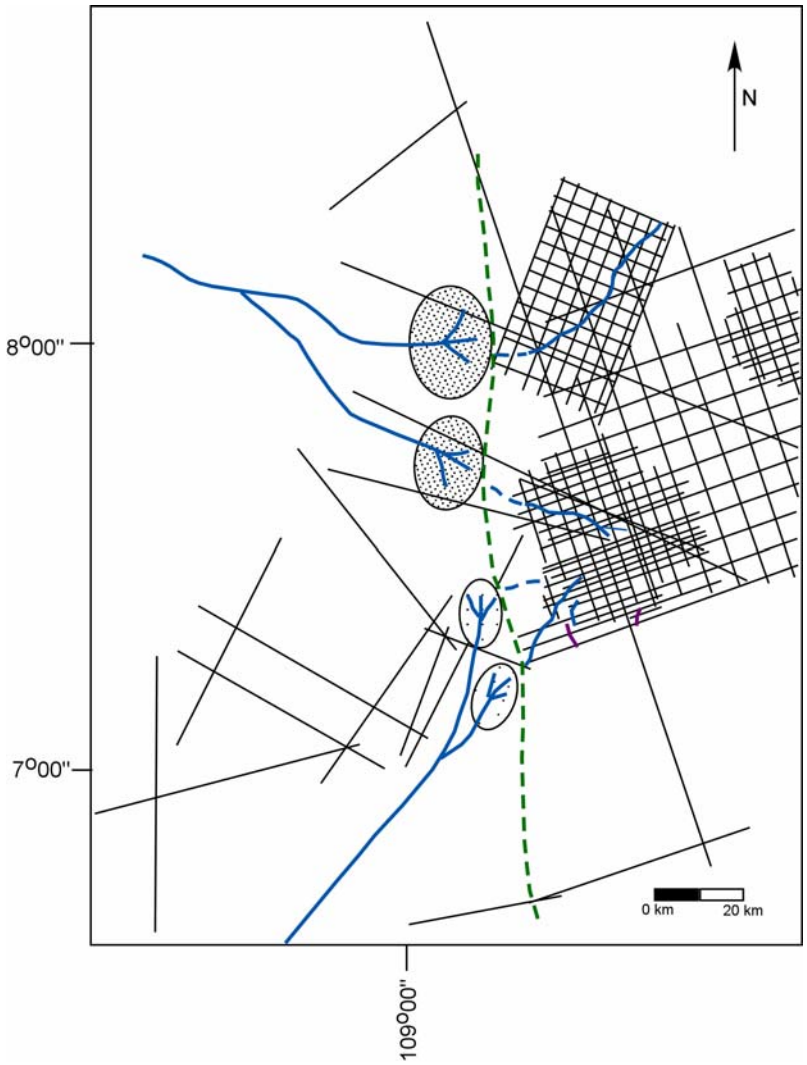


**Figure 6.7:** Illustration depicting possible depositional environments during the LGM lowstand. The paleo-Mekong River deposited sediment along the shelf edge in the northwestern part of the study area and linked to basin floor channels that extend obliquely from the shelf edge. The Molengraaff River deposits near the shelf edge in the southern part of the study area. The shelf-edge position of the Molengraaff Delta fed upper slope canyons and basin-floor channels in the south. Stippled pattern represents paleo-Mekong Belta lobes. Dot pattern represents paleo-Molengraaff Delta lobes. Green dash indicates approximate location of LGM shelf edge. Blue lines indicate channels. Purple lines represent areas of upper slope canyon incision.

those reported by Wong et al. (2003). Thus, the asymmetric sand ridges in the study area are also interpreted as early transgressive deposits that formed during the post-LGM sea-level rise.

## Seafloor Channels and Sediment Dispersal Pathways

### *Northern Shelf and Basin Floor*

The distribution of channel cross-sections on seismic profiles and relatively consistent channel widths suggest a single, deep-water trunk channel trended NE-SW, across the basin floor (Figure 6.7). Only two comparatively large width measurements might be explained by an oblique cross-section through this channel. Depth measurements record overall increasing channel depth from the southwest to the northeast away from the shelf edge with an abrupt decrease near the northeastern part of the study area. Gradients on the seafloor decrease in the northeastern part of the study area as evidenced by wider spacing of contour lines near the first location of decreasing channel depth (Figure 6.8). Flows likely accelerated downslope and onto the basin floor deeply incising and building levees. As deep-water flows approached the subtle change in gradient the efficiency of the flow decreased leading to less deeply incised channels. Levees are present in updip reaches, but levee deposits decrease in thickness and width away from the present-day shelf edge, suggesting the channel originates somewhere on the present-day slope. No up-slope canyons or shelf-edge incisions are observed in the northern part of the study area. They may be present, but are not observable due to the wide spacing between seismic lines. Sediment dispersal pathways, evidenced by fluvial

and basin floor channels, in the northern part of the study area were likely linked to the shelf-edge location of the paleo-Mekong River Delta. Sea-level fall during the LGM lowered sea-level sufficiently to bring the paleo-Mekong Delta to an outer shelf or shelf edge location (Figure 6.7).

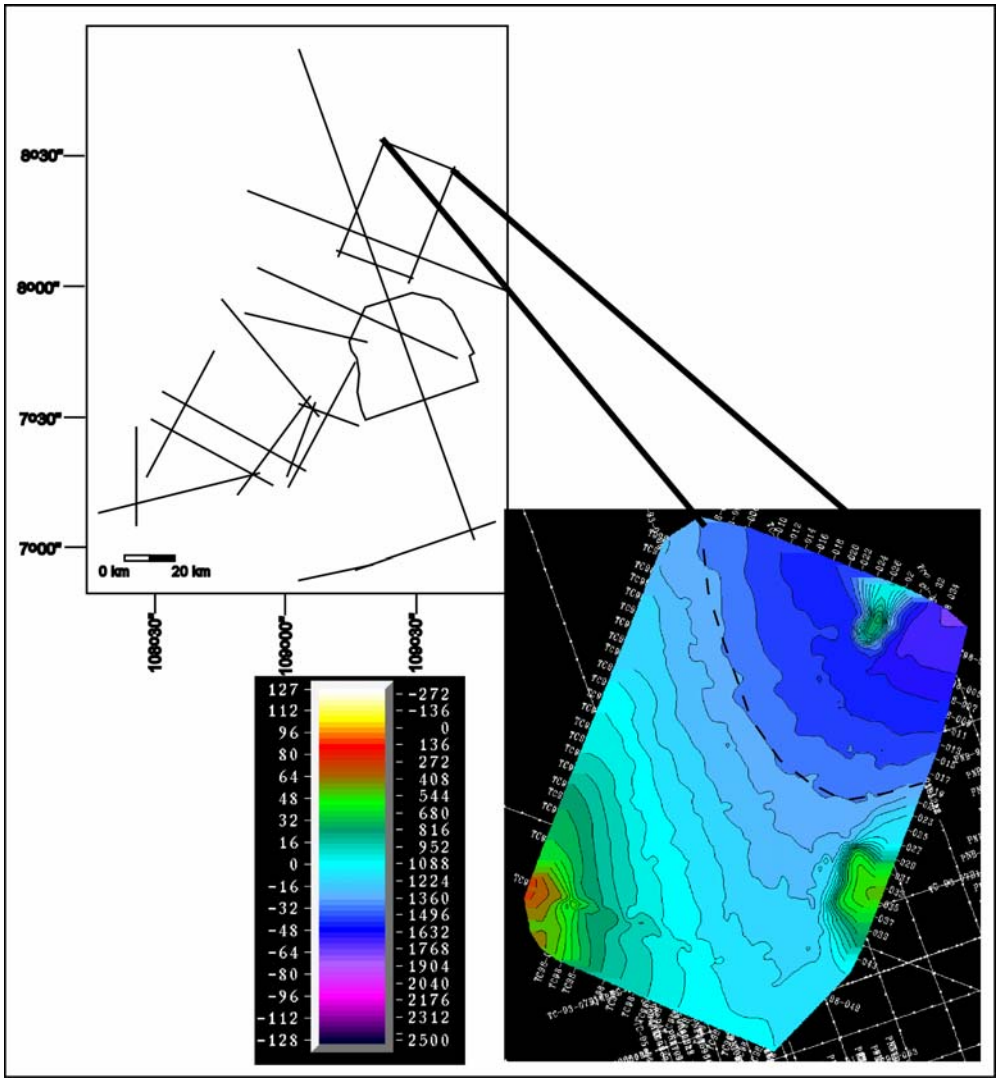


**Figure 6.8:** The gradient of the seafloor in the northern part of the study area shallows down dip. Black dashed line marks the approximate location of decreased gradient.

*Southern Shelf and Basin Floor*

Basin floor channels in the southern part of the study area cluster into two groups based on the trend of channels clusters with respect to the LGM shelf edge. The close proximity and similar trend with slope canyons up-dip suggests that basin-floor channels may have been directly linked to the up-dip canyons. One group of basin-floor channels formed close to the central shelf region and was likely linked to the paleo-Mekong Delta when the delta avulsed and delivered sediment to the slope farther south. The second group of basin-floor channels is located in the southernmost part of the study area. Channel width and depth decreases away from the shelf suggesting that flows originated from the shelf  and was likely linked to fluvial systems that flowed across the Sunda Shelf, such as the Molengraaff River, which incised the shelf during sea-level lowstands (Hanebuth et al., 2000; ) (Figure 6.7).

# CONCLUSIONS

This study focused on the depositional features and incisions on the modern seafloor in the ENCSB, offshore Vietnam. These features are believed to represent deposition and sediment dispersal patterns that were active during latest Pleistocene to Recent time, including the LGM. The Mekong River was a significant sediment source to the ENCSB during this time. The paleo-Mekong Delta was situated at the terminal shelf edge in the northwestern ENCSB and linked with a deep-water channel that flowed northeastward at an oblique angle to the LGM shelf edge.

Anomalous subsidence in the ENCSB yields depth estimates for LGM deposits that are approximately 40-50 m deeper than expected. This indicates average subsidence rates of ~2.2 m/kyr to ~2.7 m/kyr. The current depth of the LGM deltaic wedge may reflect either renewed rapid tectonic subsidence during the last 18,000 yrs, possible compaction effects, or a combination of these.

In the southwestern ENCSB, the Sunda Shelf was primarily a sediment-bypass surface during the LGM lowstand event, which is in agreement with other studies (Hanebuth et al. 2000). Channels on the basin floor can be loosely arranged into two groups based on proximity to and overall trend with up-dip canyon systems. These basin floor systems are likely related to the locations of shelf-edge deltas of the paleo-Mekong and Molengraaff Rivers during the LGM.

# CHAPTER VII

# CONCLUSIONS

The SCS is a region of significant importance in terms of the records of SE Asian tectonics, including Tibetan Plateau uplift, and the onset and evolution of the East Asian monsoon. The Mekong River, which drains the eastern Tibetan Plateau, deposits sediment in the southwestern SCS, has been a dominant sediment source since at least late Miocene time. Understanding the Pliocene to Recent stratigraphy of the paleo-Mekong Delta and associated shelf-edge deposits, offshore Vietnam, aids in understanding changes in accommodation, sea level, and sediment supply, which might then be used to interpret the long-term history of basin evolution in the NCSB.

Nine sequence boundaries and associated sequences are recognized along the early Pliocene to latest Pleistocene shelf in the ENCSB. Comparison and correlation of the Pliocene to Recent stratigraphic boundaries with published sea level curves of Wornardt et al. (2001) allow loosely defined age constraints to be assigned. Regional accommodation is controlled by shelf-edge compaction, rift-related thermal subsidence and non-rift-related anomalous subsidence, and eustatic change. More localized accommodation on the shelf is influence by avulsion of shelf margin systems and shelf edge faulting.

One of the major objectives of the study was to determine if changes in sediment flux from SE Asia could be ascertained with this data set and if this record could be used as a proxy for evaluating uplift of the eastern Tibetan Plateau and evolution of the East Asian monsoon since Early Pliocene time. It was determined that the high resolution

record of changing sediment flux from the paleo-Mekong River that was needed to make reasonably confident inferences about Tibetan Plateau uplift and changes in the East Asian monsoon could not be determined from this data set and additional data would be needed to investigate these events.

Sediment was supplied to ENCSB by two primary point sources, which are likely the paleo-Mekong River and a fluvio-deltaic system originating from the Sunda Shelf, such as the Molengraaff River. Changes in areal extent and relative thickness of Pliocene to Recent shelf-edge delta deposits reflect changes in accommodation and sediment supply over time. Changes in geographic location of shelf edge delta accumulations reflect progradation of the shelf edge during Pliocene to Recent time and avulsion of the shelf edge delta due to local sediment infilling.

This study also focused on the depositional features and incisions on the modern seafloor. These features are believed to represent deposition and sediment dispersal patterns that were active during latest Pleistocene to Recent time, including the LGM. The paleo-Mekong and Molengraaff Rivers were significant sediment sources to the ENCSB throughout latest Pleistocene time. The paleo-Mekong and Molengraaff accumulations were situated at the latest Pleistocene shelf edge in the northwestern and southwestern ENCSB at the LGM. Deep-water channels on the basin floor were likely linked to these updip fluvio-deltaic system at the LGM.

Anomalous subsidence in the ENCSB yields depth estimates for LGM deposits that are approximately 40-50 m deeper than expected, which indicates average subsidence rates of ~2.2 m/kyr to ~2.7 m/kyr. The magnitude and rates estimated in this

study closely match those by previous studies (Wong et al., 2003), both of which far exceed the calculated subsidence rate of 49 m/Myr average non-rift-related subsidence reported by Wheeler and White (2002). Thus, the current depth of the LGM deltaic wedge must reflect renewed rapid tectonic subsidence during the last 18,000 yrs, compaction effects, or a combination of these.

Future studies could include continued investigation of the evolution of the East Asian monsoon as recorded by paleo-Mekong Delta deposits during Pliocene to Recent time. Although it was determined that this data set does not include sufficient data to speculate on the history of monsoon development and strengthening, the record of monsoon evolution is likely recorded in paleo-Mekong Delta deposits. Deposits of the paleo-Mekong Delta have been used by other authors to investigate the Late Pleistocene changes in monsoon strengthening (Liu et al., 2005). It is reasonable to assume that similar processes influenced sediment supply from the paleo-Mekong Delta further in the geologic past. Additional data, however, would be needed.

Within this data set additional work could include: investigation of carbonate growth since Miocene time; the nature of interplatform fill in the eastern part of the study area where carbonate buildups are common; stratigraphic history of westward prograding systems, which are observed in the easternmost part of the data set; and detailed investigation of fault patterns on the basin floor, which may prove difficult due to poor data quality.

## REFERENCES CITED

An, Z., J.E. Kutzbach, W.L. Prell, and Porter, S.C., 2001, Evolution of Asian monsoons and phased uplift of the Himalaya-Tibetan plateau since Late Miocene times: Nature, v. 411, p. 62-66.

Beaumont, C., R.A. Jamieson, M.H. Nguyen, and S. Medvedev, 2004, Crustal channel flows: 1. Numerical models with applications to the tectonics of the Himalayan-Tibetan orogen: Journal of Geophysical research, v. 109, no. B06406, p. 1-29.

Briais, A., P.Patriat, and P. Tapponnier, 1993, Updated interpretation of magnetic anomalies and seafloor spreading stages in the South China Sea; implications for Tertiary tectonics of Southeast Asia: Journal of Geophysical Research, B, Solid Earth and Planets, v. 98, no. 4, p. 6299-6328.

Chang, C., N. Chen, M.P. Coward, W. Deng, J.F. Dewey, A. Gansser, N.B.W. Harris, C. Jin, S.F. Kidd-Williams, M.R. Leeder, H. Li, L. Jinlu, M. Houjun, P. Molnar, P.Yun, P. Yusheng, J. Pearce, R.M. Shackleton, A.B. Smith, Y. Sun, M. Ward, D.R. Watts, J. Xu, R. Xu, J. Yin, and Y. Zhang, 1986, Preliminary conclusions of the Royal Society and Academia Sinica 1985 geotraverse of Tibet: Nature, v. 323, no. 6088, p. 501-507.

Chen, M., R. Wang, L. Yang, J. Han, and J. Lu, 2003, Development of east Asian summer monsoon environments in the late Miocene: radiolarian evidence from Site 1143 of ODP Leg 184: Marine Geology, v. 201, p. 169-177.

Chung, S., M. Chu, Y. Zhang, Y. Xie, C. Lo, T. Lee, C. Lan, X. Li, Q. Zhang, and Y. Wang, 2005, Tibetan tectonic evolution inferred from spatial and temporal variations in post-collisional magmatism: Earth Science Reviews, v. 68, p. 173-196.

Clark, M.K. and L.H. Royden, 2000, Topographic ooze: Building the eastern margin of Tibet by lower crustal flow: Geology, v. 28, p. 703-706.

Clark, M.K, L.M. Schoembohm, L.M. Royden, K.X. Whipple, B.C. Burchfiel, X. Zhang, W. Tang, C. Wang, and L. Chen, 2004: Tectonics, v. 23, no. 1, TC1006 doi:10.1029/2002TC001402.

Clift, P., I.H. Campbell, M.S. Pringle, A. Carter, X. Zhang, K. Hodges, A.A. Khan, and C.M. Allen, 2004, Thermochronology of the modern Indus River bedload: New insight into the controls on the marine stratigraphic record: Tectonics, v. 23, p. TC5013, doi:10.1029/2003TC001559.

Clift, P. and C. Gaedicke, 2002, Accelerated mass flux to the Arabian Sea during the middle to late Miocene: Geology, v. 30, no. 3, p. 207-210.

Clift, P., J. Lin, and U. Barckhausen, 2002, Evidence of low flexural rigidity and low viscosity lower continental crust during continental break-up in the South China Sea: Marine and Petroleum Geology, v. 19, p. 951-970.

Dettman, D.L., X. Fang, G.N. Garzione, and J. Li, 2003, Uplift-driven climate change at 12 Ma: a long d18O record from the NE margin of the Tibetan plateau: Earth and Planetary Science Letters, v. 214, p. 267-277.

Dewey, J.F., S. Cande, and W.C. Pitman III, 1989, Tectonic evolution of the India/Eurasia Collision Zone: Eclogae Geologicae Helvetiae, v. 82, no. 3, p. 717-734.

Ding, Z.L., and S.L. Yang, 2000, C3/C4 vegetation evolution over the last 7.0 Myr in the Chinese Loess Plateau: Evidence from pedogenic carbonate d13C: Palaeogeography, Palaeoclimatology, Palaeoecology, v. 160, p. 291-299.

Fairbanks, R.G., 1989, A 17,000-year glacio-eustatic sea level record; influence of glacial melting rates on the Younger Dryas event and deep-ocean circulation; Nature, v. 342, no. 6250, p. 637-642.

Fielding, E.J., 1996, Tibet uplift and erosion: Tectonophysics, v. 260, p. 55-84.

Filipelli, G.M., 1997, Intensification of the Asian monsoon and a chemical weathering event in the late Miocene-early Pliocene; implications for late Neogene climate change: Geology v. 25, no. 1, p. 27-30.

Garzione, C.N., P.G. DeCelles, D.G. Hodkinson, T.P. Ojha, and B.N. Upreti, 2003, East-west extension and Miocene environmental change in the southern Tibetan Plateau; Thakkhola Graben, central Nepal: Geological Society of America Bulletin, v. 115, no. 1, p. 3-20.

Ginger, D.C., J. Pothecary, and R.J. Hedley, 1994, New insights into the inversion history of the West Natuna Basin, AAPG Bulletin, v. 78, no. 7, p. 1142-1143.

Guo, Z., T. Liu, N. Federoff, L. Wei, Z. Ding, N. Wu, W. Jian, and Z. An, 1998, Climate extremes in Loess of China coupled with the strength of deep-water formation in the North Atlantic: Global and Planetary Change, v. 18, p. 113-128.

Guo, Z., S. Peng, Q. Hao, P.E. Biscaye, Z. An, and T. Liu, 2004, Late Miocene-Pliocene development of Asian aridification as recorded in the Red-Earth Formation in northern China: Global and Planetary Change, v. 41, p. 135-145.

Gupta, A., 2004, The Mekong River: Morphology, evolution and paleoenvironment: Journal Geological Society of India, v. 64, p. 525-533.

Hall, R., 1996, Reconstructing Cenozoic SE Asia, *in* R. Hall and D. Blundell, eds., Tectonic evolution of southeast Asia: London, Geological Society Special Publication, v. 106, p. 153–184.

Hall, R., and C.K. Morley, 2004, Sundaland basins, *in* P. Clift, P. Wang, W. Kuhnt, and D. Hayes, eds., Continent-Ocean Interactions Within East Asian Marginal Seas: American Geophysical Union, Geophysical Monograph 149, p. 55-85.

Hamilton, W., 1979, Tectonics of the Indonesian region: U.S. Geological Survey Professional Paper 1078: Reston, VA, U. S. Geological Survey, v. 345, p.324-325.

Hanebuth, T., K. Stattegger, and P.M. Grootes, 2000, Rapid flooding of the Sunda Shelf: A late-glacial sea-level record: Science, v. 288, p. 1033-1035.

Hanebuth, T., K. Stattegger, A. Schimanski, T. Ludmann, and H.K. Wong, 2003, Late Pleistocene forced-regressive deposits on the Sunda Shelf (Southeast Asia): Marine Geology, v. 199, p. 139-157.

Harrison, T.M., P. Copeland, W.S.F. Kidd, and A. Yin, 1992, Raising Tibet: Science, v. 255, p. 1663-1667.

Harrison, T.M., A. Yin, and F.J. Ryerson, 1998, Orographic evolution of the Himalaya and Tibetan Plateau: *in* T.J Crowley and K.C. Buree, eds, Tectonic Boundary Conditions for Climate Reconstructions: Oxford, United Kingdom, Oxford University Press, p. 39-72.

Haq B. U., J. Hardenbol, and P.R. Vail, 1987, Chronology of fluctuating sea levels since the Triassic: Science, v. 235, p. 1156-1167.

Hess, S., and W. Kuhnt, 2005, Neogene and Quaternary paleoceanographic changes in the southern South China Sea (Site 1143): The benthic foraminiferal record, Marine Micropaleontology, v. 54, p. 63-87.

Holloway, N.H., 1982, North Palawan Block, Philippines, its relation to Asian mainland and role in evolution of South China Sea: AAPG Bulletin, v. 66, p. 1355-1383.

Houseman, G.A., D.P. McKenzie, and P. Molnar, 1981, Convective instability of a thickened boundary layer and its relevance for the thermal evolution of continental convergent belts: Journal of Geophysical Research B, v. 86, no. 7, p. 6115-6132.

Howes, J.V.C., 1997, Petroleum resources and petroleum systems of SE Asia, Australia, Papua New Guinea, and New Zealand: Proceedings of the petroleum systems of SE Asia and Australasia conference: Indonesian Petroleum Association, Jakarta, Indonesia, p. 81-100.

Huchon, P., X. Le Pichon, and C. Rangin, 1994, Indochina peninsula and the collision of India and Eurasia: Geology, v. 22, p. 27–30.

Huchon, P., T. N. H. Nguyen, and N. Chamot-Rooke, 1998, Finite extension across the South Vietnam basins from 3D gravimetric modeling: relation to South China Sea kinematics: Marine and Petroleum Geology, v. 15, no. 7, p. 619-634.

Jamieson, R.A., C. Beaumont, S. Medvedev, and M.H. Nguyen, 2004, Crustal channel flows: 2. Numerical models with implications for metamorphism in the Himalayan-Tibetan orogen: Journal of Geophysical Research, v. 109, no. B06407, p. 1-24.

Jolivet, L., P. Huchon, and C. Rangin, 1989, Tectonic setting of Western Pacific marginal basins: Tectonophysics, v. 160, p. 23–47.

Karig, D.E., 1971, Origin and development of marginal basins in the western Pacific: Journal of Geophysical Research, v. 76, p. 2543-2561.

Kukla, G. and Z. An, 1989, Loess stratigraphy in central China: Palaeogeography, Palaeoclimatology, Palaeoecology, v. 72, p. 203-225.

Kutzbach, J.E., W.L. Prell, and W.F. Ruddiman, 1993, Sensitivity of Eurasian climate to surface uplift of the Tibetan Plateau: The Journal of Geology, v. 101, no. 2, p. 177-190.

Lacassin, R., A. Replumaz, and P.H. Leloup, 1998, Hairpin river loops and slip-sense inversion on Southeast Asian strike-slip faults: Geology, v. 26, no. 8, p. 703-706.

Lee, G.H., K. Lee, and J.S. Watkins, 2001, Geologic evolution of the Cuu Long and Nam Con Son basins, offshore southern Vietnam, South China Sea: AAPG Bulletin, v. 85, no. 6, p. 1055-1082.

Lee, T.-Y. and L.A. Lawver, 1994, Cenozoic plate reconstructions of the South China Sea region: Tectonophysics, v. 235, p. 149–180.

LeLoup, P.H., R. Lacassin, P. Tapponnier, and T.M. Harrison, 2001, Comment on "Onset timing of left-lateral movement along the Ailao Shan-Red river shear zone: 40Ar/39Ar dating constraint from the Nam Dinh area, northeastern

Vietnam" by Wang et al., 2000. Journal of Asian Earth Sciences 18, 281-292: Journal of Asian Earth Sciences, v. 20, p. 95-99.

Li, B., J. Wang, B. Huang, Q. Li, Z. Jian, Q. Zhao, X. Su, and P. Wang, 2004, South China Sea surface water evolution over the last 12 Myr: A south-north comparison from Ocean Drilling Program Sites 1143 and 1146: Paleoceanography, v. 19, p. PA 1009, doi: 10.1029/2003PA000906.

Liu, X., J.E. Kutzbach, Z. Liu, Z. An, and L. Li, 2003, The Tibetan Plateau as amplifier of orbital-scale variability of the East Asian monsoon: Geophysical Research Letters, v. 30, no. 16, 1839, p. 1-4.

Liu, Z., C. Colin, A. Trentesaux, D. Blamart, F. Bassinot, G. Siani, and M.A. Sicre, 2004, Erosional history of the eastern Tibetan Plateau since 190 kyr ago: clay mineralogical and geochemical investigations from the southwestern South China Sea: Marine Geology, v. 209, p. 1-18.

Liu, Z., C. Colin, A. Trentesaux, G. Siani, N. Frank, D. Blamart, and S. Farid, 2005, Late Quaternary climatic control on erosion and weathering in the eastern Tibetan Plateau and the Mekong Basin: Quaternary Research, v. 63, p. 316-328.

Madon, M.B., 1997, The kinematics of extension and inversion in the Malay Basin, offshore Peninsular Malyasia: Bulletin Geological Society of Malaysia, v. 41, p. 127-138.

Matthews, S.J. and S.P. Todd, 1993, A tectonostratigraphic model for the southern Nam Con Son Basin, offshore Vietnam: Warta Geologi, v. 19, no. 6, p. 276.

Matthews, S.J., A.J Fraser, S. Lowe, S.P. Todd, and F.J. Peel, 1997, Structure, stratigraphy, and petroleum geology of the SE Nam Con Son Basin, offshore Vietnam, *in* A.J. Fraser, S.J. Matthews, and R.W. Murphy, eds., Petroleum Geology of Southeast Asia: Geological Society Special Publication, v. 126, p. 89-106.

Mitchum, R.M., P.R. Vail, and J.B. Sangree, 1977, Seismic stratigraphy and global changes of sea level, part 6: Stratigraphic interpretation of seismic reflection patterns in depositional sequences: Memoir - American Association of Petroleum Geologists, v. 26, Pages 117-133.

Molnar, P., B.C. Burchfiel, Z. Zhao, K. Liang, S. Wang, and M. Huang, 1987, Geologic evolution of northern Tibet; results of an expedition to Ulugh Muztagh: Science, v. 235, p. 299-305.

Molnar, P., P. England, and J. Martinod, 1993, Mantle dynamics, uplift of the Tibetan Plateau and the Indian monsoon: Reviews of Geophysics, v. 31, no. 4, p. 357-396.

Murphy, M.A., A. Yin, T.M. Harrison, S.B. Durr, Z. Chen, F.J. Ryerson, W.S.F. Kidd, X. Wang and X. Zhou 1997, Did the Indo-Asian collision alone create the Tibetan Plateau?: Geology, v. 25, no. 8, p. 719-722.

Murray, M.R. and S.L. Dorobek, 2004, Sediment supply, tectonic subsidence, and basin-filling patterns across the Southwestern South China Sea during Pliocene to Recent time, Continent-Ocean Interactions Within East Asian Marginal Seas: Geophysical Monograph Series 149, p. 235-253.

Normark, W.R., H. Posamentier, and E. Mutti, 2003 Turbidite systems: State of the art and future directions: Reviews of Geophysics, v. 31, no. 2, p. 91-116.

Olson, C., 2001, Timing and tectonic implications of basin inversion in the Nam Con Son basin and adjacent areas: M.S. Thesis, Texas A&M University, College Station, TX.

Olson, C. and S. Dorobek, 2000, Timing and tectonic implications of structural inversion in the Nam Con Son Basin and adjacent areas, southern South China Sea: Abstracts with Programs-Geological Society of America, v. 32, no. 7, p 237.

Oppo, D.W. and Y. Sun, 2005, Amplitude and timing of sea-surface temperature change in the northern South China Sea: Dynamic link to the East Asian monsoon: Geology, v. 33, no. 10, p. 785-788.

Peltzer, G. and P. Tapponnier, 1988, Formation and evolution of strike-slip faults, rifts, and basins during the India-Asia collision; an experimental approach: Journal of Geophysical Research, B, Solid Earth and Planets, v. 93, p. 15,085-15,117.

Powell, C.M., 1986, Continental underplating model for the rise of the Tibetan Plateau: Earth and Planetary Science Letters, v. 81, p. 79-94.

Powell, C.M., and P.J. Conaghan, 1973, Plate tectonics and the Himalayas: Earth and Planetary Science Letters, v. 20. p. 5-12.

Prell, W.L. and J.E. Kutzbach, 1992, Sensitivity of the Indian monsoon to forcing parameters and implications for its evolution: Nature, v. 360, no. 6405, p. 647-652.

Prell, W. L. and J. E. Kutzbach, 1997, The impact of Tibet-Himalayan elevation on the

sensitivity of the monsoon climate system to changes in solar radiation, *in* Ruddiman, W.E., ed. Tectonic uplift and climate change: New York, Plenum Press, p. 171-201.

Qiang, X.K., Z.X. Li, C.M. Powell, and H.B. Zheng, 2001, Magnetostratigraphic record of the Late Miocene onset of the East Asian monsoon, and Pliocene uplift of northern Tibet: Earth and Planetary Science Letters, v. 187, p. 83-93.

Rangin, C., H. Bellon, L. Benard, J. Letouzey, C. Müller, and T. Sanudin, 1990, Neogene arc-continent collision in Sabah, northern Borneo (Malaysia): Tectonophysics v. 183, p. 305–319.

Raymo, M.E. and W.F. Ruddiman, 1992, Tectonic forcing of late Cenozoic climate: Nature, v. 359, p. 117-122.

Replumaz, A., R. Lacassin, P. Tapponnier, and P.H. Leloup, 2001, Large river offsets and Plio-Quaternary dextral slip rate on the Red River Fault (Yunnan, China) : Journal of Geophysical Research, B, Solid Earth and Planets, v. 106, no. 1, p. 819-836.

Roberts, A., L.S. Goh, M.D. Jong, H. Veltmeyer, R. Hooper, 1999, Quantitative analysis of structural development and subsidence in the Nam Con Son Basin, offshore Vietnam: Differential stretching ahead of a propagating ocean? AAPG International Conference and Exhibition, p. 432-434.

Roberts, H.H., R.H. Fillon, B. Kohl, J.M. Robalin, and J.C. Sydow, 2004, Depositional architecture of the Lagniappe Delta; sediment characteristics, timing of depositional events, and temporal relationship with adjacent shelf-edge deltas: Special Publication-Society for Sedimentary Geology, v. 79, p. 143-188.

Royden, L.H., B.C. Burchfiel, R.W. King, E. Wang, Z. Chen, F. Shen, and Y. Liu, 1997, Surface deformation and lower crustal flow in eastern Tibet: Science, v. 276, p. 788-790.

Ruddiman, W.F and J.E. Kutzbach, 1991, Plateau uplift and climate change: Scientific American, v. 264, no. 3, p. 66-75.

Ruddiman, W.F., M.E. Raymo, W.L. Prell, and J.E. Kutzbach, 1997, The climate-uplift connection: A synthesis: Tectonic Uplift and Climate Change, p. 471-515.

Schimanski, A. and K. Statteger, 2005, Deglacial and Holocene evolution of the Vietnam shelf:stratigraphy, sediments and sea-level change: Marine Geology, v. 214, p. 365-387.

Schluter, H.U., K. Hinz, and M. Block, 1996, Tectono-stratigraphic terranes and detachment faulting of the South China Sea and Sulu Sea: Marine Geology, v. 130, p. 39-78.

Su, D., N. White, and D. McKenzie, 1989, Extension and subsidence of the Pearl River mouth basin, northern South China Sea: Basin Research, v. 2, no. 4, p. 205-222.

Sun, J. and T. Liu, 2000, Stratigraphic evidence for uplift of the Tibetan Plateau between ~1.1 and ~0.9 myr ago: Quaternary Research, v. 54, p. 309-320.

Sun, X. and P. Wang, 2005, How old is the Asian monsoon system?-Paleobotanical records from China: Palaeogeography, Palaeoclimatology, Palaeoecology, v. 222, p. 181-222.

Tapponnier, P., G. Peltzer, A.Y. Le Dain, R. Armijo, P. Cobbold, 1982, Propagating extrusion tectonics in Asia: New insights from simple experiments with plasticine: Geology, v. 10, p. 611-616.

Tapponnier, P., G. Peltzer, and R. Armijo, 1986, On the mechanics of the collision between India and Asia, *in* M.P. Coward, and A.C. Ries, eds., Collision Tectonics, Geological Society Special Publication 19, p. 115-157.

Tapponnier, P., X. Zhiqin, F. Roger, B. Meyer, N. Arnaud, G. Wittlinger, and Y. Jingsui, 2001, Oblique stepwise rise and growth of the Tibet Plateau: Science, v. 294, p. 1671-1677.

Taylor, B., and D. E. Hayes, 1983, Origin and history of the South China Sea Basin, *in* D. E. Hayes, ed., Tectonic and geologic evolution of southeast Asian seas and islands: Union Geophysical Monographs, p. 23-56.

Thi, K., N.Van Lap, I. Kobayashi, M. Tateishi, and Y. Saito, 2001, Late Pleistocene-Holocene stratigraphy and delta progradation, the Mekong River delta, south Vietnam: Gondwana Research, v. 4, no. 4, p. 799-800.

Tian, J., P. Wang, and X. Cheng, 2004, Development of the East Asian monsoon and Northern Hemisphere glaciation: Oxygen isotope records from the South China Sea: Quaternary Science Reviews, v. 23, p. 2007-2016.

Tija, H.D., 1994, Inversion tectonics in the Malay Basin: Evidence and timing of events, Geological Society of Malaysia Bulletin, v. 36, p. 119-126.

Tjia, H. D., and K. K. Liew, 1996, Changes in tectonic stress field in northern Sunda Shelf basins, *in* R. Hall, and D. J. Blundell, eds., Tectonic evolution of Southeast

Asia: Geological Society Special Publications, London, Geological Society of London, p. 291-306.

Van Wagoner, J.C., R.M. Mitchum, K.M. Campion, and V.D. Rahmanian, 1990, Siliciclastic sequence stratigraphy in well logs, cores, and outcrops: Concepts for high-resolution correlation of time and facies: AAPG Methods in Exploration, series 7, p. 1-55.

Wang, L., M. Sarnthein, H. Erlenkeusser, J. Grimalt, P. Grootes, S. Heilig, E. Ivanova, M. Kienast, C. Pelejero, and U. Pfaumann, 1999, East Asian monsoon climate during the Late Pleistocene: High-resolution sediment records from the South China Sea: Marine Geology, v. 156, p. 245-284.

Wang, L.W., and H.L. Lin, 2004. Data report: Carbonate and organic carbon contents of sediments from Sites 1143 and 1146 in the South China Sea. *In* W.L. Prell, P. Wang, P. Blum, D.K. Rea, and S.C. Clemens, (Eds.), Proc. ODP, Sci. Results, 184 [Online], <http://www.odp.tamu.edu.ezproxy.tamu.edu:2048/publications/184_SR/207/207.htm>.

Wang, P., W.L. Prell, P. Blum, 2000, Leg 184 summary: Exploring the Asian monsoon through drilling in the South China Sea: Proceedings of the Ocean Drilling Program, Initial Reports, v. 184, p. 1-76.

Wang, P., Z. Jian, Q. Zhao, Q. Li, R. Wang, Z. Liu, G. Wu, L. Shao, J. Wang, B. Huang, D. Fang, J. Tian, J. Li, X. Li, G. Wei, X. Sun, Y. Luo, X. Su, S. Mao, and M. Chen, 2003, Evolution of the South China Sea and monsoon history revealed in deep-sea records: Chinese Science Bulletin, v. 48, no. 23, p. 2549-2561.

Wang, Y. and T. Deng, 2005, A 25 m.y. isotopic record of paleodiet and environment change from fossil mammals and paleosols from the NE margin of the Tibetan Plateau: Earth and Planetary Science Letters, v. 236, p. 322-338.

Wehausen, R. and H.J. Brumsack, 2002, Astronomical forcing of the East Asian monsoon mirrored by the composition of Pliocene South China Sea sediments: Earth and Planetary Science Letters, v. 201, p. 621-636.

Wehausen, R., J. Tian, H.J. Brumsack, C. Xinrong, and P. Wang, 2003, Geochemistry of Pliocene sediments from ODP Site 1143 (southern South China Sea), *in* W.L. Prell, P. Wang, P. Blum, D.K. Rea, and S.C. Clemens, (Eds.), Proc. ODP, Sci. Results, 184 [Online]. Available from World Wide Web: <http://www.odp.tamu.edu.ezproxy.tamu.edu:2048/publications/184_SR/201/201.htm>.

Wheeler, P. and N. White, 2002, Measuring dynamic topography: An analysis of Southeast Asia: Tectonics, v. 21, no. 5, p. 1-26.

Willett, S.D. and C. Beaumont, 1994, Subduction of Asian lithospheric mantle beneath Tibet inferred from models of continental collision: Nature, v. 369, p. 642-645.

Wong, H.K., T. Ludmann, C. Haft, A. Paulsen, C. Hubscher, and J. Geng, 2003, Quaternary sedimentation in the Molengraaff paleo-delta, northern Sunda Shelf (southern South China Sea): Topical Deltas of Southeast Asia-Sedimentology, Stratigraphy, and Petroleum Geology, SEPM Special Publication No. 76, p. 201-216.

Wornardt, W.W., B. Shaffer, and P.R. Vail, 2002, Revision of the Late Miocene, Pliocene and Pleistocene sequence cycles: Gulf Coast Assoc. of Geological Societies Transactions, v. L1, p. 477-481.

Xiong, S.F., S.L. Ding, W.Y. Jian, S.L. Yang, and T.S. Liu, 2003, Initial intensification of East Asian winter monsoon at about 2.75 Ma as seen in the Chinese eolian loess-red clay deposit: Geophysical Research Letters, v. 30, no. 10, doi:10.1029/2003GL017059,2003.

Yarbrough, C., 2005, Pliocene to Recent Stratigraphy of the Cuu Long and Nam Con Son Basins, Offshore Vietnam, M.S. Thesis, Texas A&M Universtiy, College Station, TX.

Yin, A.T.M., T.M. Harrison, F.J. Ryerson, W. Chen, W.S.F. Kidd, and P. Copeland, 1994, Tertiary structural evolution of the Gangdese thrust system, southeastern Tibet: Journal of Geophysical Research, v. 99, no. 18, p. 201.

Zheng, H., C.M. Powell, D.K. Rea, J. Wang, and P. Wang, 2004, Late Miocene and mid-Pliocene enhancement of the East Asian monsoon as viewed from the land and sea: Global and Planetary Change, v. 41, p. 147-155.

Zhou, D.A., 1994, Cenozoic rifting and seafloor spreading of the South China Sea region independent of Indochina extrusion: AAPG Annual convention, p. 290.

Zhou, D., K. Ru, and H. Chen, 1995 , Kinematics of Cenozoic extension on the South China Sea continental margin and its implications for the tectonic evolution of the region: Tectonophysics, v. 251, p. 161-177.

Zhao, W. and W.J. Morgan, 1985, Uplift of the Tibetan Plateau: Tectonics, v. 4, p. 359-369.

Zhao, W. and W.J. Morgan, 1987, Injection of Indian crust into Tibetan lower crust; a

two-dimensional finite element model study: Tectonics, v. 6, no. 4, p. 489-504.

# APPENDIX A

## CHANNEL MEASUREMENT DATA

| | | x1 | x2 | width (m) | d1 | d2 | depth (ms) | depth (m) TWT | depth (m)OWT |
|---|---|---|---|---|---|---|---|---|---|
| northern region NS | line | | | | | | | | |
| | tc98001 | 346595 | 346904.7 | 309.7 | 1688.8 | 1710.4 | 21.6 | 32.4 | 16.2 |
| | tc98003 | 345372 | 345861.2 | 489.26 | 1654.67 | 1694.67 | 40 | 60 | 30 |
| | tc98005 | 343778.3 | 344256.9 | 478.59 | 1621 | 1670 | 49 | 73.5 | 36.75 |
| | tc98007 | 341438.1 | 342126.7 | 688.54 | 1580 | 1633 | 53 | 79.5 | 39.75 |
| | tc98009 | 339225 | 340186.4 | 961.39 | 1539.2 | 1596 | 56.8 | 85.2 | 42.6 |
| | tc98011 | 338860.9 | 339327.5 | 466.6 | 1533.6 | 1567.2 | 33.6 | 50.4 | 25.2 |
| | tc98013 | 336980.2 | 337353.5 | 373.31 | 1507 | 1535 | 28 | 42 | 21 |
| | tc98013 | 337353.5 | 337890 | 536.49 | 1508 | 1535 | 27 | 40.5 | 20.25 |
| | tc98015 | 335897.5 | 336550.6 | 653.13 | 1480 | 1519 | 39 | 58.5 | 29.25 |
| | tc98017 | 334536.7 | 334932.5 | 395.79 | 1460 | 1502 | 42 | 63 | 31.5 |
| | tc98019 | 333958 | 334436.8 | 478.76 | 1433 | 1480 | 47 | 70.5 | 35.25 |
| | tc98021 | 333708 | 334104.8 | 396.84 | 1408 | 1445 | 37 | 55.5 | 27.75 |
| | tc98023 | 332742 | 333267.7 | 525.7 | 1383 | 1425 | 42 | 63 | 31.5 |
| | tc98025 | 330968.1 | 331399.7 | 431.55 | 1357 | 1379 | 22 | 33 | 16.5 |
| | tc98027 | 329675.4 | 330306.5 | 631.13 | 1324 | 1357 | 33 | 49.5 | 24.75 |
| | tc98029 | 327597.3 | 328542.3 | 945.01 | 1293 | 1319 | 26 | 39 | 19.5 |
| | tc98031 | 326886 | 327317.1 | 431.1 | 1268 | 1292 | 24 | 36 | 18 |
| | tc98033 | 325054.8 | 325556.4 | 501.59 | 1243 | 1272 | 29 | 43.5 | 21.75 |
| | tc98035 | 322939.7 | 323454.1 | 514.45 | 1200 | 1221 | 21 | 31.5 | 15.75 |
| | tc98037 | 319990.4 | 320527 | 536.56 | 1149 | 1161 | 12 | 18 | 9 |
| | tc98039 | 318793.6 | 319388.3 | 594.63 | 1128 | 1142 | 14 | 21 | 10.5 |
| | tc98041 | 316734.9 | 317346.9 | 611.92 | 1092.8 | 1108.8 | 16 | 24 | 12 |
| | tc98043 | 0 | 0 | 0 | 0 | 0 | 0 | 0 | 0 |
| | tc98049 | 0 | 0 | 0 | 0 | 0 | 0 | 0 | 0 |

| | | | | | | | | | |
|---|---|---|---|---|---|---|---|---|---|
| southern region NS | tc98063 | 0 | 0 | 0 | 0 | 0 | 0 | 0 | 0 |
| | pnt9503RE | 0 | 0 | 0 | 0 | 0 | 0 | 0 | 0 |
| | tc98065 | 0 | 0 | 0 | 0 | 0 | 0 | 0 | 0 |
| | tc9809B2W | 0 | 0 | 0 | 0 | 0 | 0 | 0 | 0 |
| | tc98067 | 0 | 0 | 0 | 0 | 0 | 0 | 0 | 0 |
| | pnt9507R | 0 | 0 | 0 | 0 | 0 | 0 | 0 | 0 |
| | tc98069 | 0 | 0 | 0 | 0 | 0 | 0 | 0 | 0 |
| | pnt9509 | 0 | 0 | 0 | 0 | 0 | 0 | 0 | 0 |
| | tc98071 | 0 | 0 | 0 | 0 | 0 | 0 | 0 | 0 |
| | pnt9511 | 0 | 0 | 0 | 0 | 0 | 0 | 0 | 0 |
| | tc9309B3 | 0 | 0 | 0 | 0 | 0 | 0 | 0 | 0 |
| | tc98075 | 0 | 0 | 0 | 0 | 0 | 0 | 0 | 0 |
| | pnt9515 | 0 | 0 | 0 | 0 | 0 | 0 | 0 | 0 |
| | tc98077 | 0 | 0 | 0 | 0 | 0 | 0 | 0 | 0 |
| | pnt95017 | 0 | 0 | 0 | 0 | 0 | 0 | 0 | 0 |
| | tc98079 | 0 | 0 | 0 | 0 | 0 | 0 | 0 | 0 |
| | pnt9519r | 0 | 0 | 0 | 0 | 0 | 0 | 0 | 0 |
| | tc98081 | 0 | 0 | 0 | 0 | 0 | 0 | 0 | 0 |
| | tc93011 | 0 | 0 | 0 | 0 | 0 | 0 | 0 | 0 |
| | tc98083 | 0 | 0 | 0 | 0 | 0 | 0 | 0 | 0 |
| | pnt9523 | 0 | 0 | 0 | 0 | 0 | 0 | 0 | 0 |
| | tc98085 | 0 | 0 | 0 | 0 | 0 | 0 | 0 | 0 |
| | pnt9525 | 0 | 0 | 0 | 0 | 0 | 0 | 0 | 0 |
| | tc98087 | 338374.7 | 338516.9 | 142.14 | 1058 | 1064 | 6 | 9 | 4.5 |
| | | 339192 | 339369.7 | 177.73 | 1055.2 | 1059.2 | 4 | 6 | 3 |
| | pnt9527 | 0 | 0 | 0 | 0 | 0 | 0 | 0 | 0 |
| | tc98089 | 0 | 0 | 0 | 0 | 0 | 0 | 0 | 0 |
| | tc9311B1 | 0 | 0 | 0 | 0 | 0 | 0 | 0 | 0 |
| | pnt9531RE | 325273.6 | 325535.5 | 261.83 | 950 | 954.67 | 4.67 | 7.005 | 3.5025 |
| | pnt9533 | 0 | 0 | 0 | 0 | 0 | 0 | 0 | 0 |
| | pnt9535R | 0 | 0 | 0 | 0 | 0 | 0 | 0 | 0 |
| | tc9311B2W | 361472.4 | 363900 | 2427.6 | 1157 | 1201 | 44 | 66 | 33 |
| | | 364115.4 | 364971.8 | 856.4 | 1154 | 1194 | 40 | 60 | 30 |

| | | | | | | | | | |
|---|---|---|---|---|---|---|---|---|---|
| southern (cont.) | pnt9539 | 347350.6 | 348317.4 | 966.8 | 1032 | 1066.67 | 34.67 | 52.005 | 26.0025 |
| | tc9511A11R | | | 0 | | | 0 | 0 | 0 |
| | tc9511A1 | 322768 | 323603.2 | 835.2 | 819 | 939 | 120 | 180 | 90 |
| | tc9311B3ARE | 314641.2 | 315109.6 | 468.4 | 659 | 673 | 14 | 21 | 10.5 |
| | | 321040.4 | 324414.1 | 3373.7 | 796 | 952 | 156 | 234 | 117 |
| | tc9511B3RE | 321073 | 324556.8 | 3483.8 | | | | | 180 |
| | | 324663 | 325445.6 | 782.6 | | | 0 | 0 | 108 |
| | | 331337 | 332540 | 1203 | | | 0 | 0 | 92 |
| | | 332646 | 333797 | 1151 | | | 0 | 0 | 132 |
| | tc9311B3RE | 312643 | 313971.8 | 1328.8 | 535 | 610.67 | 75.67 | 113.505 | 56.7525 |
| | | 316760.3 | 317365 | 604.7 | 594.67 | 614.67 | 20 | 30 | 15 |
| | | 320458.9 | 321330.5 | 871.6 | 756 | 784 | 28 | 42 | 21 |
| | | 321446.5 | 323963.8 | 2517.3 | 704 | 906.67 | 202.67 | 304.005 | 152.0025 |
| | | 325469.8 | 325948.2 | 478.4 | 737.33 | 772 | 34.67 | 52.005 | 26.0025 |
| | | 326341 | 326880.5 | 539.5 | 769.33 | 854.67 | 85.34 | 128.01 | 64.005 |
| | | 327562.8 | 328084.2 | 521.4 | 742 | 796 | 54 | 81 | 40.5 |
| | | 328647.4 | 329237.6 | 590.2 | 730.67 | 766.67 | 36 | 54 | 27 |
| | | 332289.5 | 333091 | 801.5 | 706.67 | 738.67 | 32 | 48 | 24 |
| | | 333173.6 | 333423.2 | 249.6 | 708 | 724 | 16 | 24 | 12 |
| | | 334252 | 334678.5 | 426.5 | 718 | 768 | 50 | 75 | 37.5 |
| | | 336065 | 336236.2 | 171.2 | 697.33 | 710.67 | 13.34 | 20.01 | 10.005 |
| | | 337384.4 | 337925.1 | 540.7 | 697.3 | 721.33 | 24.03 | 36.045 | 18.0225 |
| | tc9511A3RE | 335131 | 335866.4 | 735.4 | 705.33 | 786.67 | 81.34 | 122.01 | 61.005 |
| | tc93013T | 312678.6 | 313693.6 | 1014.99 | 497.33 | 529.33 | 32 | 48 | 24 |
| | | 313873.3 | 314274.8 | 401.46 | 500 | 509.33 | 9.33 | 13.995 | 6.9975 |
| | | 314980.4 | 315223.1 | 242.74 | 505.33 | 510.67 | 5.34 | 8.01 | 4.005 |
| | | 315294.3 | 315748.1 | 453.87 | 509.33 | 525.33 | 16 | 24 | 12 |
| | | 315829.7 | 316469.5 | 639.81 | 521.33 | 552 | 30.67 | 46.005 | 23.0025 |
| | | 318369.3 | 318783.5 | 414.17 | 566.67 | 589.33 | 22.66 | 33.99 | 16.995 |
| | | 322898.1 | 324952.2 | 2054.19 | 696 | 856 | 160 | 240 | 120 |
| | | 327107 | 327835.3 | 728.28 | 690.67 | 729.33 | 38.66 | 57.99 | 28.995 |
| | | 328835.3 | 329195.6 | 360.24 | 772 | 804 | 32 | 48 | 24 |
| | | 329264.6 | 329959.9 | 695.31 | 776 | 820 | 44 | 66 | 33 |
| | | 334162.5 | 335061.4 | 898.99 | 688 | 742.67 | 54.67 | 82.005 | 41.0025 |
| | | 335144.8 | 335706 | 561.19 | 689.33 | 737.33 | 48 | 72 | 36 |
| | | 335802 | 336158 | 356 | 733.67 | 740 | 6.33 | 9.495 | 4.7475 |

# APPENDIX B

## SHELF EDGE THICKNESS DATA

| PL4 shelf edge thickness | | | |
|---|---|---|---|
| line | z1 (m) | z2 (m) | z2-z1 (m) |
| TC98-041 | 428 | 1240 | 812 |
| TC98-055 | 420 | 1132 | 712 |
| TC98-057 | 408 | 968 | 560 |
| Seas95-15-2 | 0 | 0 | 0 |
| vn-06-45 | 0 | 0 | 0 |
| vn-06-57 | 0 | 0 | 0 |
| Seas95-01-2A | 0 | 0 | 0 |
| Seas95-15-1 | 0 | 0 | 0 |
| vn-06-08 | 428 | 776 | 348 |
| Seas95-01-1 | 0 | 0 | 0 |
| TC93-11B1WT | 472 | 880 | 408 |
| vn-06-44 | 0 | 0 | 0 |
| Seas95-01-3 | 0 | 0 | 0 |
| Seas95-13-12 | 0 | 0 | 0 |
| | | | |
| PL3 shelf edge thickness | | | |
| line | z1 (m) | z2 (m) | z2-z1 (m) |
| TC98-041 | 688 | 1344 | 656 |
| TC98-055 | 656 | 1315 | 659 |
| TC98-057 | 692 | 1232 | 540 |
| Seas95-15-2 | 0 | 0 | 0 |
| vn-06-45 | 0 | 0 | 0 |
| vn-06-57 | 0 | 0 | 0 |
| Seas95-01-2A | 0 | 0 | 0 |
| Seas95-15-1 | 0 | 0 | 0 |
| vn-06-08 | 608 | 1216 | 348 |
| Seas95-01-1 | 624 | 1024 | 400 |
| TC93-11B1WT | 664 | 1236 | 572 |
| vn-06-44 | 0 | 0 | 0 |
| Seas95-01-3 | 0 | 0 | 0 |
| Seas95-13-12 | 0 | 0 | 0 |

PL2 shelf edge thickness

| line | z1 (m) | z2 (m) | z2-z1 (m) | |
|---|---|---|---|---|
| TC98-041 | 792 | 1084 | 292 | |
| TC98-055 | 832 | 992 | 160 | faulted |
| TC98-057 | 860 | 1304 | 444 | |
| Seas95-15-2 | 0 | 0 | 0 | |
| vn-06-45 | 0 | 0 | 0 | |
| vn-06-57 | 0 | 0 | 0 | |
| Seas95-01-2A | 0 | 0 | 0 | |
| Seas95-15-1 | 0 | 0 | 0 | |
| vn-06-08 | 824 | 1428 | 604 | |
| Seas95-01-1 | 780 | 1348 | 568 | |
| TC93-11B1WT | 0 | 0 | 0 | |
| vn-06-44 | 0 | 0 | 0 | |
| Seas95-01-3 | 0 | 0 | 0 | |
| Seas95-13-12 | 0 | 0 | 0 | |

PL1 shelf edge thickness

| line | z1 (m) | z2 (m) | z2-z1 (m) |
|---|---|---|---|
| TC98-041 | 1060 | 1276 | 216 |
| TC98-055 | 1012 | 1352 | 340 |
| TC98-057 | 1056 | 1520 | 464 |
| Seas95-15-2 | 0 | 0 | 0 |
| vn-06-45 | 892 | 1120 | 228 |
| vn-06-57 | 0 | 0 | 0 |
| Seas95-01-2A | 0 | 0 | 0 |
| Seas95-15-1 | 1020 | 1316 | 296 |
| vn-06-08 | 824 | 1424 | 600 |
| Seas95-01-1 | 0 | 0 | 0 |
| TC93-11B1WT | 0 | 0 | 0 |
| vn-06-44 | 0 | 0 | 0 |
| Seas95-01-3 | 0 | 0 | 0 |
| Seas95-13-12 | 0 | 0 | 0 |

P5 shelf edge thickness

| line | z1 (m) | z2 (m) | z2-z1 (m) |
|---|---|---|---|
| TC98-041 | 1032 | 1464 | 432 |
| TC98-055 | 1152 | 1400 | 248 |
| TC98-057 | 1188 | 1512 | 324 |
| Seas95-15-2 | 0 | 0 | 0 |
| vn-06-45 | 924 | 1456 | 532 |
| vn-06-57 | 0 | 0 | 0 |
| Seas95-01-2A | 960 | 1436 | 476 |
| Seas95-15-1 | 960 | 1448 | 488 |
| vn-06-08 | 0 | 0 | 0 |
| Seas95-01-1 | 0 | 0 | 0 |
| TC93-11B1WT | 0 | 0 | 0 |
| vn-06-44 | 0 | 0 | 0 |
| Seas95-01-3 | 0 | 0 | 0 |
| Seas95-13-12 | 0 | 0 | 0 |

P4 shelf edge thickness

| line | z1 (m) | z2 (m) | z2-z1 (m) |
|---|---|---|---|
| TC98-041 | 1280 | 1588 | 308 |
| TC98-055 | 1244 | 1552 | 308 |
| TC98-057 | 1232 | 1328 | 96 |
| Seas95-15-2 | 1220 | 1380 | 160 |
| vn-06-45 | 1092 | 1308 | 216 |
| vn-06-57 | 0 | 0 | 0 |
| Seas95-01-2A | 1104 | 1404 | 300 |
| Seas95-15-1 | 0 | 0 | 960 |
| vn-06-08 | 0 | 0 | 0 |
| Seas95-01-1 | 0 | 0 | 0 |
| TC93-11B1WT | 0 | 0 | 0 |
| vn-06-44 | 0 | 0 | 0 |
| Seas95-01-3 | 0 | 0 | 0 |
| Seas95-13-12 | 0 | 0 | 0 |

P3 shelf edge thickness

| line | z1 (m) | z2 (m) | z2-z1 (m) |
|---|---|---|---|
| TC98-041 | 1312 | 1528 | 216 |
| TC98-055 | 0 | 0 | 0 |
| TC98-057 | 0 | 0 | 0 |
| Seas95-15-2 | 1336 | 1672 | 336 |
| vn-06-45 | 1324 | 1580 | 256 |
| vn-06-57 | 0 | 0 | 0 |
| Seas95-01-2A | 1316 | 1556 | 240 |
| Seas95-15-1 | 0 | 0 | 0 |
| vn-06-08 | 0 | 0 | 0 |
| Seas95-01-1 | 0 | 0 | 0 |
| TC93-11B1WT | 0 | 0 | 0 |
| vn-06-44 | 0 | 0 | 0 |
| Seas95-01-3 | 0 | 0 | 0 |
| Seas95-13-12 | 0 | 0 | 0 |

P2 shelf edge thickness

| line | z1 (m) | z2 (m) | z2-z1 (m) | |
|---|---|---|---|---|
| TC98-041 | 0 | 0 | 0 | |
| TC98-055 | 0 | 0 | 0 | |
| TC98-057 | 0 | 0 | 0 | |
| Seas95-15-2 | 1284 | 1388 | 104 | |
| vn-06-45 | 1332 | 1628 | 296 | |
| vn-06-57 | 1312 | 1564 | 252 | |
| Seas95-01-2A | 1324 | 1556 | 232 | shelf break |
| Seas95-15-1 | 0 | 0 | 0 | |
| vn-06-08 | 0 | 0 | 0 | |
| Seas95-01-1 | 0 | 0 | 0 | |
| TC93-11B1WT | 0 | 0 | 0 | |
| vn-06-44 | 0 | 0 | 0 | |
| Seas95-01-3 | 0 | 0 | 0 | |
| Seas95-13-12 | 0 | 0 | 0 | |

Shelf break removed by erosion

P1 shelf edge thickness

| line | z1 (m) | z2 (m) | z2-z1 (m) |
|---|---|---|---|
| TC98-041 | 0 | 0 | 0 |
| TC98-055 | 0 | 0 | 0 |
| TC98-057 | 0 | 0 | 0 |
| Seas95-15-2 | 1468 | 1864 | 396 |
| vn-06-45 | 1388 | 1728 | 340 |
| vn-06-57 | 1424 | 1680 | 256 |
| Seas95-01-2A | 1456 | 1708 | 252 |
| Seas95-15-1 | 0 | 0 | 0 |
| vn-06-08 | 0 | 0 | 0 |
| Seas95-01-1 | 0 | 0 | 0 |
| TC93-11B1WT | 0 | 0 | 0 |
| vn-06-44 | 0 | 0 | 0 |
| Seas95-01-3 | 1392 | 1668 | 276 |
| Seas95-13-12 | 0 | 0 | 0 |

**Note: “0” value denotes shelf edge not observed at that location.**

# VITA

Christine M. Wright received a Bachelor of Science in geology from Central Missouri State University in December 1998, where she studied trilobites of the Roubidoux Formation with Dr. James Loch. She completed a Master of Science in geology at Louisiana State University in December 2002. While at LSU, Christine studied variability of ancient deltaic deposits with Dr. Arnold Bouma. Christine came to Texas A&M University in Fall 2002 and completed this project under the direction of Dr. Steve Dorobek. After graduation, Christine will join Chevron in Houston as a geoscientist. She can be contacted c/o Texas A&M University Department of Geology, College Station, TX.